ALMA MATER STUDIORUM
UNIVERSITÀ DI BOLOGNA
Dipartimento di Scienze della Terra e Geologico-Ambientali

DOTTORATO DI RICERCA IN SCIENZE DELLA TERRA
XXIII° CICLO
Settore scientifico-disciplinare: GEO/02

Coordinatore: Prof. Roberto Barbieri

RICOSTRUZIONE DELLE FLUTTUAZIONI EUSTATICHE QUATERNARIE CON PARTICOLARE RIFERIMENTO ALL'ULTIMA DEGLACIAZIONE (TERMINAZIONE I) NEL BACINO ADRIATICO (MAR MEDITERRANEO)

…

THE STRATIGRAPHIC RECORD OF THE QUATERNARY SEA LEVEL FLUCTUATIONS AND THE IMPACT OF THE POST-GLACIAL SEA LEVEL RISE (TERMINATION I) IN THE ADRIATIC BASIN (MEDITERRANEAN SEA)

Presentata da:
Dott. Vittorio Maselli

Relatore
Dott. Fabio Trincardi

Esame Finale Anno 2011

CONTENTS

RIASSUNTO

La configurazione attuale dei margini continentali clastici è il risultato dell'interazione tra vari processi geologici che agiscono su molteplici scale spaziali e temporali. Tra questi, le oscillazioni del livello del mare, le variazioni nei tassi di sedimentazione e il regime tettonico regionale, sono i principali fattori che hanno regolato la deposizione e la preservazione delle sequenze deposizionali di piattaforma durante il Quaternario. Nei tre anni di Dottorato, ho cercato di ricostruire e quantificare l'impatto che ha avuto ogni processo nella formazione dei corpi deposizionali centro e nord adriatici, con lo scopo finale di investigare le oscillazioni eustatiche tardo Quaternarie.

Nel corso degli ultimi decenni, vari autori hanno cercato di quantificare le oscillazioni eustatiche utilizzando sia indicatori diretti di livello del mare, come sistemi barriera laguna o reef a coralli costituiti da specie che vivono prossime al livello del mare, sia indiretti, come il segnale isotopico del $\delta^{18}O$, oppure utilizzando simulazioni numeriche. Le curve ottenute utilizzando indicatori diretti del livello del mare offrono un segnale composito, che oltre ad aver registrato la componente eustatica, riflettono anche l'effetto di fenomeni locali, come il regime tettonico o processi di *rebound* glacio-isostatico: il segnale eustatico va quindi ricostruito filtrando frequenze spurie che riflettono il contributo di questi fattori. Il primo livello di studio è consistito quindi nel quantificare lo stile tettonico del bacino centro adriatico, in modo da ridurre gli errori sulle ricostruzioni delle oscillazioni del livello del mare nel passato. Questo risultato è stato ottenuto mediante un approccio numerico, integrato con dati diretti di sismica ad alta risoluzione. In particolare, i risultati ottenuti dal "backstripping" del pozzo PRAD1.2 (un pozzo a carotaggio continuo lungo ca. 71 m e perforato a sud della Depressione Meso Adriatica - MAD - a ca. 185 metri di profondità durante il Progetto Europeo Promess1 - *Profile across Mediterranean Sedimentary Systems*, Part 1) sono stati integrati e confermati dallo studio di paleo-linee di riva di stazionamento basso, formatesi durante i periodi glaciali a partire dallo Stadio Isotopico (*Marine Isotopic Stage* - MIS) 10. Il trend tettonico di subsidenza ottenuto, che spiega la geometria in backstepping delle ultime quattro sequenze deposizionali, poiché maggiore del tasso di sedimentazione medio, è stato ulteriormente confrontato con le associazioni di foraminiferi bentonici campionate nel pozzo PRAD1.2, che hanno registrato un'evoluzione da un ambiente deposizionale di spiaggia durante il MIS 10, ad un ambiente di piattaforma esterna durante il MIS 2.

Una volta ricostruito il regime tettonico dell'area centro adriatica, definendo quantitativamente i tassi di subsidenza, il secondo livello di studio è stato analizzare l'impatto che hanno avuto le oscillazioni eustatiche e climatiche post glaciali, tra cui i due *Meltwater*

Pulses 1A e 1B e l'evento climatico freddo del Dryas recente, e degli apporti sedimentari, nel costruire i corpi sedimentari trasgressivi post glaciali associati all'ultima risalita eustatica (*Transgressive Systems Tract* – TST). Il record trasgressivo adriatico, che copre un intervallo temporale di circa 14 ka a partire dalla fine del periodo glaciale avvenuta ca. 19 ka BP (Last Glacial Maximum, LGM), è costituito da tre depositi lateralmente equivalenti: lungo la piattaforma centro adriatica e nella MAD, dove i depositi trasgressivi sono caratterizzati da Facies di ambiente prevalentemente marino; lungo la piattaforma nord adriatica, dove i depositi trasgressivi sono invece caratterizzati da corpi sedimentari costieri, e quindi buoni indicatori del livello del mare.

In particolare, la piattaforma centro adriatica, limitata a nord dalla MAD e a sud dal promontorio del Gargano, è caratterizzata da un corpo sedimentario trasgressivo composito, formato da tre unità deposizionali separate da 2 superfici erosive di estensione regionale. Ogni unità del corpo trasgressivo ha registrato un preciso intervallo temporale dell'ultima risalita eustatica, come indicato da una serie di età ^{14}C calibrate. In particolare l'unità intermedia, costituita da due sotto-unità progradazionali, ha registrato l'intervallo compreso tra i due *Meltwater Pulses* 1A e 1B e in particolare l'evento freddo del Dryas recente. Una serie di simulazioni è stata eseguita mediante due modelli numerici (sviluppati dal *Community Surface Dynamics Modeling System* - CSDMS) per ricostruire la stratigrafia del margine adriatico post-LGM, in particolare: *HydroTrend 3.0* ha fornito simulazioni dei tassi di sedimentazione medi dal massimo glaciale ad oggi; e *2D Sedflux 1.0C* ha permesso di ricostruire il riempimento del bacino adriatico e la geometria interna dei depositi trasgressivi. I risultati ottenuti dalle simulazioni, integrati con analisi sismo-stratigrafiche e dati di carota, indicano che: 1 - il corpo progradante del Dryas recente è la conseguenza di un aumento negli apporti di sedimenti dovuti ad una diminuzione nella copertura vegetale delle aree di drenaggio e ad una variazione nel ciclo idrologico; 2 - la bipartizione dell'unità intermedia è la conseguenza di un periodo di stazionamento (o possibilmente di una breve caduta) del livello del mare avvenuta durante il Dryas recente.

La piattaforma nord adriatica, per le sue caratteristiche morfo-batimetriche, fornisce informazioni complementari a quelle ottenute studiando i depositi trasgressivi dell'area centro adriatica. In quest'area, infatti, l'ultima trasgressione marina è stata registrata in piattaforma da una serie di depositi barriera-laguna di età decrescente al diminuire della profondità e in una geometria in "*backstepping*". Il modello profondità-età dei livelli di torba campionati alla base e all'interno di depositi di laguna, datati con metodo ^{14}C, è in accordo con le curve eustatiche pubblicate da precedenti autori e conferma l'andamento eustatico post glaciale. Una maggiore complessità è registrata invece nei depositi del Dryas recente, caratterizzati da due sistemi

deposizionali lagunari quasi coevi a profondità molto differenti da zona a zona. Questa complessità, probabilmente legata all'interazione di vari processi, non è ancora del tutto spiegata, ma sono state poste le basi per future ricerche.

ABSTRACT

The modern stratigraphy of clastic continental margins is the result of the interaction between several geological processes acting on different time scales, among which sea level oscillations, sediment supply fluctuations and local tectonics are the main mechanisms. During the past three years my PhD was focused on understanding the impact of each of these process in the deposition of the central and northern Adriatic sedimentary successions, with the aim of reconstructing and quantifying the Late Quaternary eustatic fluctuations.

In the last few decades, several Authors tried to quantify past eustatic fluctuations through the analysis of *direct* sea level indicators, among which drowned barrier-island deposits or coral reefs, or *indirect* methods, such as Oxygen isotope ratios ($\delta^{18}O$) or modeling simulations. Sea level curves, obtained from direct sea level indicators, record a composite signal, formed by the contribution of the global eustatic change and regional factors, as tectonic processes or glacial-isostatic rebound effects: the eustatic signal has to be obtained by removing the contribution of these other mechanisms.

To obtain the most realistic sea level reconstructions it is important to quantify the tectonic regime of the central Adriatic margin. This result has been achieved integrating a numerical approach with the analysis of high-resolution seismic profiles. In detail, the subsidence trend obtained from the geohistory analysis and the backstripping of the borehole PRAD1.2 (the borehole PRAD1.2 is a 71 m continuous borehole drilled in -185 m of water depth, south of the Mid Adriatic Deep - MAD - during the European Project PROMESS 1, *Profile Across Mediterranean Sedimentary Systems*, Part 1), has been confirmed by the analysis of lowstand paleoshorelines and by benthic foraminifera associations investigated through the borehole. This work showed an evolution from inner-shelf environment, during *Marine Isotopic Stage* (MIS) 10, to upper-slope conditions, during MIS 2. Once the tectonic regime of the central Adriatic margin has been constrained, it is possible to investigate the impact of sea level and sediment supply fluctuations on the deposition of the Late Pleistocene-Holocene transgressive deposits.

The Adriatic transgressive record (TST - Transgressive Systems Tract) is formed by three correlative sedimentary bodies, deposited in less then 14 kyr since the Last Glacial Maximum (LGM); in particular: along the central Adriatic shelf and in the adjacent slope basin the TST is formed by marine units, while along the northern Adriatic shelf the TST is represented by costal deposits in a backstepping configuration.

The central Adriatic margin, characterized by a thick transgressive sedimentary succession, is the ideal site to investigate the impact of late Pleistocene climatic and eustatic fluctuations, among which Meltwater Pulses 1A and 1B and the Younger Dryas cold event. The central

Adriatic TST is formed by a tripartite deposit bounded by two regional unconformities. In particular, the middle TST unit includes two prograding wedges, deposited in the interval between the two Meltwater Pulse events, as highlighted by several ^{14}C age estimates, and likely recorded the Younger Dryas cold interval. Modeling simulations, obtained with the two coupled models *HydroTrend 3.0* and *2D-Sedflux 1.0C* (developed by the *Community Surface Dynamics Modeling System* - CSDMS), integrated by the analysis of high resolution seismic profiles and core samples, indicate that: 1 - the prograding middle TST unit, deposited during the Younger Dryas, was formed as a consequence of an increase in sediment flux, likely connected to a decline in vegetation cover in the catchment area due to the establishment of sub glacial arid conditions; 2 - the two-stage prograding geometry was the consequence of a sea level still-stand (or possibly a fall) during the Younger Dryas event.

The northern Adriatic margin, characterized by a broad and gentle shelf (350 km wide with a low angle plunge of 0.02° to the SE), is the ideal site to quantify the timing of each steps of the post LGM sea level rise. The modern shelf is characterized by sandy deposits of barrier-island systems in a backstepping configuration, showing younger ages at progressively shallower depths, which recorded the step-wise nature of the last sea level rise. The age-depth model, obtained by dated samples of basal peat layers, is in good agreement with previous published sea level curves, and highlights the post-glacial eustatic trend. The interval corresponding to the Younger Dyas cold reversal, instead, is more complex: two coeval coastal deposits characterize the northern Adriatic shelf at very different water depths. Several explanations and different models can be attempted to explain this conundrum, but the problem remains still unsolved.

PREFACE

In the last few decades several Authors focused their attention on the study of past climatic changes with the aim of improving the knowledge of the mechanisms governing their evolution. Since the 1990, when the first IPCC report was released (IPCC Scientific Assessment, 1990), most of the scientific interest was dedicated to the prediction of future climate evolutions and, in particular, of future sea level changes and their impact on coastal regions (Stanley and Warne, 1994; Siddall et al., 2010; Paul, 2011). To achieve this goal, several approaches were introduced, ranging from direct reconstructions of past climate indicators to complete modeling simulations (Alley 2000; Church et al., 2001; Lambeck and Chappell, 2001). The reconstruction of past climatic oscillations, on different time scales and with different degrees of resolution, is the only way to test and improve our hypotheses of future climate change, because past climate regimes show the full range of climatic variability, including abrupt changes of higher magnitude than commonly observed today (Barber et al., 1999; Clark et al., 2002a). In this view it is crucial to understand the stability of ice caps and their response to climatic oscillations, driven by astronomical forcing, that control the changing of the insolation of our Planet, and by internal land-ocean feedback processes (Ruddiman, 2006). As sea level and ice sheets can be considered interlinked systems, reconstructing past sea level oscillations is a direct measurement of the total ice sheet volume changes (Shackleton, 1987; Peltier, 1994). Since the early ’60 (Fairbridge, 1961; Shackleton and Opdyke, 1973), several Authors tried to reconstruct eustatic oscillations by using a variety of direct sea level indicators, as coral reefs or drowned shoreline deposits (Bard et al., 1996; Hanebuth et al., 2000). In any case, several corrections need to be introduced, in particular referring to the local tectonics.

During my three-years PhD thesis work, I combined numerical simulation models and a sequence stratigraphy approach to understand and recognize the fingerprint of sea level fluctuations in the western Adriatic margin on different time scales, giving particular attention to the last sea level rise (Termination I, Broecker and Van Donk, 1970; Mix and Ruddiman, 1985). In order to better constrain the rate of sea level changes since the Middle Pleistocene, the first goal was to understand the local tectonics of the central Adriatic basin. This result was obtained by coupling geohistory analysis with a detailed investigation of drowned lowstand shoreline deposits. Once the local tectonic trend was constrained, I applied two numerical models to reconstruct the central Adriatic margin stratigraphy, in order to understand the impact of the step-wise nature of the last sea level rise on the deposition and preservation of the transgressive sedimentary succession. The attention was focused particularly on the study of the impact of the Younger Dryas cold event on sediment flux and sea level: several hypotheses were tested by

comparing modeling results to the analysis of high resolution seismic profiles and paleo-climatic reconstructions of previous studies.

The hypotheses made on the reconstruction of the last sea level rise and tested through the numerical modeling of the central Adriatic transgressive sequence are then compared with the reconstructed sea level curve obtained by the direct investigation of drowned shoreline deposits in northern Adriatic region.

The outline of this thesis reflects the above reported goals as follows:

Chapter 1) Introduction

Chapter 2) Study Area

Chapter 3) Maselli, V., F. Trincardi, A. Cattaneo, D. Ridente and A. Asioli (2010) "Subsidence pattern in the central Adriatic and its influence on sediment architecture during the last 400 kyr". Journal of Geophysical Research - Solid Earth (vol. 115, doi: 10.1029/2010JB007687).

Chapter 4) Maselli, V., E. Hutton, A. Kettner, J. Syvitski and F. Trincardi. "High-frequency sea level and sediment supply fluctuations during Termination I: an integrated sequence-stratigraphy and modeling approach from the Adriatic Sea". Marine Geology (Paper accepted, under revision).

Chapter 5) The record of the last sea level rise in the northern Adriatic shelf. The Younger Dryas Conundrum: Hypotheses and future investigations.

Conclusion.

At the end of my PhD one Paper has been published on *Journal of Geophysical Research*, and a second Paper has been accepted on *Marine Geology*.

CHAPTER I

- Introduction -

Introduction

Sea level oscillations are the consequence of the interaction between local, regional and global processes, acting on different temporal and spatial scales. Geological processes, the formation of ocean basins and plate motions, dominate over the long-term intervals (several Ma, Cloetingh, 1986; Haq et al., 1988), while climatic and isostatic effects are the main factors controlling sea level on intermediate to short-term time scales (Imbrie et al., 1984; Lambeck et al., 1998).

During the Quaternary, cyclical changes in orbital parameters led to variations in solar radiation reaching the Earth surface causing important climatic oscillations (Martinson et al., 1987; Ruddiman, 2006). Earth orbital cycles are characterized by three specific frequencies, as a consequence of the interaction between the gravitational fields of the Solar System Planets: 1) eccentricity, a parameter which defines the shape of the orbit and so the distance between the Earth and the Sun, characterized by period of ca. 100 kyr; 2) obliquity, with a period of ca. 41 kyr, recording variations in the tilt of the Earth rotational axis; 3) precession, with a period of ca. 21 kyr, reflecting changes in the direction of the Earth rotational axis (Berger, 1984; Berger and Pestiaux, 1984). Following the pioneeristic ideas of Adhemar (1842) and Croll (1875), Milankovitch (1941) proposed the theory relating Quaternary glaciations to astronomical events and explained how changes in orbital parameters control the insolation of the Earth and, as a consequence, the waxing and waning of ice caps. Global sea level changes are mainly a consequence of ice caps growth and retreat, although several other factors control eustatism, as changes in the ocean Geoid (Mörner, 1996) and steric variations due to temperature changes of the water masses (Bryan, 1996).

When referring to regional and local spatial scales, moreover, sea level fluctuations (i.e. relative sea level) can be the consequence of different kind of processes that control the vertical oscillations of the Earth surface, as glacio-isostatic rebound effects, local tectonics and compaction processes of the sedimentary cover (Reynolds et al., 1991; Lambeck et al., 1998). In order to obtain the eustatic signal from a relative sea level curve, it is important to remove the contributions of all these processes.

Sea level reconstructions

On the last few decades, several Authors reconstructed eustatic oscillations by analyzing different sea level indicators, with contributions from geomorphology, geology, geochemistry and archaeology (Lambeck et al., 2004). Sea level elevation can be obtained *directly* by

investigating geologic and geomorphologic features, or archaeological remains; otherwise the eustatic signal can be reconstructed *indirectly* by analyzing biological proxies that recorded the chemical composition of Ocean water or ice and gas composition of ice cores.

Direct sea level indicators

Marine erosion features, such as benches or tidal notches may provide quite accurate determinations of paleo-sea level elevations: an example is discussed in Antonioli et al. (2007), who also determines sea level elevation, or tectonics, by the modern elevation of archeological findings, among which seaports. Marine deposits are useful sea level indicators, mostly because clearly identifiable through their stratigraphic features and fauna assemblages. Moreover, barrier-island-lagoon deposits (Törnqvist et al., 2004) or drowned paleo-shorelines are often associated with remains of coastal plants and vegetation, which accumulate as peat layers or mangrove deposits and can be dated with ^{14}C radiocarbon dating (Hanebuth et al., 2000). The most reliable paleo sea level indicator is probably the coral reef deposit of species living close to sea level, such as *Acropora Palmata* reef (Fairbanks, 1989) and other fossil coral reef terraces (Bard et al., 1996; Bard et al., 2010). It is important to note that all these different indicators are based on the assumption that the tectonic evolution of the area (uplift or subsidence rates) is known, and, possibly, glacio-hydro isostatic contributions are introduce or estimated (Lambeck et al., 2002).

Indirect sea level indicators

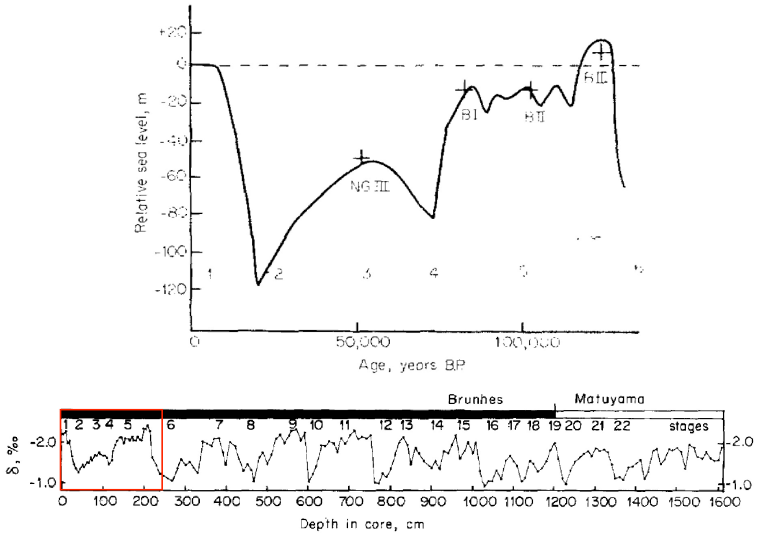

Beside the methods mentioned above, past eustatic oscillations can be reconstructed by using two indirect methods: Oxygen isotopes ratio (see Figure 1.1), obtained from foraminifer's shells, and modeling simulations (Lambeck and Chappell, 2001; Lea et al., 2002). The ratio between ^{18}O and ^{16}O ($\delta^{18}O$) in the ocean is a

Figure 1.1 - An example of indirect estimation of global sea level oscillation. Glacio-eustatic sea level curve for the last 130 kyr derived from Oxygen isotopic composition of *G. sacculifer* (modified from Shackleton and Opdyke 1973).

function of the climate-driven oscillations of the hydrological cycle. Evaporation processes remove preferentially the lighter ^{16}O fraction from the ocean: during glacial periods the ^{16}O tends to remain preferentially trapped in ice caps and the $\delta^{18}O$ proportionally increases in the water ocean. On the contrary, during interglacial intervals, the melting of ice caps brings back the ^{16}O to the ocean, and so the proportion of $\delta^{18}O$ in the water decreases; the relation between $\delta^{18}O$ and sea level is then obtained through empirical relations: a variation of 0.1‰ of the $\delta^{18}O$ corresponds to a variation in sea level of about 10 meters (Shackleton and Opdyke, 1973; Chappell and Shackleton, 1986; Shackleton et al., 1987).

It is important to underline that sea level curves, based on the conversion of $\delta^{18}O$, can be affected by large uncertainties because the $\delta^{18}O$ may vary as a function of many factors, among which the water temperature and salinity (Rohling et al., 1998; Waelbroek et al., 2002; Siddall et al., 2003).

The last Glacial-Interglacial cycle

The 4-order cyclicity (ca. 100 kyr) dominates the eustatic signal after the Mid-Pleistocene revolution (MPR, ca. 800 kyr BP); this term is used to describe the transition between 41 kyr and 100 kyr glacial-interglacial cycles (see Figure 1.2; Maslin and Ridgwell, 2005). The 100 kyr cycles are markedly asymmetric: the time interval recording a sea level fall, as a consequence of the slow growth of the ice caps, it is more then three times greater then the time interval occurred for sea level rise, as a consequence of ice melting.

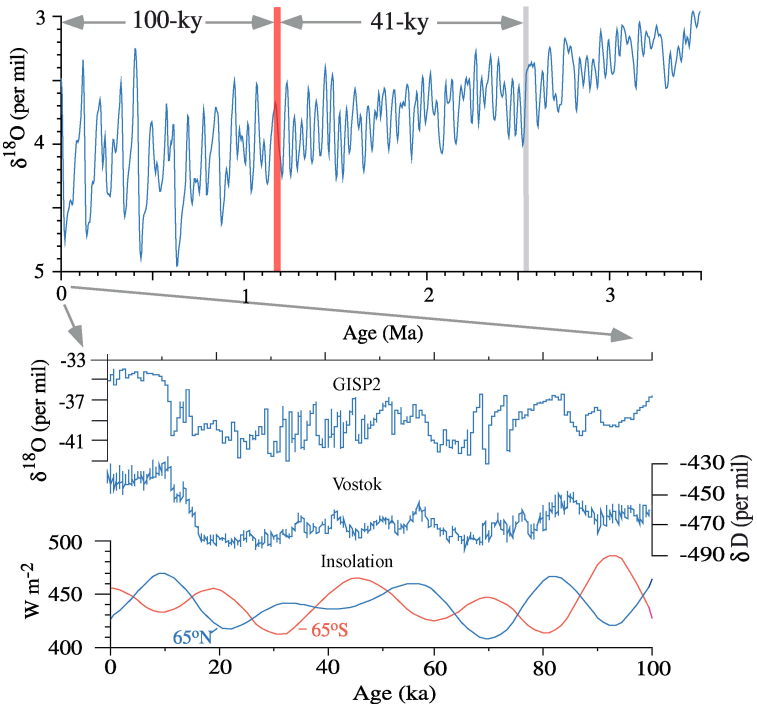

Figure 1.2 - Top: The marine $\delta^{18}O$ record as a proxy for changes in global ice volume over the past 3.5 My. The red line marks the transition between 41 kyr and 100 kyr glacial-interglacial cycles. Bottom: the comparison between the $\delta^{18}O$ curve derived from Greenland ice core GISP2 and Antarctic ice core Vostok, and the insolation at 65°N for July and 65° S for January (modified from Clark et al., 1999).

During the last glacial-interglacial transition, started about 20 kyr ago at the end of the Last Glacial Maximum (LGM), sea level rose from about -120 meters to

modern position (Clark et al., 2009). As highlighted by several Authors, the last sea level rise (encompassing the interval between ca. 19 and 5.5 kyr BP; all ages refer to calendar year Before Present) was not monotonic, but punctuated by two main steps of enhanced ice melting and by minor eustatic events (Fairbanks, 1989).

In agreement with the Milankovitch theory, the increasing amount of northern summer insolation allows the northern ice sheet to retreat ca. 21-19 kyr BP. The high flux of fresh water due to ice melting lead to a sea level rise of about 10 meters in less then 500 yr and to a slowing of the Atlantic circulation (see Figure 1.3; Clark et al., 2004).

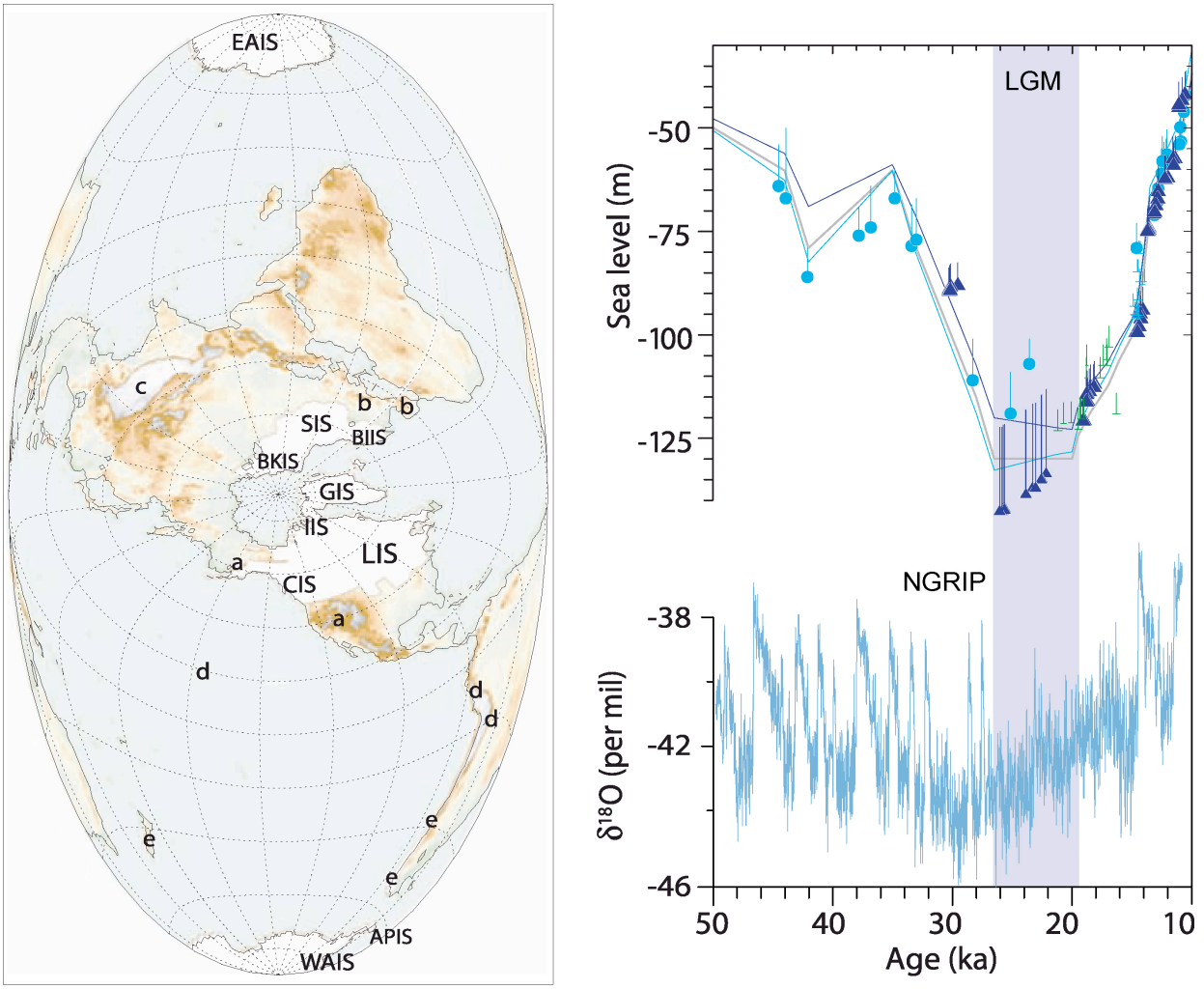

Figure 1.3 - Left: Distribution of ice sheets at the Last Glacial Maximum: APIS, Antarctic Peninsula Ice Sheet; EAIS, East Antarctic Peninsula Ice Sheet; WAIS, West Antarctic Peninsula Ice Sheet; LIS, Laurentide Ice Sheet; GIS, Greenland Ice Sheet, SIS, Scandinavian Ice Sheet; CIS, Cordilleran Ice Sheet; BKIS, Barents-Kara Ice Sheet; BIIS, British-Irish Ice Sheet; IIS, Innuitian Ice Sheet. Mountain Glaciers: a, western North America; b, Europe; c, Tibet; d, tropics and subtropics; e, Southern Hemisphere (modified from Clark et al., 2009). Right top: Sea level prediction for New Guinea (blue line), Barbados (purple line) compared to RSL data (vertical bars represent depth uncertainty) from New Guinea (blue circle), Barbados (purple triangle), Bonaparte Gulf (green bar) and Sunda Shelf (blue bar). The gray bar represents the time of the Last Glacial Maximum (LGM). Right Bottom: Oxygen isotope ratio obtain from NGRIP ice core (modified from Clark et al., 2009).

The switching-off of the North Atlantic conveyor, ca. 18 kyr BP, produced an abrupt warming of Antarctica and surrounding ocean: the bipolar see-saw, a term used to define the opposite relation between northern and southern hemisphere climate (Broecker, 1998), was in the "warm-south" mode (Severinghaus, 2009). Furthermore, CO_2 levels in the atmosphere began to rise (Stephens and Keeling, 2000) and led to warming the entire Planet through the greenhouse effect (Paillard, 2001). The bipolar see-saw changed in "warm-north" mode ca. 14.7 kyr BP, as a consequence of the gradual warming in the Southern Ocean and of a consequent reduction of the densification process controlling the formation of deep ocean water (Knorr and Lohmann, 2003). The resumption of Atlantic circulation, together with high values of atmospheric CO_2 and strong June insolation, led to the Bölling climatic optimum and to the Meltwater Pulse 1A (MWP-1A, Fairbanks, 1989). During the MWP-1A sea level rose of about 20 meters in the interval between ca. 14.3 to 13.8 kyr BP, as a consequence of the collapses both Laurentide and Antarctic ice sheets (see Figure 1.4; Bard et al., 1996, Clark et al., 2002b; Rohling et al., 2004; Siddall et al., 2010). The large amount of fresh water originated by ice melting and delivered in the North Atlantic Ocean led to a reduction of oceanic surface water density and of the Thermohaline circulation: a cooling phase started in the Northern Hemisphere, while a contemporaneous warming was recorded in the Southern Hemisphere, indicating that a large reduction in North Atlantic Deep Water Formation (NADW) led to a decreased meridional heat transport across the South Atlantic (Clark et al., 2002b). This cooling trend, started with the MWP-1A and culminated with the cold Younger Dryas event: during this interval, sub-glacial conditions were recorded in the northern Atlantic region and the bipolar see-saw turned back in the "south-warm" mode (Alley et al., 1999). The abrupt end of the Younger Dryas, ca. 11.5 kyr BP, was probably a consequence of the re-establishment of warm surface currents flowing northward in the Atlantic Ocean, most likely due to the resumption of North Atlantic Deep Water circulation (Severinghaus et al., 1998). The switch of the bipolar see-saw in a "north-warm" condition led to a second important phase of Laurentide ice sheet collapse culminating in the Meltwater Pulse 1B (Fairbanks et al., 1989; Bard et al., 1996): in less then 1000 yr sea level rose of about 20 meters (see Figure 1.4; Fairbanks, 1989).

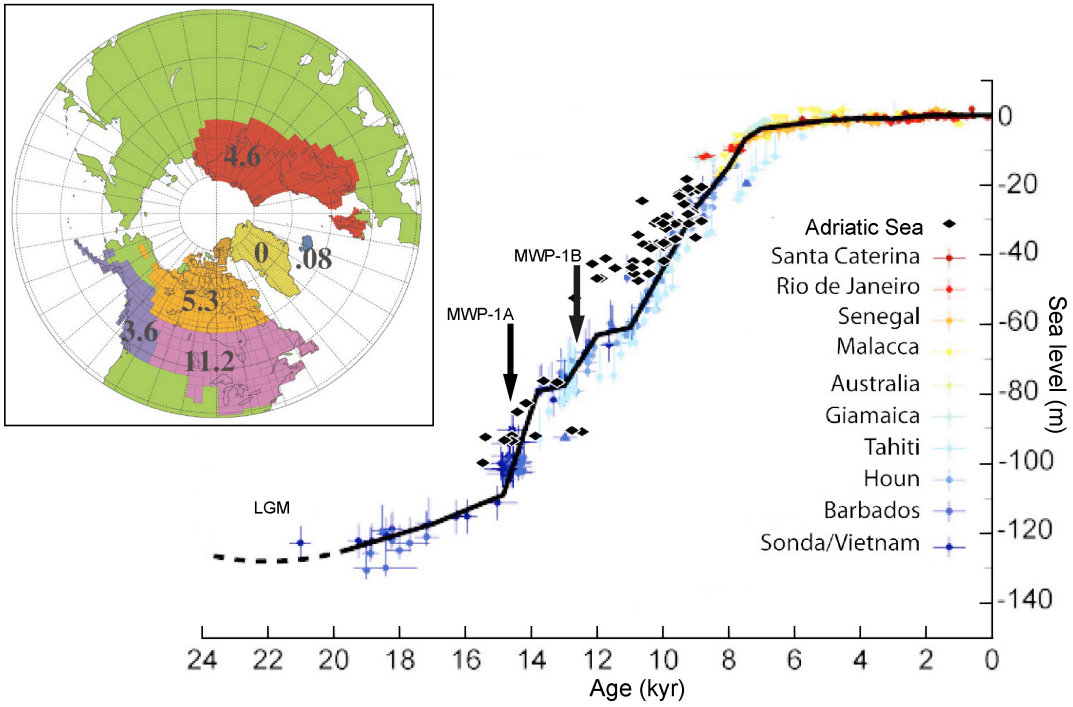

Figure 1.4 - Composite sea level curve for the post- LGM time interval and the timing of the Meltwater Pulses 1A and 1B (modified from Fleming et al 1998). Inset box represents the contribution (in meters) of sea level rise during the MWP-1A from individual region of the Northern Hemisphere (modified from Peltier, 2004).

The Younger Dryas event

Termination I, recording the last glacial-Holocene transition (Mix and Ruddiman, 1985), was characterized by oscillating phases of warm and cold climate conditions: an abrupt warming at the start of the Bölling was followed by a period of gradual cooling, which culminated in the sub-glacial condition of the Younger Dryas (Lehman et al., 1992). The Younger Dryas event, which began approximately 12.8 kyr BP, was characterized by a large-scale reorganization of the pattern of atmospheric and oceanic circulations, as highlighted by proxy-based reconstructions on several different geological archives and modeling simulations (Isarin et al., 1998; Alley et al., 2000). The YD was likely originated by an intense freshwater discharge, derived from ice melting and released in the north Atlantic, which caused a density decline of the north Atlantic surface water (North Atlantic Meridional Overturning; Broecker et al., 1988). A reduced density of the waters flowing from the south led to a southward shift in sites of deep water formation and to a decline of cross equatorial flow of warm surface waters (Stocker et al., 1992). These processes led to the cooling of the high-latitude portion of the northern Hemisphere (Fig. 1.5) and to a reduction in African and Asian Monsoon with a consequent reduction of CH_4 content in ice core records which likely reflects a decrease in the extent of tropical wetlands (Chappellaz et al., 1997; Dällenbach et al., 2000).

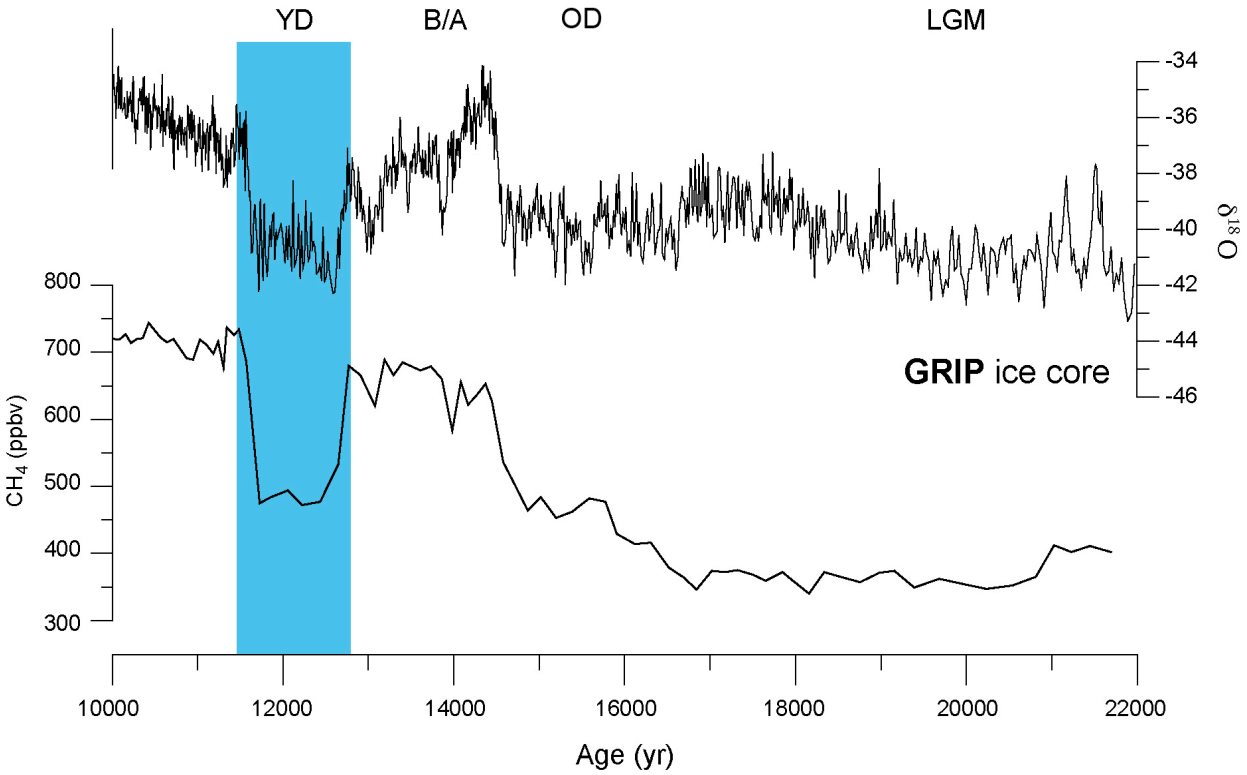

Figure 1.5 - $\delta^{18}O$ and CH_4 curve from the Last Glacial Maximum (LGM) to the end of the Younger Dryas (YD) derived from the GRIP ice core (modified from Alley et al., 2000). The Younger Dryas period is characterized by heavier $\delta^{18}O$, reaching values comparable to those of the LGM. A similar trend in Methane curve reflects a contemporaneous decrease in the extent of tropical wetlands (Chappellaz et al., 1997). The end of the YD cold event was abrupt and possibly occurred in less then a 50 yr (Taylor et al., 1997); B/A: Bölling-Allerød; OD: Oldest Dryas.

Moreover, the reduction of the north Atlantic circulation led to an increased heat transport toward the south, producing a warming in the Antarctic regions (Alley et al., 1999). Whether the onset of the YD was the culmination of a cooling trend started ca. 1500 yr before, its end was abrupt, and warmer condition were reached in a very short time interval ca. at 11.5 kyr BP. As highlighted by Taylor et al., (1997) through the analysis of the Greenland ice core-record, the end of the YD was divided into three steps, spread over about 40 yr. This result was supported by Alley et al. (1993), who identified that changes in snow accumulation probably cover a shorter time interval, and by Severinghaus et al. (1998), who document a large warming in Greenland on a decadal time scale, followed by an increase in CH_4 concentration, which probably indicates widespread increase in tropical wetland areas (Fig. 1.5).

The sea level record during the Younger Dryas

During the last few decades, several Authors have tried to reconstruct sea level changes on different time scales. Reconstructing sea level changes during the last glacial-interglacial cycle,

constrained by more precise dating techniques and higher resolution methods of investigation, provides a way of understanding the mechanisms and process-response relations governing the ice sheet dynamics and climate change. Although it is possible to reconstruct sea level history with a sub-millennial time resolution, especially for the last 8-10 kyr BP, some uncertainties remain in a critical time interval, amid the last post-glacial sea level rise, corresponding to the Younger Dryas cold event (Bard et al., 2010). In this short interval, a slower rate of sea level rise compared to the previous and the subsequent intervals was demonstrated by several Authors, and this is consistent with the overall climate cooling in the northern Hemisphere (Tahiti corals: Bard et l., 1996; Bard et al., 2010; Huon Peninsula: Edwards et al., 1993; Cutler et al., 2003; Vanuatu: Cabioch et al., 2003; Barbados: Peltier and Faibanks, 2006). However, an exact quantification of the elevation reached by sea level before the onset of the Younger Dryas is more difficult to achieve. In the Tahiti record the YD sea level lays at a depth between -60 and -70 meters with respect to modern sea level (Bard et al., 2010), plus error bars depending on tectonics or isostatic rebound effects at regional scale. The Vanuatu record highlights deeper sea level for the YD, at a depth of ca. -70 meters. Sea level reconstructions obtained by converting the $\delta^{18}O$ signal obtained for the YD a sea level of -70 m +/- 12 m with respect to modern elevation (Siddall et al., 2003). Moreover, another important indication for sea level elevation during the YD can be derived from numerical models: in Siddall et al. (2010), a model simulation forced by temperature changes obtained from ice sheets, both in the northern (GRIP ice core) and southern (Dome-C ice core) hemispheres, indicates a -75 meters sea level for the Younger Dryas as a consequence of a minor sea level fall in the interval between the Meltwater Pulses 1A and 1B.

CHAPTER II

- Study Area -

Geodynamic and stratigraphic setting

The modern Adriatic Sea is the marine portion of the foreland domain of three different orogens: the Apennines, the Alps and the Dinaric chains. In detail, it represents the foredeep and foreland of the SW-directed Apennine subduction (see Figure 2.1; Carminati et al., 2003), the foreland basin of the NE-directed Dinaric subduction (Di Stefano et al., 2009), and the retrobelt foreland of the SE- directed Alpine subduction (Doglioni and Carminati, 2002). The western side of the central and northern Adriatic is a Plio-Quaternary foredeep basin, representing the last of a series of foredeep basins originated during the formation of the Apennine chain and then migrated eastward (Argnani e Ricci Lucchi, 2001). The eastward retreat of the subduction is the most plausible explanation for the progressive eastward migration of the thrust fronts (Malinverno and Ryan, 1986; Royden et al., 1987; Doglioni et al., 1994). Below the Po plain the northern Apennine thrust fronts are well constrained by seismic and well data, and consist of three arcuate thrusts systems: the Monferrato, the Emilia and the Ferrara-Romagna arcs, named from west to east (Pieri and Groppi, 1981). Moving toward the southeast, the external front of the Apennine accretionary prism is traced few kilometers offshore, in the area between the city of Ancona and Pescara (see Figure 2.1; Patacca et al., 1990; Argnani and Frugoni, 1997). In this area, the Plio-Quaternary Adriatic foredeep is characterized by two depocenters (see Figure 2.1 and 2.2), located north of the city of Ancona

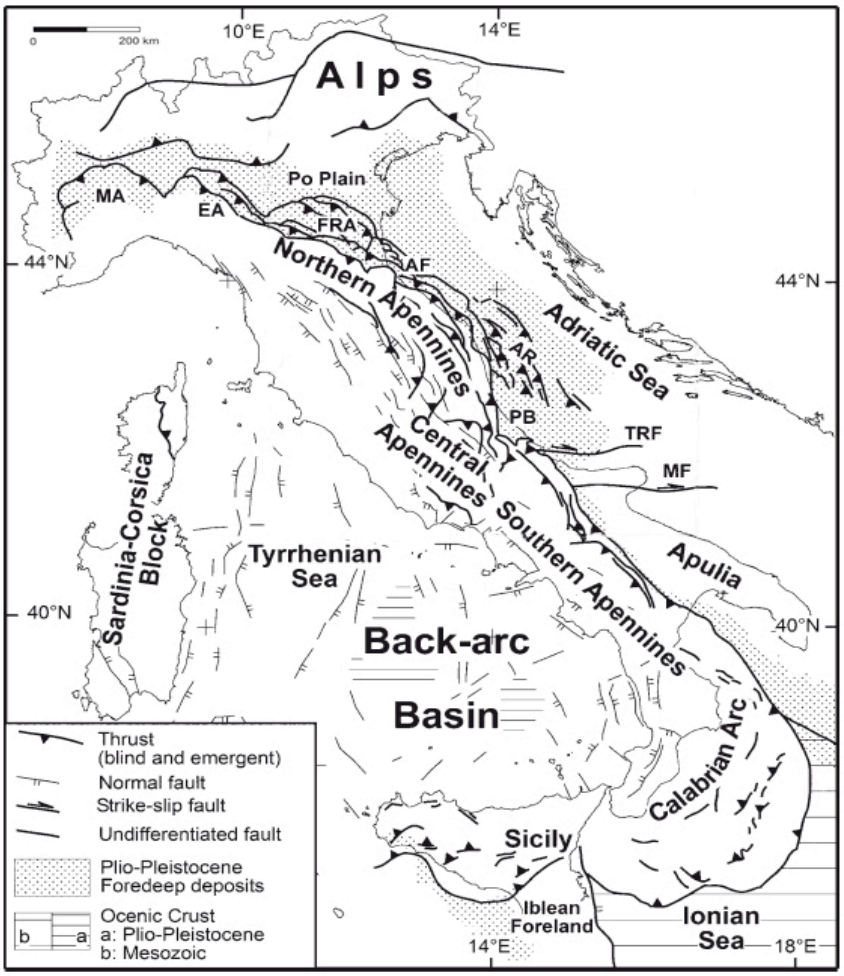

Figure 2.1 - Main structural elements of Italy (modified from Scrocca et al., 2007). MA: Monferrato Arc; EA: Emilia Arc; FRA: Ferrara-Romagna Arc; AF: Adriatic Folds; AR: Adriatic Ridge; PB: Pescara Basin; TRF: Tremiti Fault; MF: Mattinata Fault.

and offshore the city of Pescara (Argnani and Frugoni, 1997). In a distal position, the central Adriatic Sea is characterized by the presence a WNW-ESE trending belt of structural highs, defined as the "Mid-Adriatic Ridge" or "Central Adriatic Deformation Belt" (Argnani and Frugoni, 1997). The majority of these highs have been interpreted as thrust-related folds, also characterized by the evidence of salt diapirism (Scrocca, 2006).

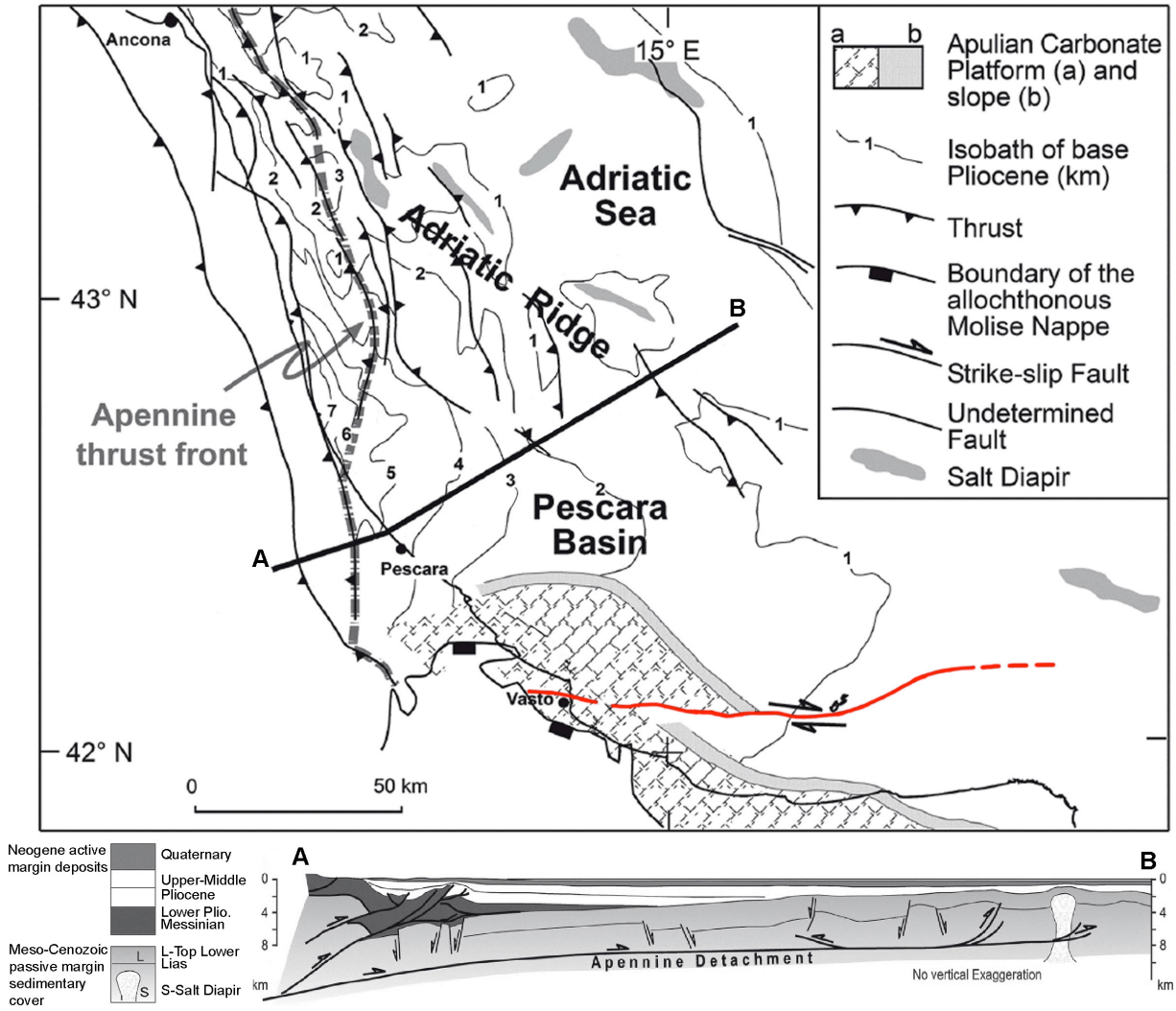

Figure 2.2 - Structural map of the western side of the central Adriatic margin (modified from Scrocca et al., 2007). The black thick line reported in the lower part of the figure (section **AB**) is the geologic section across the Apennine trust front and the Adriatic Ridge. The red line is the tectonic lineament of the Tremiti-Pianosa structural high.

The central Adriatic thrust front is separated by the southern Apennine chain by a lithospheric fault, corresponding to the Tremiti-Pianosa structural high, a tectonic lineament which allowed the accommodation of the different tectonic behaviors between the northern subsiding Adriatic margin and the uplifting Apulia region (Doglioni et al., 1994). The Apulia region represents the uplifted flexural outer bulge of the foreland domain of the westward subducting Adria Plate (Doglioni et al., 1996).

Geodynamic and sedimentary reconstructions of the geological history of the Adriatic basin document a progressive evolution from a Mesozoic carbonate passive margin, bordering the Tethys Ocean, to a Cenozoic foredeep-foreland domain, as a consequence of the collision between the African and European Plates (Channell et al., 1979; D'Argenio and Horvath, 1984). The stratigraphy encountered in exploration boreholes (Ori et al., 1986), indicates, typically, an evolution from Triassic-Early Jurassic carbonate platform to Middle Jurassic-Late Cretaceous carbonate pelagic sedimentation: this stratigraphy recorded the rifting and subsequent continental break up that led the opening of the Tethys Ocean. A significant change in sedimentation occurred during the Tertiary: during this interval the hemipelagic clastic sedimentation increased progressively, recording the compressive deformation produced by the convergence of the African and European Plates. Seismic and well log data collected for hydrocarbon exploration made it possible the analysis and the reconstruction of the progressive fill of confined basins of tectonic origin, that recorded the foredeep deposition during the growth and eastward migration of the Apennine chain since the Oligocene (Ori et al., 1986; Ricci Lucchi, 1986). The eastward migration of the Apennine thrust front produced a series of piggyback basins that were filled by Late Pliocene to Early Pleistocene deposits (Ori and Friend, 1984). Since the Middle Pleistocene the depositional style changed from a tectonically controlled foredeep successions to a cyclical deposition driven by glacio-eustatic sea level fluctuations (Trincardi and Correggiari, 2000; Ridente and Trincardi, 2002).

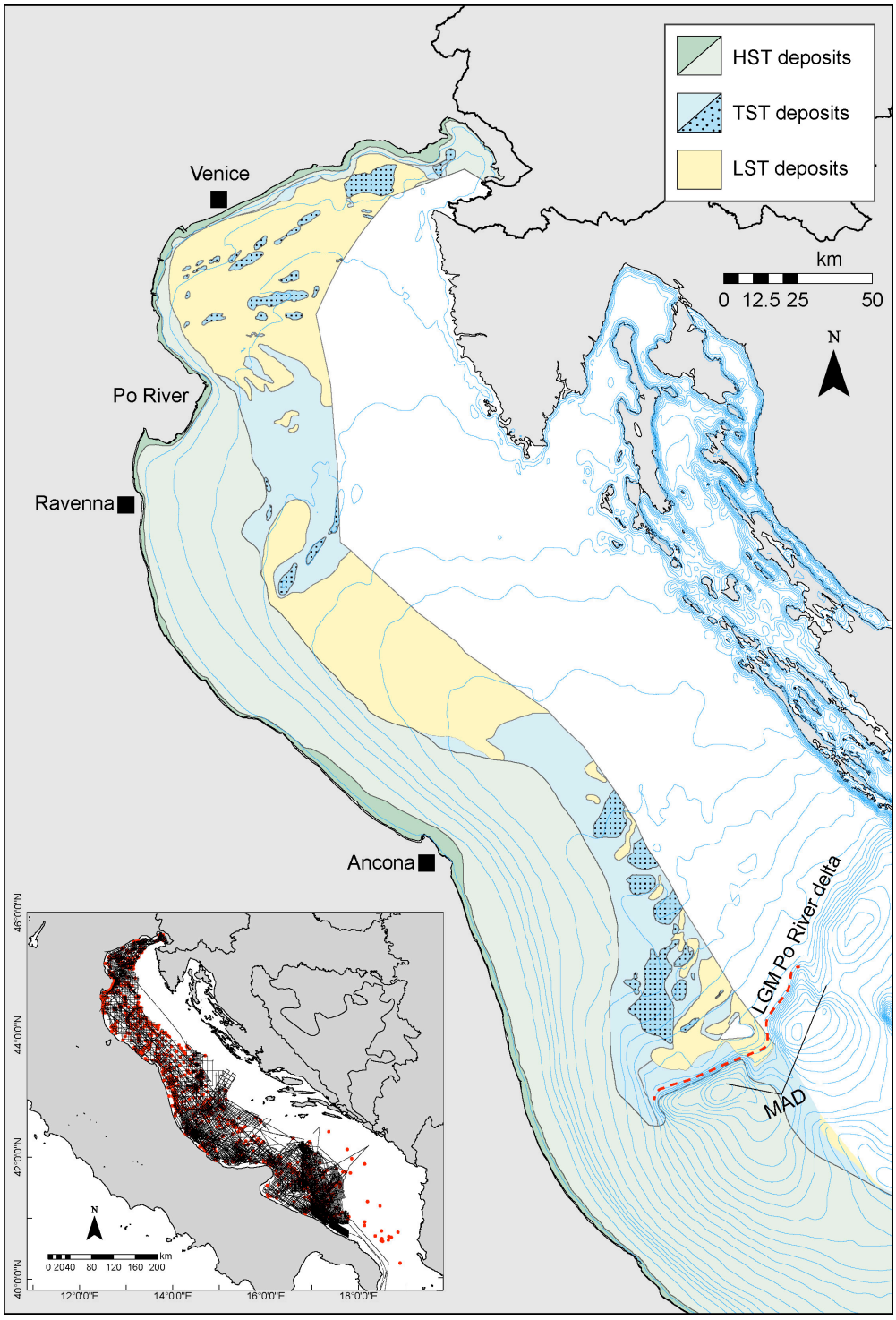

Figure 2.3 - Sea floor stratigraphy of the central and northern Adriatic Sea (modified from Trincardi and Argnani, 2001; Trincardi et al., in press, a, b). Inset map shows the coverage ISMAR-CNR seismic profiles (black lines) and cores (red dots) used to map the stratigraphy. The red dashed line shows the location of the Po River delta during LGM.

The Adriatic Sea is a mud dominated epicontinental Sea, elongated in the southeast direction more than 800 km. On the basis of shelf morphology, the western side of the Adriatic

margin can be divided into three sectors (the northern, the central and the southern Adriatic basin) separated by the Mid Adriatic Deep (MAD) and by the Gargano promontory. The northern Adriatic Sea, extending more then 350 km from the Gulf of Venice to the south, is characterized by a very low gradient shelf (0.02° dip), which is the result of several southward progradations driven by Milankovian cyclicity. The central Adriatic includes the MAD, which is formed by two slope basin more then 250 meters depth and extending in the NE-SW direction, and is limited eastward by a 50 km wide shelf (ca 0.2° dip), and southward by the Gallignani-Pelagosa ridge (Ridente and Trincardi, 2006). The southern Adriatic, south of the Pelagosa sill, is formed by a deeper basin, more then 1200 meters of water depth, characterized by a complex shelf and slope morphology (Ridente et al., 2007).

The modern sea floor stratigraphy (Fig. 2.3), investigated through a dense grid of high resolution seismic profiles and core samples, can be divided into two different domains: the shallower portion, confined toward the land, is characterized by a continuous clinoform of late Holocene deposits, formed by the sediments delivered to the basin by the Po River and others Apennine rivers after the maximum marine ingression, and confined toward the land by marine circulation (Cattaneo et al., 2003; Cattaneo et al., 2007). Instead, the central portion of the northern Adriatic shelf is characterized by lowstand alluvial plain deposits covered by transgressive sandy deposits of relict barrier-island systems, formed during to the last sea level rise (Correggiari et al., 1996a, b).

High resolution seismic profiles integrated with multichannel seismic data reveal, on the Adriatic central Adriatic shelf and upper slope, four stacked depositional sequences (termed Sequence 1–4, top down) accumulated during the last ca. 450 kyr, each separated by shelf-wide unconformities (ES1–ES4) and their correlative conformities (see Figure 2.4; Trincardi and Correggiari, 2000; Ridente and Trincardi, 2002). Each sequence is composed of progradational units among which forced regression deposits recorded phases of sea level fall (Ridente and Trincardi, 2005). The MAD recorded a quasi-undisturbed muddy marine deposition since the Middle Pleistocene, as highlighted by the borehole PRAD1.2, drilled during the European Project PROMESS1 (Profile Across Mediterranean Sedimentary Systems, Part 1; Piva et al., 2008a, b; Ridente et al., 2008; 2009).

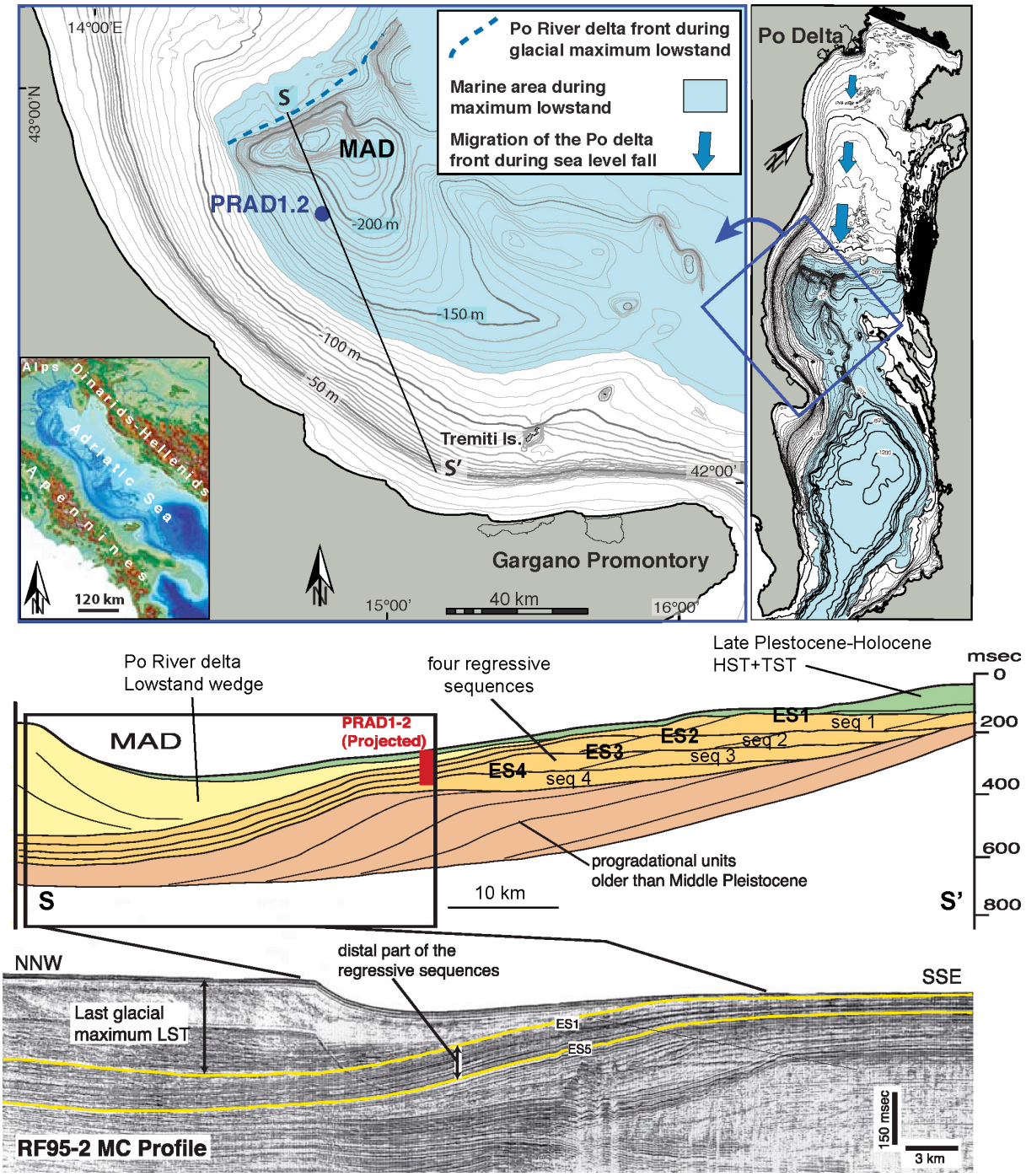

Figure 2.4 - Top: Present day bathymetry of the central Adriatic margin and its extent during the LGM (modified from Ridente et al., 2009). Bottom: Stratigraphy of the central Adriatic margin reconstructed along a NNW-SSE section (line S-S' in the map).

The shallow stratigraphic architecture of the west Adriatic margin is composed of different sedimentological units related to late Quaternary sea level changes (Cattaneo and Trincardi, 1999; Trincardi and Correggiari, 2000):

- The Prograding Pleistocene wedges are truncated at their top by a regional erosional surface (ES1) that recorded a regressive phase encompassing most of the last glacial cycle, from marine oxygen isotope stage 5e to the base of the last glacial maximum (Trincardi and

Correggiari, 2000; Ridente and Trincardi, 2002).

- The Transgressive Systems Tract (TST), resting above surface ES1, recorded distinctive phases of the last sea level rise and short-term variations of sediment supply and dispersal (Cattaneo and Trincardi, 1999), likely accompanied by changes in the oceanographic regime of the basin (Asioli et al., 2001).

- The Highstand Systems Tract (HST) consists of a shore-parallel prograding mud prism, deposited during the last 5.5 cal kyr BP, which formed above a regional downlap surface (Maximum Flooding Surface, mfs; Correggiari et al., 2001).

The south Adriatic margin shows a complex morphology, which is the result of the interaction between bottom currents, oceanic circulation, regional tectonics, sea level and sediment supply fluctuations (Ridente et al., 2007).

Oceanographic setting

The Adriatic physiographic and oceanographic settings were subjected to dramatic rearrangements during the late Quaternary eustatic oscillations, and in particular during the last sea level rise, when the northern Adriatic shelf was submerged. During the LGM, stabilized stratification of the water column allowed only weak and shallow temperature-driven winter convection in the deepest parts of the basin and, therefore, the Adriatic was characterized by a low-energy bottom current circulation (Myers et al., 1998). Moreover, short-lived but important changes of the Adriatic circulation occurred also during intervals of decreased surface water salinity that impacted the whole Mediterranean leading to the deposition of sapropel layers (Ariztegui et al., 2000; Piva et al., 2008a).

The modern Adriatic Sea is characterized by a microtidal regime and is dominated by a cyclonic circulation driven by thermohaline currents (see Figure 2.5; Malanotte-Rizzoli and Bergamasco, 1983; Bondesan et al., 1995).

Three water masses are present in the Adriatic sea (Paschini et al., 1993): (1) a surficial temperature-mixed layer (0-30 m) with the upper 10 m of less saline and cooler waters of coastal origin, mainly formed by the Po River runoff; (2) a Levantine Intermediate Water (LIW) layer (30-130 m); (3) a bottom-water region (>130 m) with very dense waters that form occasionally in the northern Adriatic and sink toward the south: the Northern Adriatic Dense Water circulation (NAdDW). The cyclonic circulation of surficial water, enhanced by the Po River plume, forces the fresh waters to flow along the western side of the basin. The along shore sediment transport, enhanced during winter by the northeasterly Bora wind, is consistent with the overall shore parallel thickness distribution of the late-Holocene clinoform (Cattaneo et al., 2007). The denser water masse of the LIW forms in the Rhodes permanent cyclonic gyre in the Levantine Basin through evaporation during the summer and cooling during winter (Lascaratos et al., 1999). This salty water mass enters the South Adriatic on the eastern side and flows out southward along the slope in intermediate depths (between 200 and 600 meters of water depth; Manca et al., 2002). The deeper water mass of the NAdDW forms, instead, in the North Adriatic shelf: during winter season the outbreaks of the cold and dry Bora wind makes the northern Adriatic surface water cooler and denser (Artegiani et al., 1989).

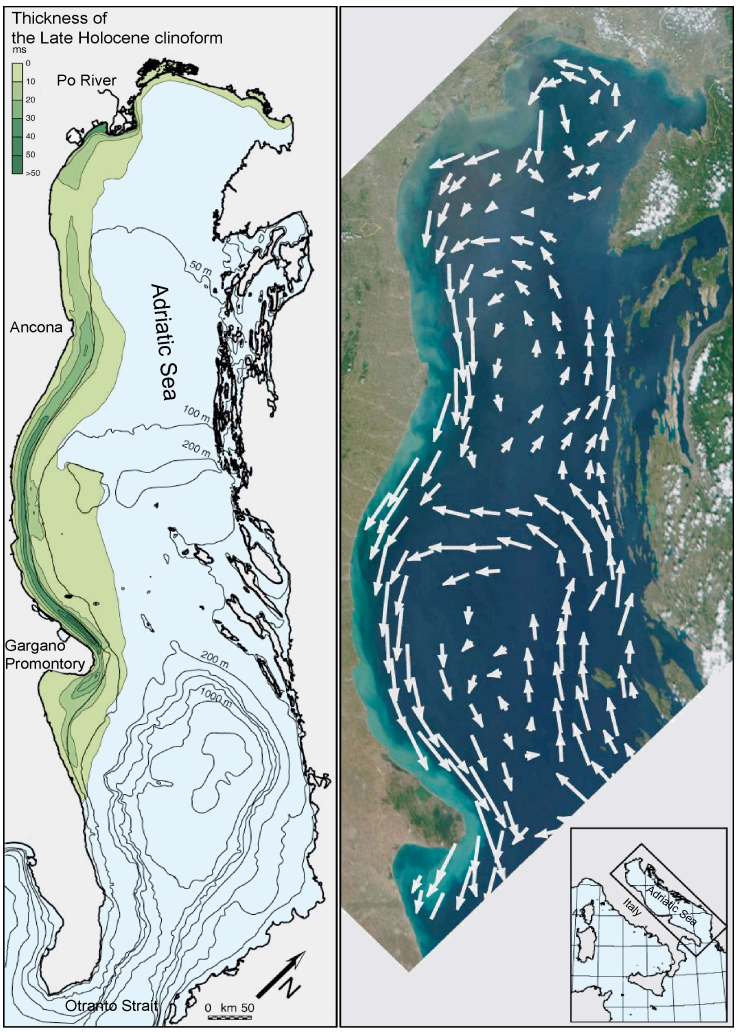

Figure 2.5 - Left: Distribution of the Late Holocene highstand deposits (thickness in msec; modified from Cattaneo et al., 2004). Right: Geostrophic circulation pattern in the Adriatic Sea (modified from Poulin, 2001).

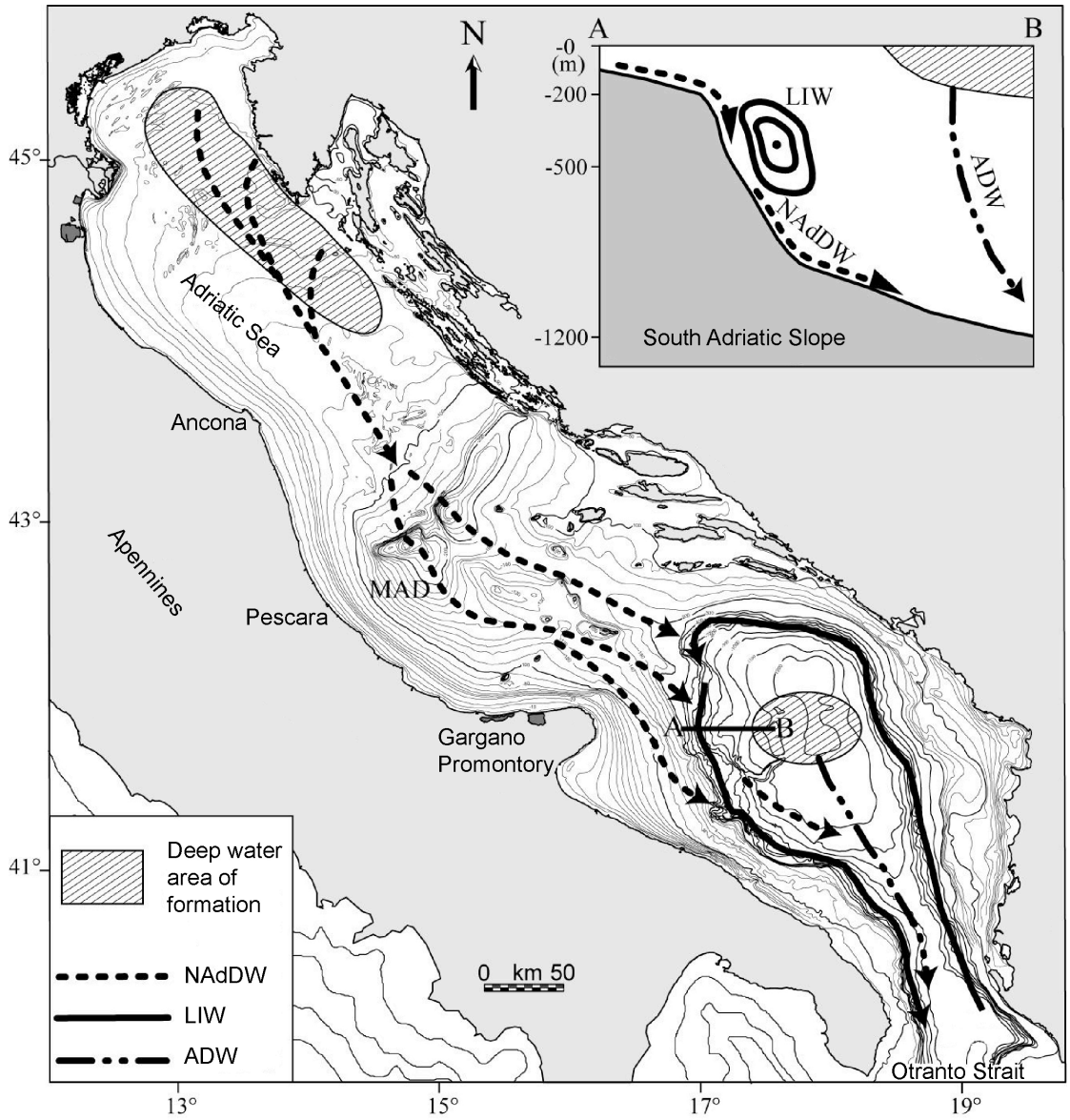

Figure 2.6 - Marine circulation in the Adriatic Sea (modified from Trincardi et al., 2007). The Northern Adriatic Dense Water (NAdDW) forms during winter in the northern Adriatic shelf and flows southward reaching the south Adriatic slope during Spring. The Levantine Intermediate Water (LIW) flows in a counterclockwise between -200 and -600 meters of water depth in the south Adriatic basin. The Adriatic Dense Water (ADW) flows southward together with the NAdDW, contributing to the outflow of dense water through the Otranto Strait.

This cold and dense water mass (Fig. 2.6) moves southward along the Italian cost passing around the Gargano promontory (Cushman-Roisin et al., 2001), cascading obliquely across the SW-Adriatic slope, where strongly interacts with its topography (Vilibic and Orlic, 2002; Trincardi et al., 2007).

CHAPTER III

Maselli, V., F. Trincardi, A. Cattaneo, D. Ridente and A. Asioli (2010), Subsidence pattern in the central Adriatic and its influence on the sediment architecture during the last 400 kyr, *Journal of Geophysical Research*, **115**, doi: 10.1029/2010JB007687.

Subsidence pattern in the central Adriatic and its influence on sediment architecture during the last 400 kyr

V. Maselli,[1,2] F. Trincardi,[2] A. Cattaneo,[3] D. Ridente,[4] and A. Asioli[5]

Received 6 May 2010; revised 10 August 2010; accepted 25 August 2010; published 28 December 2010.

[1] The western Adriatic margin (eastern Mediterranean), part of the Apennine foreland, is characterized by a differentiated tectonic setting, showing high subsidence rates (up to 1 mm/yr) in the northern area and tectonic uplift (on the order of 0.3–0.5 mm/yr) in the southern part corresponding with the so-called Apulia swell. The central Adriatic marks the transition between these two areas. To calculate subsidence values, the stratigraphy of the central Adriatic has been investigated through the borehole PRAD1.2 (European project Profiles across Mediterranean Sedimentary Systems), the first continuous Quaternary marine record in the Adriatic basin (71.2 m long) reaching the top of Marine Isotope Stage 11 (MIS 11). Subsidence calculations were performed first by applying the backstripping procedure to PRAD1.2, in order to investigate the contribution of sediment load and tectonic driving forces to subsidence. Despite the large error bars, mostly caused by the uncertainties in paleowater depth reconstructions, the values obtained demonstrate that tectonics is the main driver for subsidence in this area. In order to better estimate the subsidence rates, an independent approach is introduced, based on the correlation of the present-day burial depth of past shorelines deposited during the main glacial lowstands, from MIS 2 to MIS 10. The average subsidence rate of about 0.3 mm/yr appears greater than the average sediment supply rate (0.15 mm/yr), and this fact explains the overall backstepping of the 100 kyr regressive depositional sequences on the margin. The results obtained help to improve the understanding of the regional tectonics and can be used for quantitative reconstruction of Quaternary sea level changes in the Adriatic region. In general, the paper shows that even a short (71 m) borehole across a relatively short time span (340 kyr) can be useful for subsidence calculations, provided that a high-resolution definition of its stratigraphy is available and a correlation can be drawn with the geomorphologic proxies such as paleoshoreline deposits.

Citation: Maselli, V., F. Trincardi, A. Cattaneo, D. Ridente, and A. Asioli (2010), Subsidence pattern in the central Adriatic and its influence on sediment architecture during the last 400 kyr, *J. Geophys. Res.*, *115*, B12106, doi:10.1029/2010JB007687.

1. Introduction

[2] Subsidence is one of the key factors controlling the filling pattern of sedimentary basins and, ultimately, the geometry of sedimentary successions. In order to understand and reconstruct the burial history of a sedimentary succession, *Van Hinte* [1978] introduced the "geohistory analysis," a simple analytical method that allows quantification of the total subsidence of a basin, and calculation of the contributions of sediment and water loads and of tectonic driving forces. In the last few decades the geohistory analysis has been performed with good results in a variety of geodynamic settings, but always referring to deep boreholes (on the order of a few kilometers) or long sedimentary sections, encompassing several millions of years [*Steckler and Watts*, 1978; *Sclater and Christie*, 1980; *Carminati et al.*, 2007]. Here we apply the geohistory analysis to the borehole PRAD1.2, a 71.2 m long borehole drilled in the central Adriatic margin, encompassing the last 400 kyr. The interest in applying this method on shorter timescales is in considering key factors controlling the evolution of a continental margin such as eustatic and sediment supply fluctuations, taking advantage of a precise (millennial scale) stratigraphic resolution available.

[3] In the last decades an increasing number of sites was drilled on Quaternary continental margins through rapidly deposited successions, with accumulation rates on the order of 1 mm/yr or higher [*Sydow and Roberts*, 1994; *Rabineau et al.*, 2006]. The European project Profiles across Mediterranean Sedimentary Systems (PROMESS1) was designed to investigate the impact of Quaternary sea level changes on the deposition of continental shelf and slope sequences

[1]Dipartimento di Scienze della Terra e Geologico-Ambientali, Univerisità di Bologna, Bologna, Italy.
[2]ISMAR, Istituto di Scienze Marine (CNR), Bologna, Italy.
[3]GM-LES, Ifremer, Plouzané, France.
[4]IGAG, CNR, Rome, Italy.
[5]IGG, CNR, Padova, Italy.

0148-0227/10/2010JB007687

on two Mediterranean margins: the Adriatic and the Gulf of Lion. Continuous-recovery drilling at site of high sedimentation rates and absence of marked erosional surface are fundamental to achieve the most complete paleoenvironmental and paleoclimatic reconstructions. The aim of this paper is to test the possibility to quantify the subsidence rates in the central Adriatic Sea from a high-resolution borehole over a short geological time interval (~400 kyr). We perform this test on a section of the Adriatic margin where subsidence rates are debated [*Colantoni et al.*, 1989; *Doglioni et al.*, 1994; *Ridente and Trincardi*, 2002; *Lambeck et al.*, 2004; *Ferranti et al.*, 2006; *Antonioli et al.*, 2009], in order to better explain the geometric relationships of depositional sequences during the Quaternary and their relation with eustatic and sediment supply fluctuations. The subsidence rates are first obtained through the geohistory analysis and using the backstripping method; the results obtained are then compared with another independent approach based on the identification of paleoshorelines formed during the main eustatic lowstands [*Skene et al.*, 1998].

2. Geologic and Stratigraphic Framework

2.1. Geological Setting

[4] The Adriatic Sea is a semienclosed basin elongated in the NW–SE direction with a length of 800 km and a width of 200 km, showing a remarkable variability in shelf and slope morphology. The shelf break is about 300 km away from the Gulf of Venice, and the shelf presents a gentle dip of about 0.02° toward the SE. The Mid Adriatic Deep (MAD), south of the shelf break, represents a small remnant basin with a maximum depth of 260 m that has been progressively filled from the NW by the Po River delta deposits during each Quaternary phase of sea level fall and lowstand; the last progradational wedge originated during the Last Glacial Maximum [*Cattaneo and Trincardi*, 1999; *Asioli et al.*, 2001]. In the central Adriatic the continental shelf extends seaward about 50 km parallel to the front of the Apennine chain, with a seafloor dip of 0.3°–0.7°. The south Adriatic is a deeper basin showing a complex morphology and a maximum depth of about 1200 m (Figure 1). Overall, the Adriatic Sea is a mud-dominated system where the Po River is the most important source of sediment.

[5] During the last 25 Ma the westward subduction of the Adria plate led to the formation of the Apennine chain, while the Adriatic basin became a foreland domain. During the Pliocene and Pleistocene, the central Adriatic basin was characterized by a high subsidence rate because of the eastward rollback of the hinge of the Apennine subduction [*Royden et al.*, 1987]. The southern Adriatic basin was, instead, characterized by a different tectonic style, showing uplift since the middle Pleistocene [*Doglioni et al.*, 1994; *Scrocca*, 2006; *Ridente and Trincardi*, 2006]. This different tectonic behavior has been ascribed to differences in the thickness of the Adriatic lithosphere subducted toward the west [*Pieri and Groppi*, 1981; *Royden et al.*, 1987; *Doglioni et al.*, 1994].

[6] The modern foredeep basin in the central Adriatic is rimmed by two structures: the Gallignani-Pelagosa ridge (trending NW–SE), roughly parallel to the front of the Apennine chain, and the NE–SW Tremiti structural high, located north of the Gargano Promontory (Figure 1). The Tremiti lineament has been interpreted as the right-lateral transfer zone linking the pronounced eastward rollback of the central Adriatic slab and the buckled Apulian region [*Doglioni et al.*, 1994]. The stratigraphic and tectonic evolution of the central Adriatic since the Oligocene shows that the highest subsidence values are confined landward, toward the Apennine chain, as highlighted by the flexure of the Messinian datum corresponding to the evaporite unit and the related unconformity [e.g., *Scrocca*, 2006]. Since the middle Pleistocene, the units infilling the foredeep basin have changed from a dominant turbidite fill into a progradational margin wedge that records the Milankovich glacial-eustatic cyclicity [*Ridente et al.*, 2009].

2.2. PRAD1.2 Stratigraphy

[7] The PRAD1.2 borehole was drilled on the upper continental slope south of the MAD (42°40′34.7″N, 14°46′13.5″E) in 185.5 m water depth (Figure 2). The borehole provided a continuous core of 71.2 m with a 99.96% recovery, covering a time interval of about 400 kyr [*Piva et al.*, 2008a, 2008b]. The stratigraphy of PRAD1.2 integrates results from ecobiostratigraphic analyses of planktic and benthic foraminifera, $\delta^{18}O$ records, magnetic parameters and tephrochronology, lithology and XRF data (see Figure 4).

[8] The analysis of high-resolution seismic profiles shows that the borehole penetrates a uniform succession consisting of subparallel reflectors, with a slight plunge toward the NE (Figures 2 and 3). The sampled stratigraphic units represent the distal expression of the depositional sequences that are discernible on the shelf [*Ridente et al.*, 2008]. The stratigraphic units, starting from the youngest, are (1) highstand (HST) and transgressive (TST) deposits of the last glacial cycle, (2) lowstand progradation deposit (LST) from the Po River delta, and (3) four late Pleistocene regressive depositional sequences each recording a sea level cycle at the 100 kyr scale [*Piva et al.*, 2008a; *Ridente et al.*, 2008].

[9] The depositional pattern of each sequence upslope of the borehole may be divided into two main seismic units: (1) uniform and subparallel seismic reflectors, connected to the progradational units deposited during interglacial intervals of Marine Isotope Stage (MIS) 5, 7, and 9 [*Martinson et al.*, 1987], forming the bulk of sequences 1–3, and (2) onlapping units formed by landward converging seismic reflectors that pinch-out toward the shelf edge, corresponding to the lowstand cold intervals (Figure 3). These latter units are separated by the distal correlative of shelf erosional surfaces ES1 to ES3 that split seaward into a sequence boundary (SB) and a transgressive surface (Ts). Instead, surface ES4, as well the deepest unconformity ES5 (not reached by the borehole), maintains an erosional character on the upper slope and at the borehole site [*Ridente et al.*, 2008].

[10] The stratigraphic units recovered are mainly composed of marine mud with thin silty layers which, in some cases, correspond to pyroclastic deposits. Sand layers occur only around 58 m below the seafloor (mbsf) and correspond to the shallowest depositional environment encountered by the borehole (Figure 4).

3. Methods

[11] The reconstruction of the tectonic history of the central Adriatic continental margin follows the backstripping method, first attempted by *Sleep* [1971], and then extensively

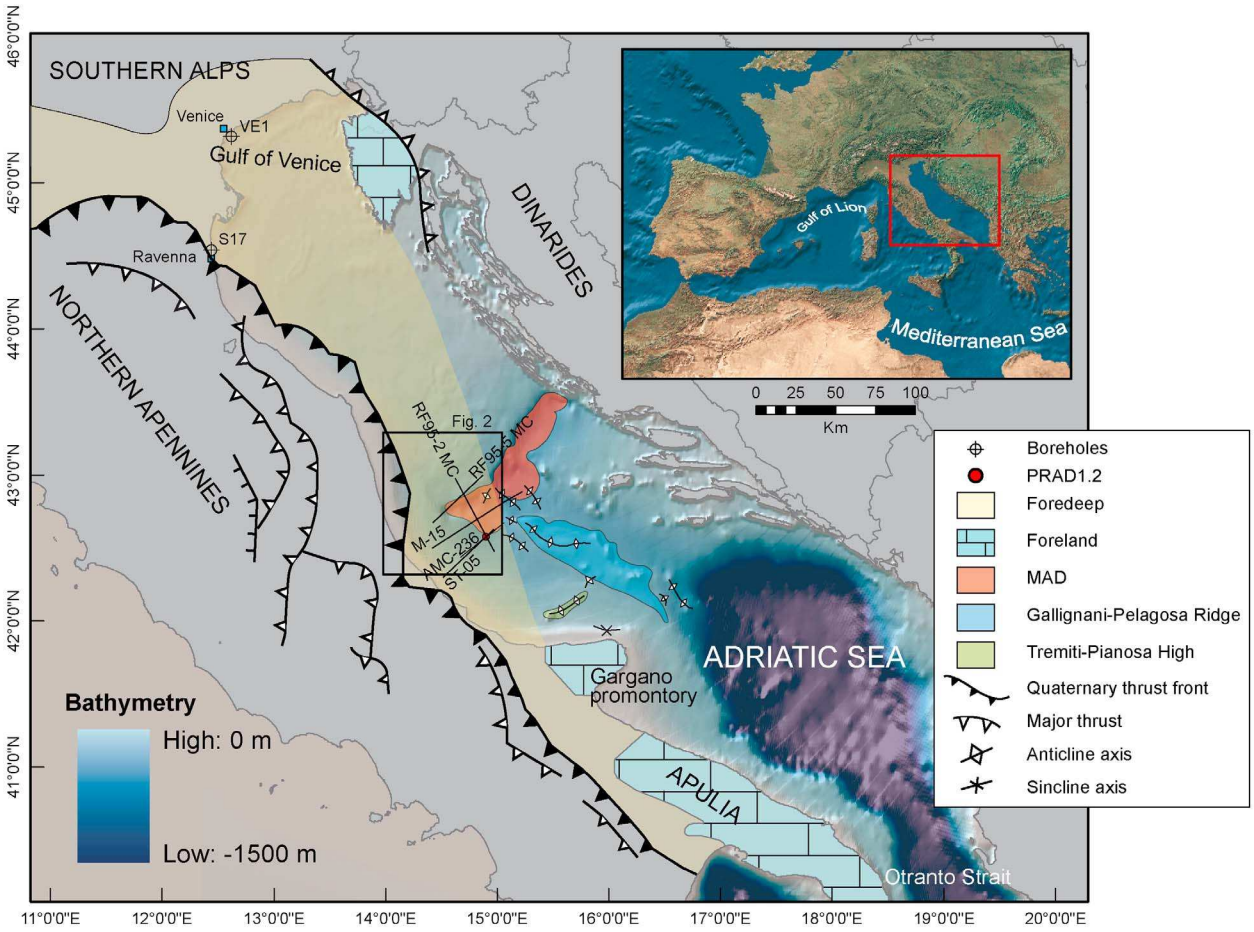

Figure 1. Bathymetry of the Adriatic Sea reporting the main structural elements of the central Apennine chain and surrounding foredeep-foreland systems (modified from *Patacca and Scandone* [2004]). Track lines refer to the seismic profiles shown in Figures 2, 4, and 12; circles denote the location of the PRAD1.2 borehole and two additional boreholes along the north Adriatic shoreline: VE1 and S17. Black box refers to the location in Figure 2. MAD, Mid Adriatic Deep.

discussed by *Watts and Ryan* [1976] and by *Steckler and Watts* [1978]. The backstripping method is a numerical stratigraphic technique with the aim of investigating the geologic history of a sedimentary basin, taking into account compaction processes of the sediment column, variations in paleowater depth and sea level changes as well as isostatic rebound effects. Backstripping is successfully applied over long timescales (millions of years); when such long intervals are taken into account, only few assumptions are necessary and the impact of errors on the reconstruction of paleowater depth is reduced; this is particularly the case when referring to long boreholes encompassing shallow water environments [*Angevine et al.*, 1990]. In contrast, applying the backstripping method to short boreholes proves more problematic, in particular when referring to recent time intervals (i.e., the last few hundreds of thousands of years), dominated by high-magnitude and high-frequency sea level oscillations which imply a more problematic reconstruction of the paleowater depth and a poorer definition of the lithospheric response to rapid load changes.

[12] Following *Angevine et al.* [1990], the borehole PRAD1.2 was divided into 16 units, and the position of each stratigraphic horizon was restored to its depth at the time of deposition on the basis of compaction corrections (see Appendix A). The units are defined on the basis of the major isotopic shifts and the available geochronological control points (see *Piva et al.* [2008a] for a detailed isotopic stratigraphy and chronology of PRAD1.2). These units, named "U" and "T," are numbered referring, broadly, to the corresponding Marine Isotopic Stages; in particular, "T" units cover periods of high rate of sea level rise (see Figure 4 and Table 1).

[13] To construct the total subsidence curve it is necessary to take into account the paleowater depth of the stratigraphic horizons and the global sea level changes. As stated by *Allen and Allen* [1990], referring to sea level changes from first- to third-order cycles, the latter correction can be avoided because of the large error bars of the eustatic curves and their uncertain origin (tectonic versus ice volume). In the case of PRAD1.2 this correction is possible and necessary, because sea level during the interval examined is the main driver for any change in water depth. Furthermore, the borehole was retrieved beyond the shelf edge and therefore the determination of paleowater depth is more uncertain for

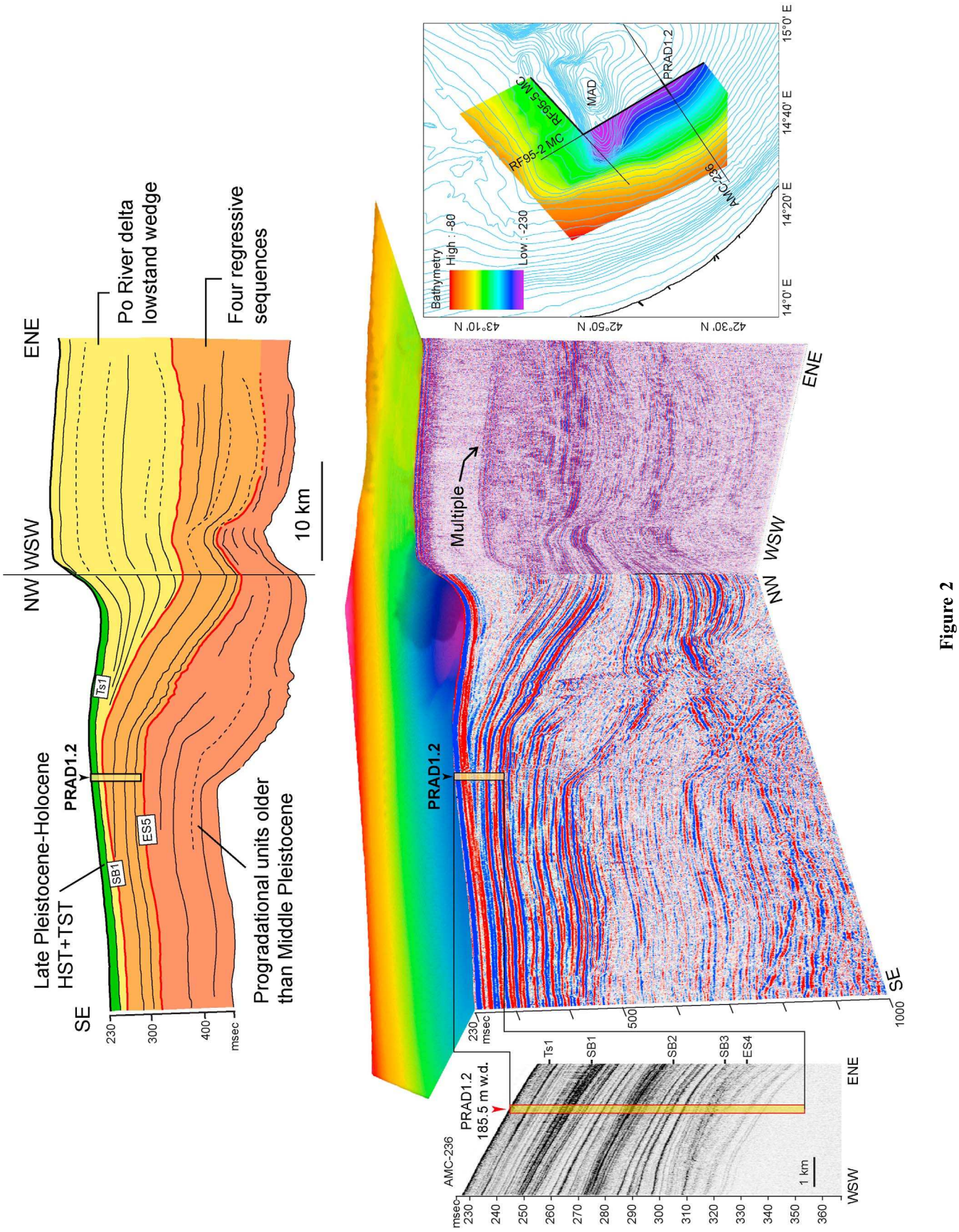
NW WSW
ENE
Po River delta
lowstand wedge
Four regressive
sequences
10 km
Late Pleistocene-Holocene
HST+TST
PRAD1.2
Ts1
SB1
ES5
Progradational units older
than Middle Pleistocene
SE
230
300
400
msec
Bathymetry
High : -80
Low : -230
RF95-2 MC
RF95-5 MC
MAD
PRAD1.2
AMC-236
42°30' N
42°50' N
43°10' N
14°0' E
14°20' E
14°40' E
15°0' E
Multiple
NW
WSW
ENE
SE
PRAD1.2
230
msec
500
1000
AMC-236
PRAD1.2
185.5 m w.d.
Ts1
SB1
SB2
SB3
ES4
1 km
WSW
ENE
msec
230
240
250
260
270
280
290
300
310
320
330
340
350
360

Figure 2

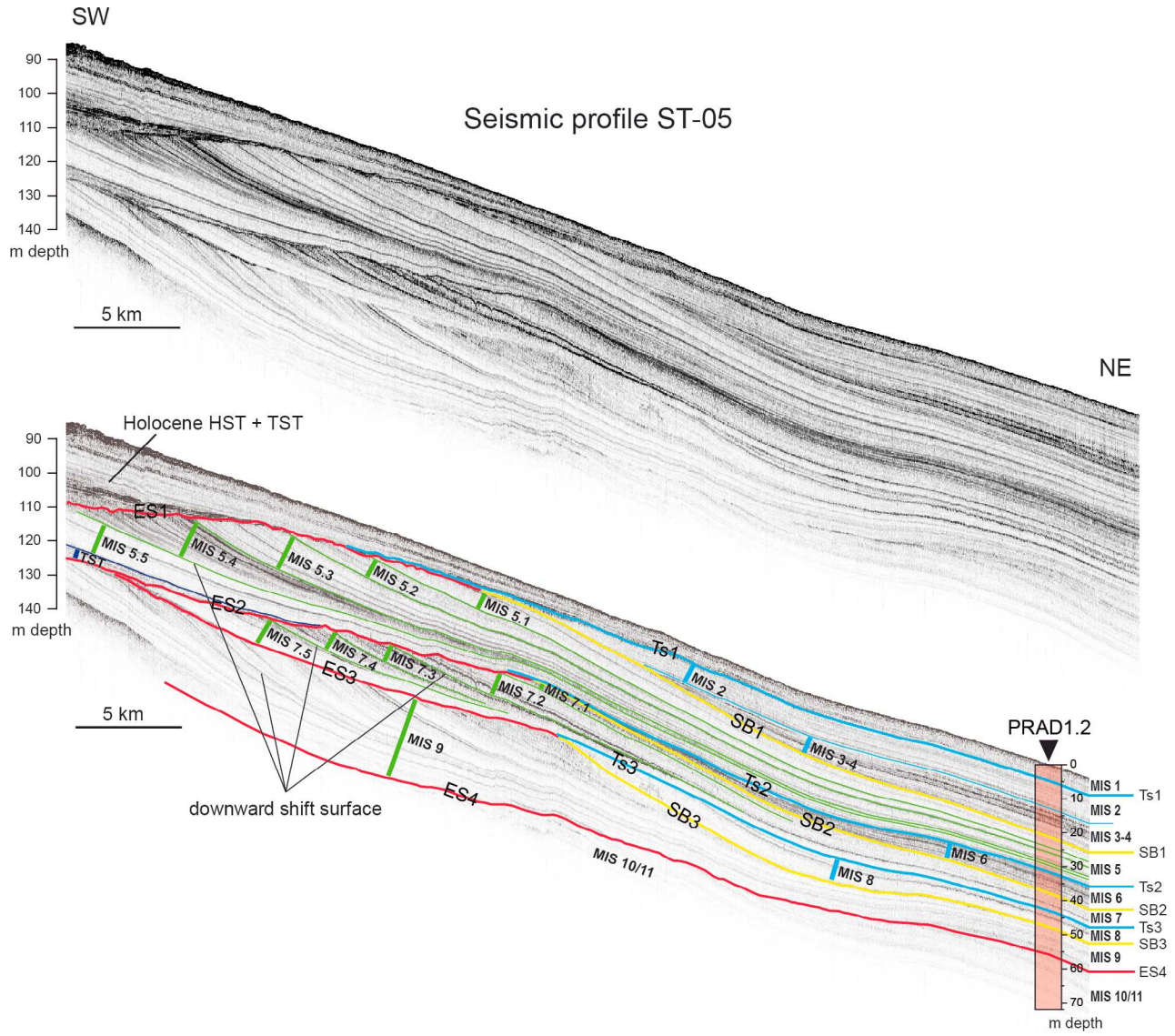

Figure 3. (top) High-resolution chirp sonar profile crossing the site of the borehole PRAD1.2. (bottom) Shelf-slope correlation of the depositional sequences across the site of the borehole PRAD1.2. Highstand, lowstand, and falling stage systems' tracts can be distinguished on the basis of their reflector geometry and biostratigraphic data [see *Piva et al.*, 2008a]. Highstand and falling sea level sequences can be correlated across the margin (green lines), while lowstand deposits remain confined to an upper slope position (blue lines). The unconformities (ES) at the base of each depositional sequence show an erosional character on the shelf, while seaward of the shelf edge they split into a sequence boundary (SB) below and a transgressive surface (Ts) above.

some stratigraphic intervals where benthic faunas are less diagnostic.

[14] All the parameters introduced above are affected by errors. The first source of error can be related to the isostatic balance model used for the backstripping procedure. Following the results of *Steckler and Watts* [1978], showing no much difference between local compensation and a more complex flexural model, we decided to use an Airy isostatic model. This approach is preferred also considering the small load of the sedimentary succession analyzed and the poor definition of the equivalent elastic thickness in the central Adriatic region.

Figure 2. Stratigraphy of the central Adriatic basin along a NNW–SSE section based on the interpretation of high-resolution multichannel seismic profiles RF95-2MC and RF95-5MC. On the left side is the high-resolution seismic stratigraphy at PRAD1.2 borehole (seismic line AMC-236); the sequence boundaries are labeled SB1–SB3 and ES4 from top to bottom. HST, highstand; TST, transgressive; m w.d., meters water depth.

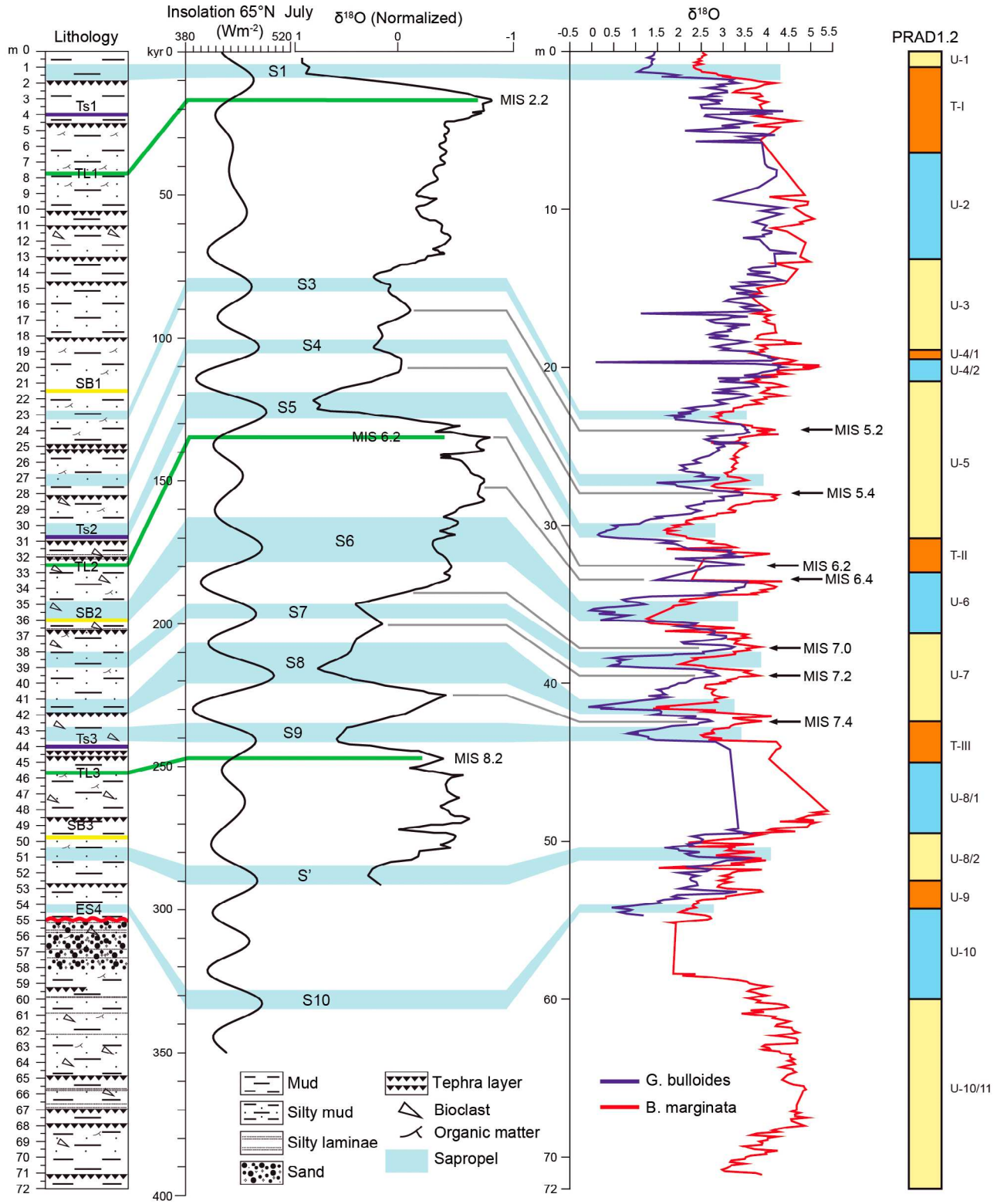
Lithology
Insolation 65°N July (Wm-2)
δ18O (Normalized)
δ18O
PRAD1.2
kyr
m
S1
S3
S4
S5
S6
S7
S8
S9
S10
S'
MIS 2.2
MIS 6.2
MIS 8.2
MIS 5.2
MIS 5.4
MIS 6.2
MIS 6.4
MIS 7.0
MIS 7.2
MIS 7.4
Ts1
Ts2
Ts3
TL1
TL2
TL3
SB1
SB2
SB3
ES4
U-1
T-I
U-2
U-3
U-4/1
U-4/2
U-5
T-II
U-6
U-7
T-III
U-8/1
U-8/2
U-9
U-10
U-10/11
Mud
Silty mud
Silty laminae
Sand
Tephra layer
Bioclast
Organic matter
Sapropel
G. bulloides
B. marginata

Figure 4

Table 1. Borehole PRAD1.2 Subdivided Into 16 Units on the Basis of the Control Points Available, to Perform the Decompaction Calculation and the Backstripping Procedure[a]

Unit Name	Base Depth (m)	Age (kyr)	Thickness (m)	Porosity (%)	Sediment Grain Density (kg/m^3)
U-1	1	7.2 (±1)[1]	1	71	1520
T-I	6.4	17.5 (±0.8)[1]	5.4	57.3	1750
U-2	13.2	27.3 (±0.8)[1]	6.8	51.6	1820
U-3	18.9	57.5 (±1.5)[2]	5.7	53.5	1820
U-4/1	19.5	61 (±1.8)[2]	0.6	51.4	1820
U-4/2	20.8	68 (±2)[2]	1.3	53.6	1820
U-5	30.7	125 (±3)[3]	9.9	53.7	1820
T-II	33	143 (±5)[4]	2.3	48.6	1850
U-6	36.8	184 (±3)[3]	3.8	52.3	1910
U-7	42.4	225 (±5)[4]	5.6	48.1	1900
T-III	45.1	248 (±4)[5]	2.7	44.6	1890
U-8/1	49.5	263 (±3)[3]	4.4	48	1900
U-8/2	52.5	315 (±3)[3]	3	53.2	1950
U-9	54.2	331 (±3)[3]	1.7	43.9	1950
U-10	60	340 (±5)[6]	5.8	42	1900
U-10/11	71.2	365 (±5)[6]	11.2	47.8	1850

[a]For each unit, Table 1 gives the depth of the bottom and the age, the thickness, the average porosity, and the sediment grain density values. Porosity was obtained indirectly by grain density values from multisensor core logger. Error bars are as follows: 1, from *Piva et al.* [2008a]; 2, from *Meese et al.* [1997]; 3, from *Lourens* [2004]; 4, from *Martinson et al.* [1987]; 5, from *Lisiecki and Raymo* [2005]; 6, from *Bassinot et al.* [1994]. T, isotopic termination. See Figure 4.

[15] The errors in PRAD1.2 age model, based on a combination of control points derived from different techniques, depend on the dating method [*Piva et al.*, 2008a]: midpoint of isotopic terminations (II and III) (error ± 4 kyr [*Lisiecki and Raymo*, 2005]) and isotopic wiggle matching with other records (error ± 5 kyr [*Martinson et al.*, 1987; *Bassinot et al.*, 1994]), biostratigraphic events (variable timescale and errors [see *Piva et al.*, 2008a]), recognition of a well-dated polarity inversion of the magnetic field [*Laj et al.*, 2006], correlation to sapropel-based stratigraphy [*Lourens*, 2004], and 6 ^{14}C AMS calibrated ages [*Piva et al.*, 2008a].

[16] Errors introduced in the decompaction process are more difficult to assess because their calculation involves iterative solutions of the nonlinear porosity-depth equation of *Athy* [1930], whereby the error at any particular depth is affected also by the error of the above section [*Waltham et al.*, 2000]. In the literature the main source of error can be identified in the decompaction parameters (initial porosity, porosity coefficient and density; see Appendix A for details), often based on empirical relations. In the case of PRAD1.2 this source of error can be neglected mainly because the porosity and density values are obtained by a sonic log and the borehole is only 71.2 m long.

[17] In the PRAD1.2 the main source of error can be identified in the paleowater depth reconstructions and in the definition of eustatic curves. Even if the latter can be avoided considering the most recent published sea level curves [*Lea et al.*, 2002], remain the problem regarding the correct evaluation of the water depth of past depositional environments. In this case, paleowater depth is obtained following the relation showed by *Van der Zwaan et al.* [1990], while error bars are given on the base of benthonic foraminifera assemblages (for a detailed description, see Appendix B).

[18] Finally, the values obtained are compared with the results of an independent approach based on the identification of lowstand paleoshorelines (over the last 340 kyr BP) on high-resolution CHIRP-sonar profiles acquired over the past 15 years by CNR-ISMAR. This technique, successfully applied in other continental margins (e.g., Gulf of Lion [*Rabineau et al.*, 2006]), gives the possibility of a detailed evaluation of the subsidence rates, with a better spatial and temporal resolution, and a better definition of uncertainties and error bars associated.

4. Results

4.1. Backstripping of PRAD1.2

[19] On the basis of the high-resolution stratigraphy and paleoenvironmental reconstructions showed by *Piva et al.* [2008a, 2008b] and *Ridente et al.* [2008], the central Adriatic margin is investigated applying the geohistory analysis to the borehole PRAD1.2, in order to quantify the total subsidence and the contribution of the sediment load and tectonic driving forces.

[20] The *first step* of the geohistory analysis was to subdivide the stratigraphic succession into elementary units, each characterized by specific porosity and grain density values; the borehole PRAD1.2 was subdivided into 16 stratigraphic

Figure 4. (left) Lithostratigraphy of PRAD1.2 (modified from *Ridente et al.* [2008]). The PRAD1.2 borehole encompasses the distal part of the last four late Quaternary depositional sequences. The borehole is characterized by an overall fine-grained lithology, punctuated by coarser (silty or sandy) layers, mainly in the lower part of the core to the ES4 surface. Note that the interval between 55 and 58 m is characterized by a thick sandy unit with reworked microfauna and an erosional base. Yellow lines refer to sequence boundaries (SB); blue lines refer to transgressive surfaces (Ts); the red line refers to erosional surface ES4; and green lines refer to time lines (TL) corresponding to the cold isotopic events 2.2, 6.2, and 8.2 (see Tables 4 and 5). (middle) Sapropel and isotopic (δ^{18}O) stratigraphy of PRAD1.2 with the main isotopic events [*Piva et al.*, 2008a]. Insolation curve 65°N refers to *Berger and Loutre* [1991]; normalized δ^{18}O curve refers to *Martinson et al.* [1987]. (right) Subdivision of PRAD1.2 for decompaction and backstripping calculations.

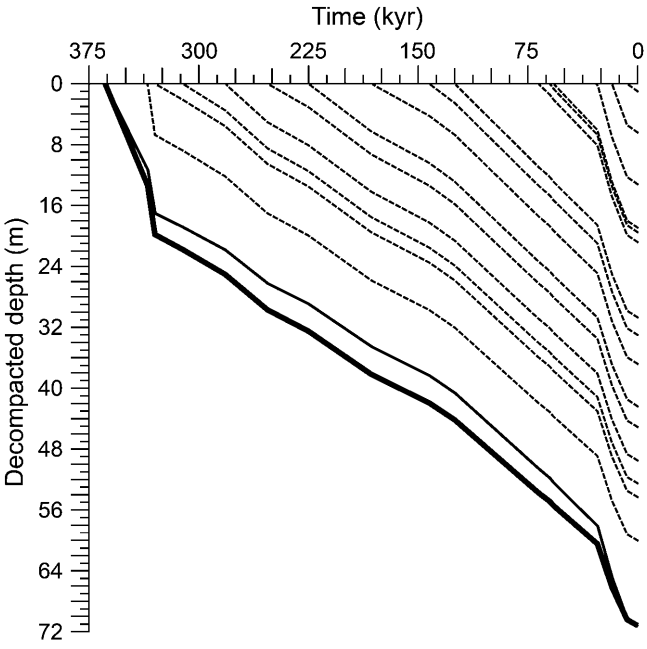

Figure 5. Decompaction plot obtained from Table A1. Each dashed line shows the depth of the borehole at each time step. The thick line is the total decompacted subsidence curve; the thin line is the present-day borehole without decompaction.

units (see Table 1 and Figure 4). In order to calculate the thickness of each individual unit at the time of its deposition, two main assumptions are necessary: (1) any change in volume of a sediment unit in the burial process is due to a change only in porosity and not in the grain size, and (2) sediment is fully compacted at the time of sampling. Following the calculations reported in Appendix A, the decompacted subsidence history of the borehole could be plotted in a diagram of depth versus age where the bottom bold line represents the subsidence at the base of the borehole (Figure 5). At this point it is also possible to calculate the sedimentation rate for each decompacted unit in mm/yr (Table 2). Figure 6 shows that the sedimentation rate is almost constant at 0.15 mm/yr, even if there are two short intervals, centered around MIS 2 and MIS 10, that appear to reach 0.72 and 0.75 mm/yr, respectively.

Table 2. Sedimentation Rates Obtained From Decompacted Thickness

Unit Name	Decompacted Thickness (mm)	Time Interval (kyr)	Sedimentation Rate (mm/yr)
U-1	1000	7.2 (±1)	0.14 (±0.02)
T-I	5427	10.5 (±0.8)	0.52 (±0.04)
U-2	7015	9.8 (±0.8)	0.72 (±0.06)
U-3	6076	30.2 (±1.5)	0.20 (±0.01)
U-4/1	656	3.5 (±1.8)	0.19 (±0.09)
U-4/2	1429	7 (±2)	0.20 (±0.06)
U-5	10895	57 (±3)	0.19 (±0.01)
T-II	2532	18 (±5)	0.14 (±0.04)
U-6	4215	41 (±3)	0.10 (±0.01)
U-7	6277	41 (±5)	0.15 (±0.02)
T-III	3079	23 (±4)	0.13 (±0.07)
U-8/1	5056	15 (±3)	0.34 (±0.02)
U-8/2	3492	52 (±3)	0.07 (±0.004)
U-9	2101	16 (±3)	0.13 (±0.02)
U-10	6720	9 (±5)	0.75 (±0.4)
U-10/11	13368	25 (±5)	0.54 (±0.1)

[21] In order to obtain the total subsidence curve it is necessary to introduce the paleowater depth of each horizon and consider the global sea level oscillation, representing the datum from which the water depths are then calculated. The total subsidence curve (see Figure 5, bottom line) takes into account all the following contributions: sediment load, tectonic load, thermal cooling (if applicable) and water load. The backstripping procedure allows one to quantify the contribution of each parameter by solving the following equations:

$$Z_i = S^* \left(\frac{\rho_a - \overline{\rho}_b}{\rho_a - \rho_w} \right) + W_{d_i} - \Delta_{sl_i}, \quad (1)$$

$$S^* = \sum_{j=1}^{i} T_j^*, \quad (2)$$

where Z_i is the tectonic subsidence ($[Z_i]$ = m), S^* is the total thickness of the decompacted sedimentary column at the time t ($[S^*]$ = m), ρ_a is the density of the underlying material, under the sediment section ($[\rho_a] = 3330$ kg/m^3), $\overline{\rho}_b$ is the bulk

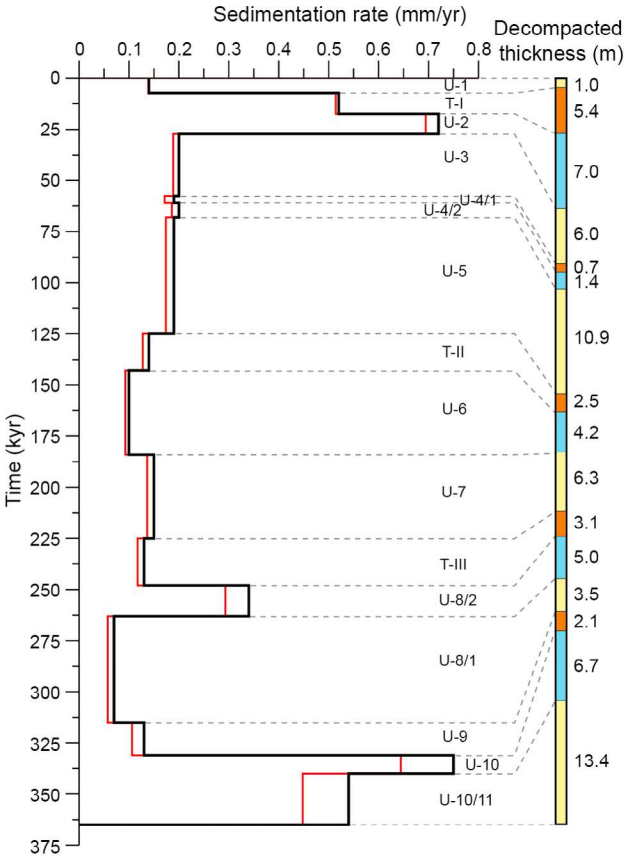

Figure 6. Undecompacted (red line) and decompacted (black line) sedimentation rate for borehole PRAD1.2, obtained from Table 2. The average sedimentation rate is about 0.15 mm/yr, even if two peaks are present at 20 kyr (0.7 mm/yr) and 340 kyr (0.75 mm/yr). On the right is the decompacted thickness of the 16 units of the borehole.

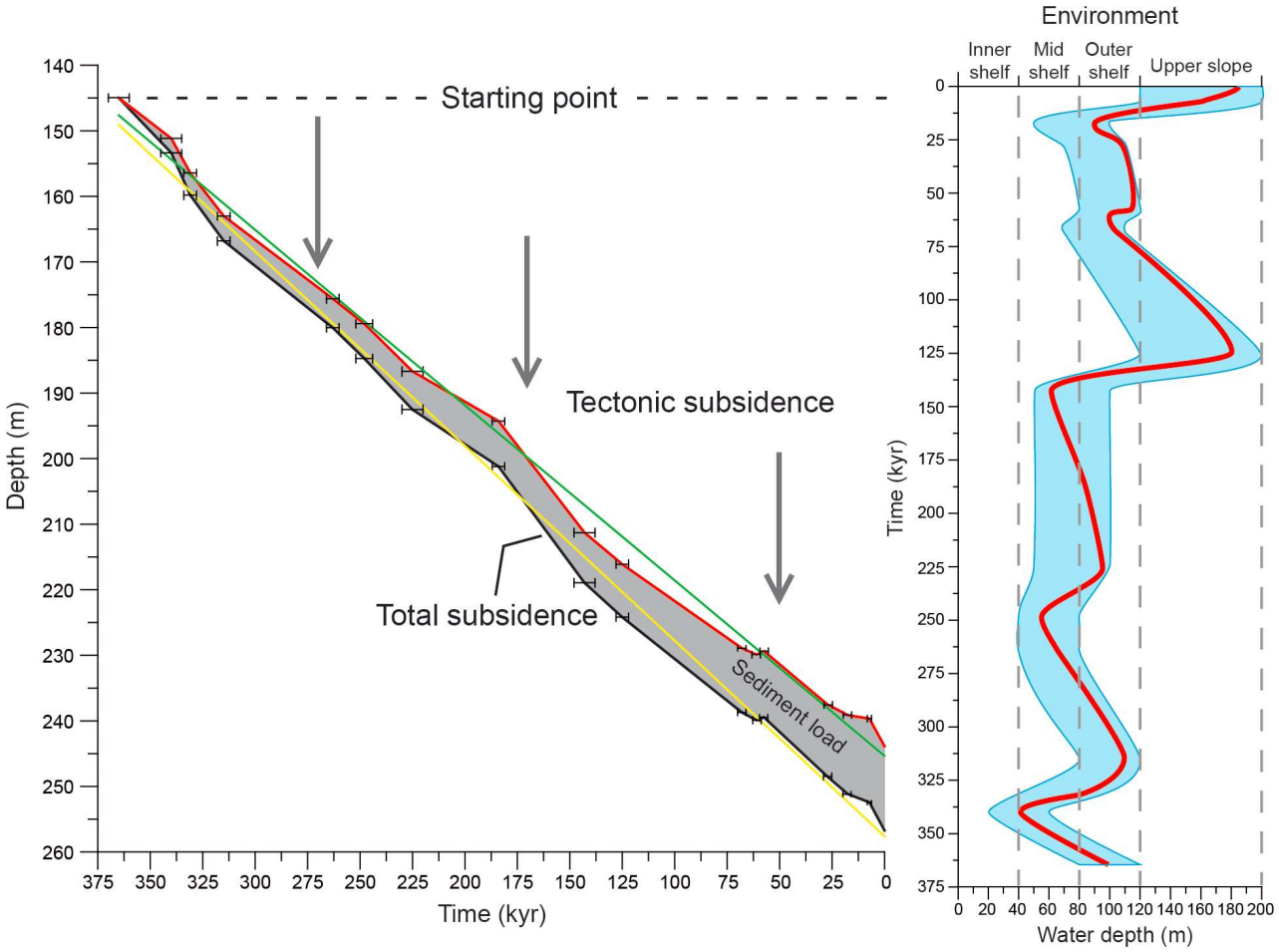

Figure 7. Backstripping diagram of borehole PRAD1.2. The black line represents the total subsidence curve (see also Figure 5), the red line is the tectonic subsidence, and the gray area is the sediment load. The two fitting curves are the total subsidence (yellow line: about 0.3 mm/yr) and the tectonic subsidence (green line: about 0.27 mm/yr). The diagram on the right represents the paleowater depths: the red line is obtained following the theory of *Van der Zwaan et al.* [1990], while the blue envelope represents the environment obtained from the foraminifera associations (see Table 3 for a detailed description of each parameter).

density of the sedimentary column ($[\overline{\rho}_b]$ = kg/m^3), ρ_w is the density of salt water ($[\rho_w]$ = 1030 kg/m^3), W_{d_i} is the paleowater depth ($[W_{d_i}]$ = m), and Δ_{sl_i} is the sea level oscillations ($[\Delta_{sl_i}]$ = m).

[22] Equation (1) is still a simplified version of the backstripping equation, because no isostatic correction is introduced for changes in water load. This simplification derives from the evidence that the Airy correction for rapid changes in water load gives nonlinear results, meaning that lithospheric adjustment for rapid changes in surface load cannot be simplified by an Airy isostatic model. Figure 7 shows the results of the backstripping procedure and the paleowater depth values used for the calculation. In detail, the red line of the diagram on the right of Figure 7 shows the paleowater depth obtained following the approach defined by *Van der Zwaan et al*. [1990], while the blue envelope, representing the confidence interval of each values, is based on the modern (present-day) range of water depths of each living benthonic foraminifera assemblage (see Table 3 and Appendix B for details). The diagram on the left of Figure 7 represents the backstripping of PRAD1.2: the black line is the total subsidence curve that reflects all processes contributing to subsidence; the red line at the top portrays the tectonic subsidence alone. The interval between the two curves shows the subsidence due to the ~72 m of sediment load. Despite the large vertical error bars due to the uncertainties in paleowater reconstructions, it is possible to estimate the contribution of sediment load and tectonics by fitting the two curves with a linear regression. The result is that the total subsidence of the borehole PRAD1.2 is about 0.3 mm/yr (yellow line), and is mostly ascribed to tectonic driving forces (0.27 mm/yr, green line). Given the inevitable large spread of uncertainty we introduce an independent method to constrain the total subsidence by defining the relative depth of shorelines during the last four glacial lowstands.

4.2. Independent Subsidence Estimates From Dated Lowstand Shorelines

[23] An independent approach for the calculation of subsidence rates, commonly applied on other continental

Table 3. Parameters Necessary for the Backstripping Procedure

Unit Name	Unit Age[a] (kyr)	Decompacted Depth[b] (m)	Sea Level[c] (m)	Water Depth[d] (m)	Foraminifera Assemblages[e]	Environment[e]	Bathymetric Range[e] (m)
Present day	0.0	71.2	0	185.50	***B. dilatata***, ***C. laevigata carinata***, *B. marginata*, *C. pachyderma*, *T. angulosa*, *U. mediterranea*, *U. peregrina*, *G. subglobosa*, *H. balthica*, *P. ariminensis*	Upper slope	120–200
U-1	7.2 (±1)[1]	70.415	−20.0	162.0	***B. dilatata***, ***C. laevigata carinata***, *B. marginata*, *G. subglobosa*, *H. balthica*, *T. angulosa*, *U. peregrina*, *C. pachyderma*, *M. barleeanum*	Upper slope	120–200
T-I	17.5 (±0.8)[1]	66.162	−95.0	90.0	***S. sellii***, ***N. depressulum***, ***E. crispum***, ***E. decipiens***, *G. laevigata*, *M. rotunda*, *B. marginata*, *Q. seminulum*	Mid-Outer shelf	50–100
U-2	27.3 (±0.8)[1]	60.461	−80.0	108.0	***C. laevigata carinata***, ***E. crispum***, *Q. seminulum*, *E. decipiens*	Mid-Outer shelf	70–110
U-3	57.5 (±1.5)[2]	55.445	−70.0	114.0	***B. marginata***, ***H. balthica***, ***E. decipiens***, *E. crispum*, *G. subglobosa*, *N. depressulum*, *Q. seminulum*, *T. angulosa*, *U. mediterranea*, *U. peregrina*	Outer shelf	80–120
U-4/1	61 (±1.8)[2]	54.899	−85.0	100.0	***C. laevigata carinata***, ***H. balthica***, ***N. depressulum***, *E. crispum*, *E. decipiens*	Mid-Outer shelf	70–110
U-4/2	68 (±2)[2]	53.709	−80.0	105.0	***B. marginata***, ***C. laevigata carinata***, ***H. balthica***, *T. angulosa*, *E. decipiens*, *E. crispum*, *P. ariminensis*, *Q. seminulum*, *U. mediterranea*, *U. peregrina*	Mid-Outer shelf	70–110
U-5	125 (±3)[3]	44.173	0	180.0	***B. dilatata***, ***B. marginata***, ***C. laevigata carinata***, ***Globobulimina***, *C. oolina*, *B. costata*, *C. bradyi*, *C. pachiderma*, *G. praegeri*, *H. balthica*, *Q. seminulum*, *U. mediterranea*, *U. peregrina*	Sapropel equivalent (Upper slope)	120–200
T-II	143 (±5)[4]	41.94	−115.0	62.0	***I. islandica***, ***Trifarina* sp. 1**, ***E. articulatum***	Mid-Outer shelf	50–100
U-6	184 (±3)[3]	38.195	−80.0	83.0	***C. laevigata carinata***, ***E. crispum***, ***E. decipiens***, ***I. islandica***, *B. marginata*, *G. praegeri*, *G. subglobosa*, *P. ariminensis*, *Q. seminulum*, *Trifarina* sp1, *T. angulosa*	Mid-Outer shelf	50–100
U-7	225 (±5)[4]	32.521	−65.0	95.0	***B. marginata***, ***C. laevigata carinata***, *B. dilatata*, *C. pachyderma*, *E. crispum*, *E. decipiens*, *G. praegeri*, *I. islandica*	Mid-Outer shelf	50–100
T-III	248 (±4)[5]	29.716	−100.0	55.0	***I. islandica***, ***E. articulatum***, ***Nonion* sp. 1**, *N. depressulum*, *E. crispum*	Midshelf	40–80
U-8/1	263 (±3)[3]	25.043	−90.0	65.0	***C. laevigata carinata***, ***I. islandica***, *B. marginata*, *B. dilatata*, *E. crispum*, *E. decipiens*, *Nonion* sp. 1	Midshelf	40–80
U-8/2	315 (±3)[3]	21.783	−35.0	110.0	***B. dilatata***, ***B. marginata***, ***C. laevigata carinata***, *B. costata*, *E. crispum*, *E. decipiens*, *E. exigua*, *M. barleeanum*, *P. ariminensis*, *T. angulosa*, *U. peregrina*	Outer shelf	80–120
U-9	331 (±3)[3]	19.81	−60.0	80.0	***B. dilatata***, ***B. marginata***, ***C. laevigata carinata***, *G. subglobosa*	Mid-Outer shelf	50–100
U-10	340 (±5)[6]	13.368	−100.0	40.0	***B. marginata***, ***Nonion* sp. 1**, *E. decipiens*, *E. crispum*, *N. depressulum*	Inner-Mid shelf	20–60
U-10/11	365 (±5)[6]	0	−45.0	100.0	*B. marginata*, *C. laevigata carinata*, *E. crispum*, *E. decipiens*, *E. exigua*	Outer shelf	80–120

[a]For errors in ages, refer to Table 1.
[b]For a detailed description of decompaction procedure, see Appendix A and Table A1.
[c]Sea level values refer to *Lea et al.* [2002]; the average error on sea level estimates is about 20 m [*Lea et al.*, 2002].
[d]Paleowater depth values are obtained following the theory explained by *Van der Zwaan et al.* [1990].
[e]The environment and bathymetric range obtained analyzing the foraminifera associations [*Piva et al.*, 2008a, 2008b]: the taxa with the highest abundances (>10%) are in bold italics, the taxa with common abundance (5–10%) are in underlined italics, and the taxa with frequency of 1–5% are in italics (see also Appendix B).

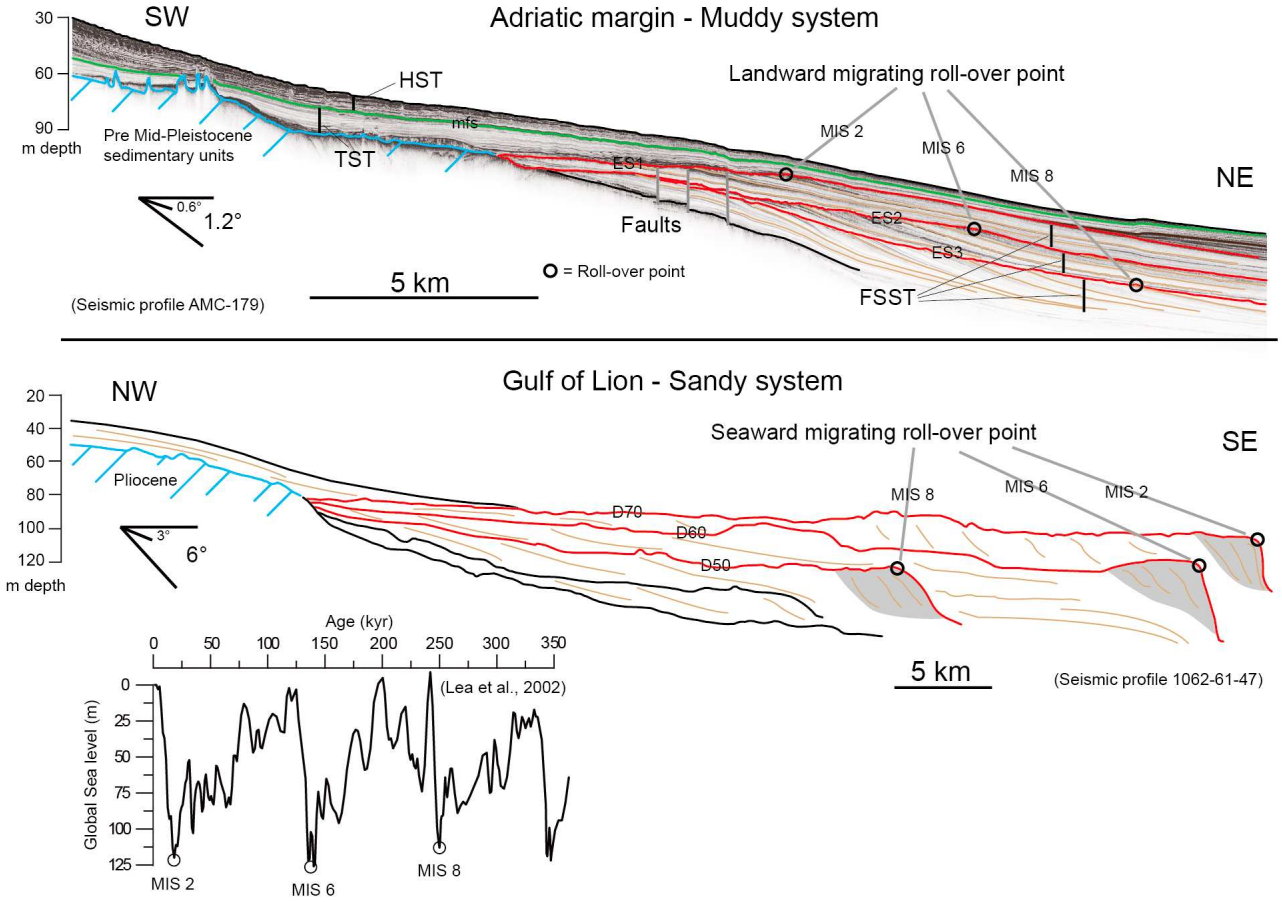

Figure 8. Comparison between the Adriatic active continental margin and the passive margin of the Gulf of Lion. (top) Line drawing along seismic profile AMC-179 (see also Figure 11). Circles represent the position of the lowstand shorelines, showing a backstepping configuration indicating that subsidence rate is greater than sediment supply. FSST, falling stage systems' tracts; mfs, maximum flooding surface. (bottom) Profile showing basinward tilt due to sedimentary load (modified from *Jouet et al.* [2006]). Progradation of the lowstand shorelines from MIS 8 to MIS 2 implies that subsidence rate is less than sediment supply. The greater subsidence of the Adriatic margin is marked by the landward shift of the landward pinch-outs of the sequences. Reference sea level curve is from *Lea et al.* [2002].

margins, is based on the identification of lowstand shoreline deposits of known age (e.g., in the Gulf of Lion [*Rabineau et al.*, 2006; *Skene et al.*, 1998]). These deposits can be identified also in the Adriatic margin from their diagnostic morphologies and internal reflector geometries on seismic profiles and their ages can then be assessed through their correlation with the stratigraphy derived from PRAD1.2 borehole.

[24] The key features to identify a drowned shoreline include (1) the rollover point between topset and foreset beds in clinoforms, although this feature can be found in water depths up to 20–30 m [*Vail et al.*, 1977; *Steckler*, 1999; *Cattaneo et al.*, 2003, 2007]; (2) the basinward limit of the lowstand subaerial erosion and/or its changes in dip and morphology; (3) the occurrence of thin packages of shingled reflectors converging and downlapping seaward; and (4) a change in seismic facies, typically characterized by higher amplitudes with respect to the surrounding seismic units (Figure 8 and Figure 9, bottom).

[25] The type of sediment delivered is an important factor controlling the formation of thick and detectable shoreline deposits. Unlike the Gulf of Lion and other Mediterranean margins characterized by coarser sediment, the Adriatic sequences are mainly pelitic. Sand-dominated systems are characterized by a well defined sedimentary prism with foreset beds dipping at high angles, typically of 3°–7° and a marked rollover point; in contrast, muddy systems are characterized by very low relief, and a shallower and less pronounced rollover point. In a first approximation, in the case of muddy systems the transition between an erosional unconformity and its correlative conformity can be considered to approximate a paleoshoreline. This assumption may lead to an error, up to several meters, because submarine erosion may extend further seaward and downward [*Thorne and Swift*, 1991].

[26] Paleoshorelines identified in this work are referred to changes in dip of the erosional surface often connected to thin reflector packages downlapping seaward. Since the Adriatic margin is characterized by a very low gradient shelf, a horizontal uncertainty of several hundreds of meters introduces an error of only a few meters in the paleoshoreline depth,

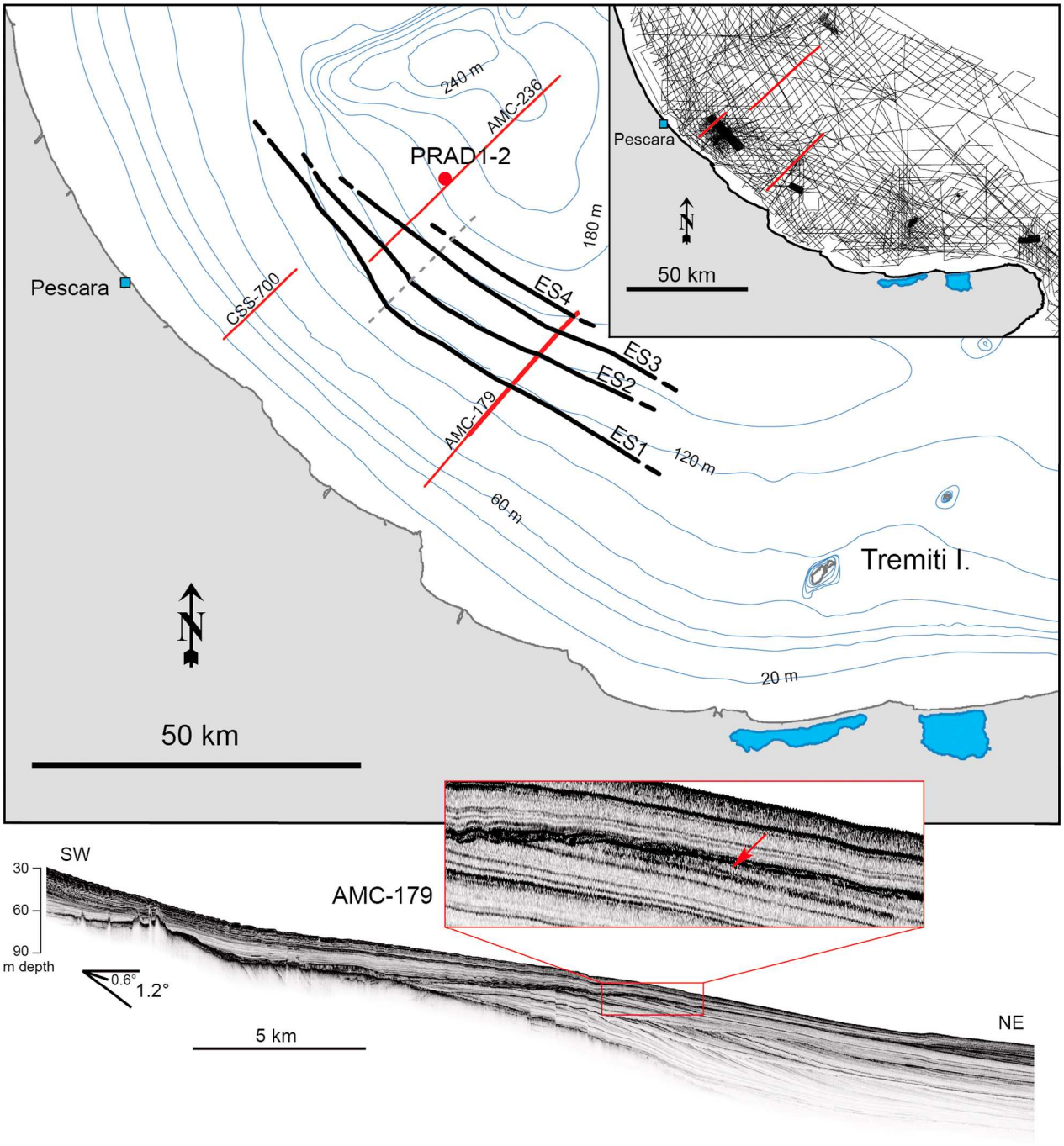

Figure 9. (top) Plane view of the lowstand shorelines (named ES1 to ES4, top down) showing a landward migration from MIS 10 (ES4) to MIS 2 (ES1). Note the basinward shift and the deepening of the lowstand shoreline ES1 and ES2 north of the dashed line (Table 4). This trend may reflect the configuration of the Eemian HST depocenter. (bottom) Detail of seismic profile AMC-179 showing a downlapping reflector interpreted as a possible shoreline deposit (red arrow).

maintaining a rather small range of uncertainty on the depth of each lowstand shoreline. The observed lowstand shorelines migrate landward from MIS 10 to MIS 2, following the backstepping pattern of the shelf perched wedge [*Trincardi and Correggiari*, 2000] (Figure 8).

[27] In plain view the lowstand shorelines become closer to each other proceeding in the NW direction, north of the dashed line in Figure 9, implying a relatively steeper margin or a faster seaward tilt during deposition. The depth of the shorelines associated to unconformities ES1–ES4 can be calculated by subdividing the margin in two areas, north and south of the dashed line in Figure 9, and averaging the values obtained analyzing the seismic profiles for each area (Table 4). To estimate the subsidence rate for each

Table 4. Depth of the Basinward Limits of the Glacial Lowstand Shorelines During the Cold Isotopic Events 2.2, 6.2, 8.2, and 10.2[a]

				North			South		
Shoreline	Age (kyr)	MIS	Eustatic Fall (m)	Average Depth (m)	Corrected Depth (m)	Subsidence Rate (mm/yr)	Average Depth (m)	Corrected Depth (m)	Subsidence Rate (mm/yr)
ES1	19 (±1.3)[4]	2.2	118 (±2)[7]	130.7 (±1.5)	12.7 (±3.5)	0.67 (±0.23)	122.1 (±0.5)	4.1 (±2.5)	0.22 (±0.16)
ES2	135 (±4.2)[4]	6.2	127 (±3)[8,9]	165.3 (±1.2)	38.3 (±4.2)	0.28 (±0.04)	154.6 (±1.1)	27.6 (±4.1)	0.2 (±0.04)
ES3	250 (±5)[6]	8.2	120 (±8)[10]	189.8 (±1.3)	69.8 (±9.3)	0.28 (±0.04)	186.9 (±2)	66.9 (±10)	0.27 (±0.05)
ES4	335 (±5)[6]	10.2	128 (±6)[10]				218.9 (±2.1)	90.9 (±8.1)	0.27 (±0.03)

[a]Subsidence rates derived by taking into account sea level falls during glacial periods following the results of different authors in the literature. The depth of each lowstand shoreline is obtained by dividing the area of interest in two sectors (north and south of the dashed line in Figure 9) and averaging the values obtained from high-resolution seismic profiles. Error bars in age are as follows: 4, from *Martinson et al.* [1987]; 6, from *Bassinot et al.* [1994]. Error bars in sea level are as follows: 7, from *Bard et al.* [1990]; 8, from *Chappell and Shackleton* [1986]; 9, from *Shackleton* [1987]; 10, from *Rohling et al.* [1998]. Errors in average depth take into account uncertainties in horizontal position and in vertical resolution of the seismic lines.

sequence, the depth of each shoreline needs to be corrected for the eustatic sea level fall; this can be done by introducing different values for each eustatic cycle [*Bard et al.*, 1990; *Chappell and Shackleton*, 1986; *Rohling et al.*, 1998; *Shackleton*, 1987; *Lea et al.*, 2002]. Table 4 shows that the western side of the Adriatic margin is subsiding at 0.3 ± 0.08 mm/yr, with small but significant changes in subsidence rate in time and even in space, higher in the northern area. Figure 10 represents the subsidence trends detected from the depths at which the lowstand shorelines are encountered for each glacial interval. Note that the lowstand shorelines for glacial intervals between MIS 2 and MIS 10 fit a linear regression implying a constant subsidence over the last ~400 kyr of about 0.3 mm/yr.

[28] By using different values for the subsidence rate, taking into account the sediment supply corrected with an Airy isostatic compensation and by introducing the sea level fall for each glacial period, it is possible to extrapolate the paleowater depth at the peak of MIS 2.2, 6.2, 8.2 and 10.2 lowstands in the borehole PRAD1.2 (Table 5) and to compare the results with the paleowater depth reconstructions obtained by foraminifera assemblages.

[29] In detail, at 54.4 mbsf, corresponding to the top of MIS 10.2, seismic profiles show the erosional surface ES4 (Figures 2 and 4). This surface was generated by submarine erosion in water depth less than 20 m, as shown in Table 5 and confirmed by the lithological and paleontological data. One of the reflectors truncated by ES4 corresponds to a sharp surface at 58 mbsf in PRAD1.2 marking the base of a coarser-grained unit that likely indicates wave reworking in an inner shelf to shoreface environment. Moreover, in the interval between 55 and 58 m, abundant benthic microfauna indicates a very proximal inner shelf assemblage, with dominance of *Ammonia perlucida*, *Islandiella islandica*,

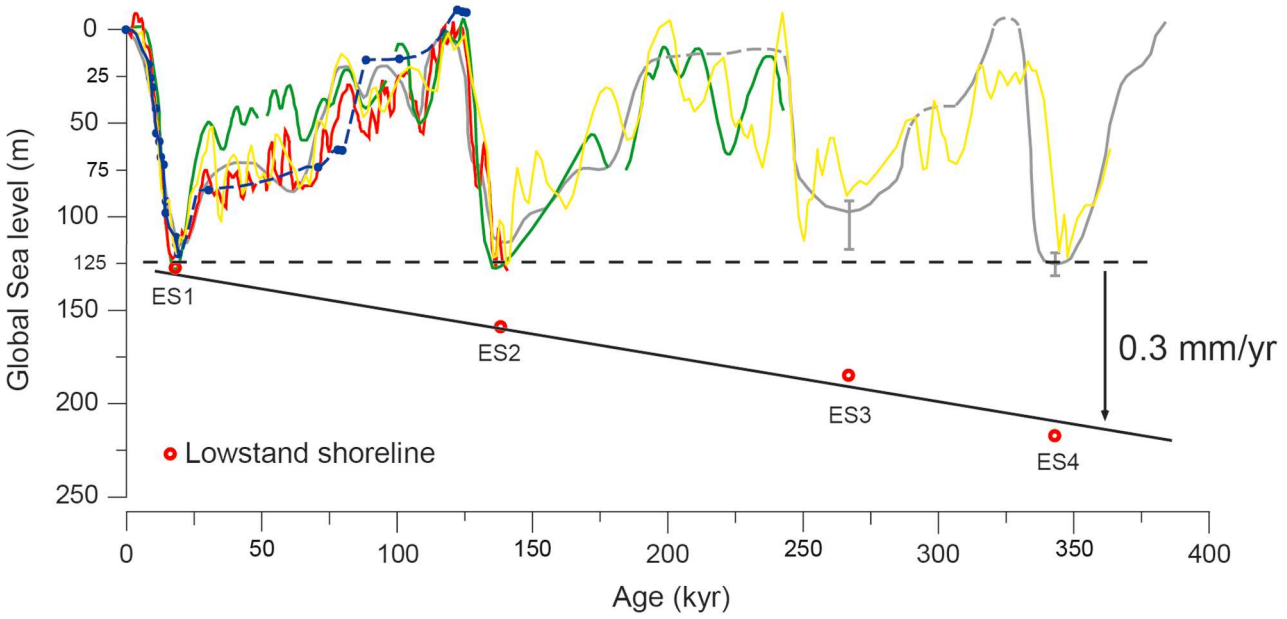

Figure 10. Present-day burial depths of paleoshorelines during major eustatic lowstands referred to isotopic stages from MIS 2 to MIS 10. The most commonly adopted eustatic curves help constrain the position of each successive lowstand shoreline: blue line is from *Bard et al.* [1990], points refer to U-Th ages, red line is from *Shackleton* [1987], green line is from *Chappell and Shackleton* [1986], gray line is from *Rohling et al.* [1998], and yellow line is from *Lea et al.* [2002]. Note that a simple regression fits the values, implying a quasi-steady subsidence rate during the last ~400 kyr.

Table 5. Paleowater Depth at the Site of PRAD1.2 During the Main Glacial Lowstands, TL1 to TL3 and ES4 (from MIS 2.2 to MIS 10.2)[a]

Boundary in PRAD1.2	Age (kyr)	MIS	Depth in PRAD1.2 (m)	Corrected Depth Airy (m)	Present-day Wd Correction (m)	Eustatic Fall (m)	Corrected Depth Eustatic Fall (m)	Subsidence Rate (mm/yr)	Subsidence Correction (m)	Paleowater Depth (m)	Foraminifera Assemblages	Environment	Bathymetric Range (m)
TL1	19 (±1.3)[4]	2.2	7.7	6.3	191.8	118 (±2)[7]	73.8 (±2)	0.45 (±0.23)	8.6 (±5)	65.2 (±7)	***C. laevigata carinata***, ***E. decipiens***, *N. depressulum*, *E. crispum*, *M. rotunda*, *S. sellii*, *G. laevigata*, *B. marginata*, *Q. seminulum*	Midshelf	40–80
TL2	135 (±4.2)[4]	6.2	32.5	26.6	212.1	127 (±3)[8,9]	85.1 (±3)	0.24 (±0.04)	32.4 (±6.4)	52.7 (±9.4)	***I. islandica***, ***Trifarina* sp1**, ***E. articulatum***, ***Nonion sp***	Midshelf	40–80
TL3	250 (±5)[6]	8.2	45.6	37.3	222.8	120 (±8)[10]	102.8 (±8)	0.27 (±0.05)	67.5 (±13.9)	35.3 (±21.9)	***I. islandica***, ***E. articulatum***, ***Nonion* sp. 1**, *N. depressulum*, *E. crispum*	Mid-Inner shelf	30–60
ES4	335 (±5)[6]	10.2	55	44.9	230.4	128 (±6)[10]	102.4 (±6)	0.27 (±0.03)	90.5 (±11.4)	11.9 (±17.4)	***I. islandica***, ***A. perlucida***, ***E. articulatum***, ***Nonion* sp. 1**, *N. depressulum*, *E. decipiens*	Inner-Mid shelf	10–30

[a]See also Figure 4. The values are obtained taking into account (1) present-day depth in core of the sequence boundaries and Airy correction for sediment unload, (2) present-day water depth (Wd) of 185.5 m, (3) sea level fall during lowstands from different eustatic curves (see Table 4 for references), and (4) reconstructed depth for different values of subsidence rate. The bathymetric range column shows the paleowater depth obtained from the foraminifera associations (see Table 3 and Appendix B).

Elphidium articulatum, and *Nonion pauciloculum* [*Piva et al.*, 2008a, 2008b].

[30] In MIS 8.2, *Piva et al.* [2008b] report a benthic assemblage dominated by *I. islandica* and *E. articulatum*. The absence of the inner shelf species *A. perlucida* (bathymetric range less then 30 m, according the local zonation reported by *Morigi et al.* [2005]) suggests a minor riverine influence along with a possible relatively deeper environment (midshelf). The calculation using a subsidence rate of 0.27 ± 0.05 mm/yr gives for MIS 8.2 a paleowater depth of about 40 m.

[31] MIS 6.2 is richer in planktic assemblages and characterized by benthic species typical of the midshelf to inner shelf environment. During the last glacial period, MIS 2.2, the PRAD1.2 borehole reached its maximum water depth as confirmed by the foraminifera assemblages, typical of a midshelf environment [*Piva et al.*, 2008b], and by the 65 m water depth calculated as above.

5. Discussion

5.1. Subsidence Rates in the Central Adriatic

[32] PRAD1.2 borehole is the only sedimentary record in the central Adriatic Sea encompassing the last ~400 kyr with a continuous core recovery. The lithological and paleontological information obtained [*Piva et al.*, 2008a, 2008b; *Ridente et al.*, 2008], correlated with a dense grid of seismic lines, made it possible to reconstruct the evolution of the margin and estimate the subsidence rate following an analytical model integrated by sedimenthological and seismostratigraphic evidences. The calculated subsidence rates of 0.3 mm/yr from PRAD1.2 borehole are consistent with the Facies and paleontological data, which record a substantial deepening of the area over the last 400 kyr. Subsidence exceeds the average rate of sediment supply, and explains the aggradational stacking pattern of the last four 100 kyr depositional sequences and the overall backstepping of their landward pinch-out [*Trincardi and Correggiari*, 2000; *Ridente and Trincardi*, 2002].

[33] While subsidence rates appear quite constant during the interval encompassed by PRAD1.2 borehole, sediment supply changed between 0.2 and 0.8 mm/yr (Figure 6). In particular, two main peaks in sediment flux are recorded during the lowstands of MIS 10 and MIS 2. These significantly increased sediment accumulation rates have two different origins: during MIS 10 the high sediment flux reflects a proximal sediment entry point (delta or prograding shoreline) which is consistent with the very shallow paleowater depth at that time; during MIS 2, instead, the site is already in 65 m of water depth even during a sea level lowstand (Table 5). The increase of the accumulation rate during MIS 2.2 reflects the influence of the rapidly advancing Po River lowstand delta toward the southern flank of the MAD, resulting in about 10 m of sediment accumulation at the site where PRAD1.2 borehole was retrieved (see Figure 11) and greater than 200 m in the northern side of the MAD (see Figure 2). Figure 11 shows a simplified scheme of the late Quaternary central Adriatic stratigraphy, related to sediment supply fluctuations and sea level oscillations. It is important to underline the relations between the unconformities and the onlapping units, in particular those deposited during MIS 2 and MIS 10 lowstands. The MIS 2

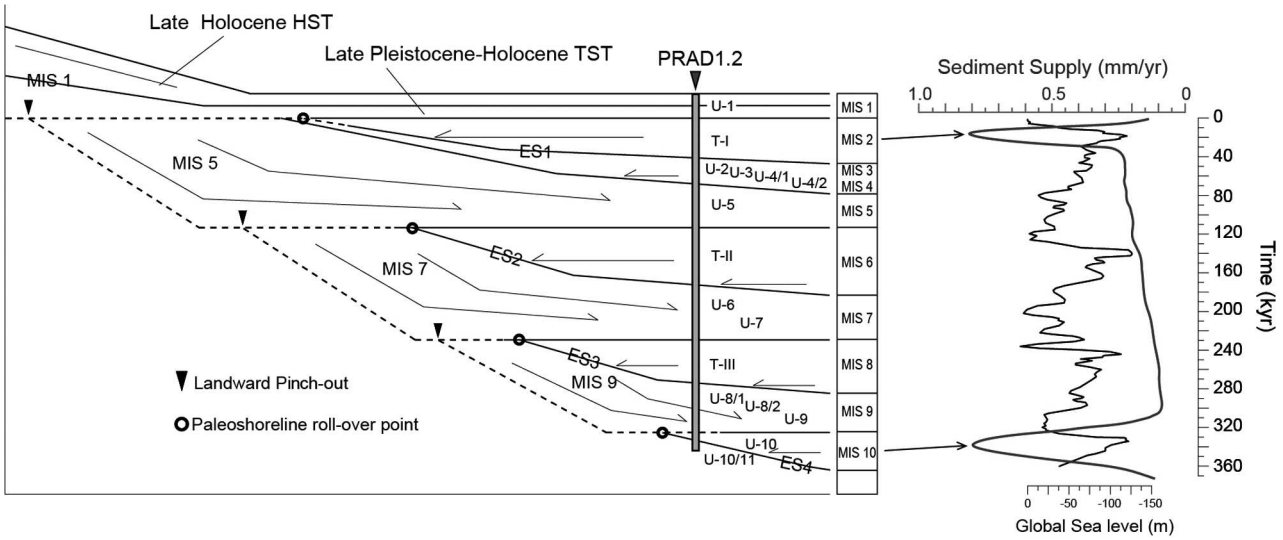

Figure 11. (left) Schematic representation of the stratigraphic relationship between progradational units on the shelf and onlapping units on the upper slope (modified from *Ridente et al.* [2008]). Dashed lines are the major unconformities (sequence boundaries). (right) Sediment supply fluctuations obtained from borehole PRAD1.2 (gray line) and global sea level oscillations (black line, modified from *Lea et al.* [2002]). The two peaks in sediment supply corresponding to sea level falls during MIS 2 and MIS 10 are correlated to the most important progradations of the late Quaternary units.

onlapping unit rests on the conformable correlative of the erosional surface, whereas during MIS 10 the erosional unconformity reached a more seaward position and affected the lowstand deposits, as highlighted by the borehole stratigraphy (see Figures 2 and 3).

[34] Previous estimates of the subsidence in the central Adriatic Sea should also be considered with caution. As an example, *Colantoni et al.* [1989] provided a subsidence rate of 3.5 mm/yr based on a single ^{14}C date of an organic-rich layer found in 200 m of water depth and interpreted as a peat layer deposited during the last glacial lowstand. However, this organic-rich layer, containing benthic foraminifera assemblage indicating riverine runoff [*Colantoni et al.*, 1989] is encased in marine sediment and most likely represents a level enriched in organic matter during MIS 2 (~LGM) on the floor of a semi-isolated basin because of the lowstand sea level and probably strongly influenced by riverine input, as also supported by similar inferences from nearby sediment cores [*Asioli*, 1996]. Moreover, the seismic stratigraphy of the area is characterized by plain-parallel reflectors that are not expected in a coastal-lagoon environment where a peat layer may form.

[35] The subsidence rates in the central Adriatic are also likely to vary laterally in response to changing tectonic/sediment load forcing. The maps of the lowstand shorelines of the four regressive sequences show that their positions along the central Adriatic margin and landward of PRAD1.2 borehole, become closer to each other proceeding to the NW suggesting that subsidence rates likely increase in this direction (Table 4 and Figure 9).

5.2. Regional Subsidence Patterns in the Adriatic Basin

[36] The area where PRAD1.2 was retrieved is considered a subsiding foredeep basin in contrast with the Apulia swell, located further south, that has been uplifted over the last 800 kyr, probably as a consequence of the lower penetration of the subducted slab, which is due to a thicker continental lithosphere [*Royden et al.*, 1987; *Doglioni et al.*, 1994]. Overall, the northern Adriatic Sea shows strong subsidence, greater in the area of Venice and Ravenna, which reflects geodynamic forcing, and is probably due to the eastward rollback of the subduction hinge [*Doglioni et al.*, 1994]. In addition to the geodynamic driving forces, it is important to consider the subsidence due to the load of the late Pleistocene to Holocene sediments, and, especially in the northern sector of the Adriatic margin, the glacio-isostatic rebound [*Antonioli et al.*, 2009].

[37] The north Adriatic has been investigated in order to quantify the rate of subsidence over long intervals (middle and late Pleistocene), and for the last century, to assess the impact of the anthropogenic subsidence, in particular in the subsiding areas of Venice and Ravenna [*Carminati et al.*, 2003; *Tosi et al.*, 2007] (Figure 1). The Venice area shows a subsidence rate between 0.18 and 0.36 mm/yr, averaged over the last million year, reaching a maximum value of 1.3 mm/yr for the late Pleistocene to Holocene, that most likely reflects sediment compaction taking place over few millennia after deposition [*Kent et al.*, 2002]. For the last 125 kyr, a complementary subsidence rate can be quantified on the basis of the work of *Massari et al.* [2004], who described the stratigraphy of two complementary boreholes (VE1 and VE1-bis) following the results of *Kent et al.* [2002]. The stratigraphy of the borehole is characterized, at 77.8 m below the ground level (which is 2 m above sea level) by shallow marine environments, ascribed to the last sea level highstand (Eemian), which gives a subsidence rate of 0.6 mm/yr for the last 125 kyr.

[38] In the Po River coastal plain north of Ravenna (Figure 1), the 173 m long continuous borehole S17

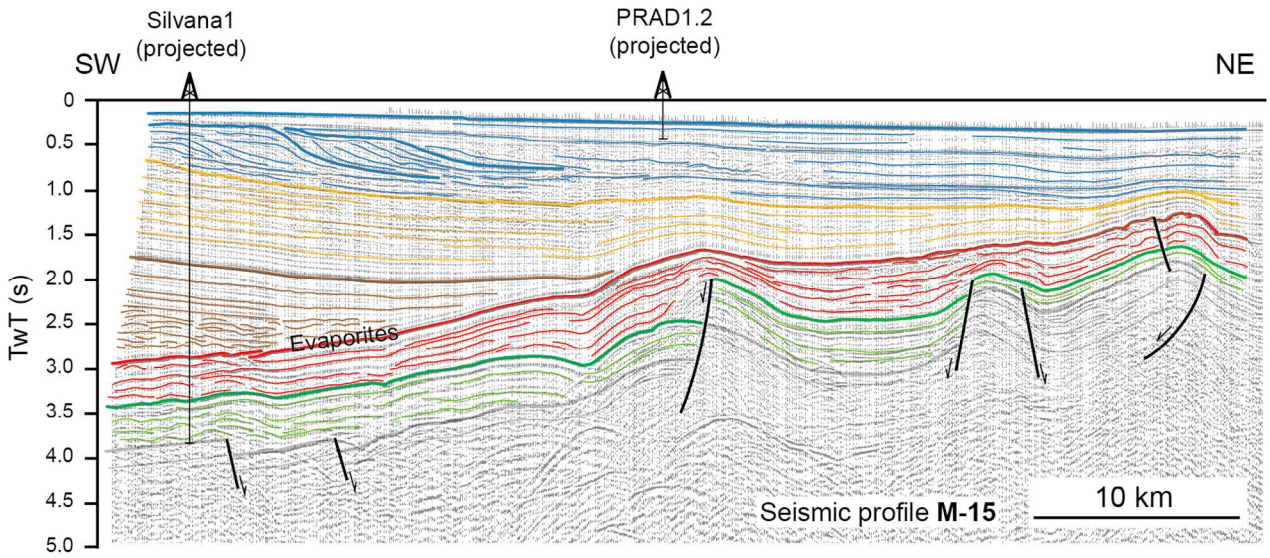

Figure 12. Interpretation of the multichannel seismic line CROP M-15 (modified from *Scrocca* [2006]) showing the stratigraphy and the main tectonic structures of the central Adriatic foredeep. Note the landward (SW) flexure of the deepest deposits, depending on the subduction of the Adria plate under the African plate, in the classical scheme of an active margin. This scheme is opposed to the youngest deposit (upper Quaternary) showing a basinward tilt typical of a passive margin. Blue unit is outer shelf to basin plain deposits (late Pleistocene to late Pliocene); yellow unit is hemipelagites and turbidites (late to middle Pliocene); brown unit is hemipelagites and turbidites (middle Pliocene to late Miocene); top red unit is evaporites (Messinian); red unit is marls and pelagic limestone (late Miocene to Early Cretaceous, Albian); green unit is cherty limestones and marls (Early Cretaceous to Early Jurassic, Lias); and grey unit is shallow water carbonates (Early Jurassic to Late Triassic, Norian). TwT, two-way travel time.

encompasses continental and marine deposits from MIS 7 to the Holocene [*Amorosi et al.*, 1999, 2004]. Facies assemblages, faunal and pollen associations allow the identification of shallow marine deposits originated during the Eemian sea level highstand 120 m below the ground. The extrapolated subsidence rate is therefore on the order of 1 mm/yr.

[39] *Ferranti et al.* [2006], on the basis of the identification of past highstand deposits, reconstructed the differentiated tectonic trends of the Italian coasts for the last 125 kyr. More detailed information, but only for the Holocene, is given by *Lambeck et al.* [2004], who tried to extract the eustatic curve. The results obtained by these authors show that the Italian coasts are characterized by variable tectonic styles; in particular referring to the Adriatic sector, the northern part is characterized by maximum subsidence rates on the order of 1.2 mm/yr, while the southern part, the Apulia swell, is characterized by uplift rate on the order of 0.2–0.3 mm/yr. The only data gap is represented by about 300 km along the central Adriatic margin, investigated in this work. The central Adriatic shelf, dominated by a subsidence rate of 0.3 mm/yr, seems to be a zone of transition between the highly subsiding northern area and the uplifting southern area.

5.3. Subsidence Rates on Foreland Versus Passive Margins

[40] Distinctive patterns of deposition in active versus passive margins, discussed by several authors [*Jordan and Flemings*, 1991; *Posamentier and Allen*, 1993], reflect the evidence that in foreland basins the subsidence-deposition ratio increases landward, while on passive margins the trend is opposite. *Rabineau et al.* [2006] used the depths of past lowstand shorelines to investigate the subsidence of the passive margin of the Gulf of Lion. The results show that the margin is characterized by a seaward progradation of the last five depositional sequences, since the glacial lowstand of MIS 12, indicating that the sediment delivered is greater than the accommodation space created (Figure 8). This observation can be explained considering that the Gulf of Lion is a passive margin, thermally cold and seismically inactive, showing a low subsidence rate principally caused by sediment load itself [*Tesson et al.*, 2005].

[41] The Adriatic margin behaves as an active margin, with subsidence-deposition ratio increasing landward, but only referring to a long time interval (millions of years). This fact is clear when observing the CROP seismic profile M-15 showing a landward tilt of the Messinian unconformity, and underlying strata, toward the Apennine chain (Figure 12; modified from *Scrocca* [2006]). On a shorter timescale, like the 300–400 kyr encompassed by borehole PRAD1.2, the Adriatic foreland shows a behavior similar to that of a passive margin that is tilting seaward. Since the sediment supply is not sufficient to exploit all the accommodation space induced by subsidence, the shoreline break of each lowstand interval moves progressively landward (Figures 8 and 9). This subsidence-driven pattern of deposition mirrors the typical pattern of a young passive margin under a significant seaward tilt.

[42] The substantial difference between the Gulf of Lion and the Adriatic margin, even if the overall geodynamic

contexts are different (passive versus active margins), is the subsidence/sedimentation ratio, which is greater in the Adriatic Sea and explains the larger landward shift of the landward pinch-outs and the backstepping of the last four depositional sequences.

5.4. Methodological Considerations

[43] To achieve accurate reconstructions of the tectonic history of a subsiding continental margin on short timescale and with high-resolution data sets, it is important to integrate different approaches, from purely analytical methods to geophysical reconstructions and paleontological/stratigraphic evidences. A particularly interesting result is that the proposed reconstructions document, for the first time, that subtle but significant changes in subsidence rate over small spatial and timescales can be resolved by high-resolution stratigraphic data in shallow slope environments (Tables 4 and 5).

[44] The backstripping procedure was introduced to investigate the evolution of a margin over intervals of tens to hundreds of millions of years and on kilometric stratigraphic sections [e.g., *Van Hinte*, 1978], in order to separate within the total subsidence the tectonic contribution and the sediment load. In the case of PRAD1.2 borehole, the backstripping procedure is still applicable and the results obtained are consistent with the results obtained with an independent method, even if significant error bars should accompany the paleowater depth reconstructions. The geohistory analysis and the application of backstripping procedure poses many problems if applied to the study of short boreholes, in particular in a time interval dominated by high-amplitude sea level fluctuations. Even if errors introduced in the decompaction calculations can be omitted, especially when porosity logs are available, the main source of error can be ascribed to the uncertainties in the reconstruction of paleowater depth and to the lithospheric response to rapid load changes driven by sea level fluctuations. Errors in paleowater depth reconstructions can be reduced by referring to long boreholes, encompassing shallow water deposits from shoreface-lagoon to midshelf environments, better defined by the benthonic communities compared to deeper water environments.

6. Conclusions

[45] By integrating two complementary geophysical and seismic-stratigraphic approaches, this paper attempts to a reconstruction of the geological history of the central Adriatic margin disentangling subsidence, eustacy and sediment-flux variations over the last 400 kyr. The results are based on the PRAD1.2 borehole, a 71.2 m continuous core, encompassing a continuous record through the last four Quaternary glacial-interglacial cycles.

[46] The geohistory analysis is first adopted to estimate the contribution of tectonic subsidence rates (0.27 mm/yr) in the total subsidence of the central Adriatic margin (0.3 mm/yr), and then compared with the subsidence rates obtained with an independent method based on the identification of dated lowstand shorelines, also resulting in a total subsidence rate of 0.3 ± 0.08 mm/yr, averaged over the last ~340 kyr. The use of lowstand shorelines made it possible to better constrain the subsidence rates and error bars associated, giving also a detailed spatial resolution on different timescales.

[47] Using the calculated subsidence rate and taking into account sediment supply fluctuations and sea level, it was possible to estimate the paleowater depths in PRAD1.2 during the last four glacial intervals, since the glacial lowstand of MIS 10. The results obtained document a progressive deepening of the central Adriatic margin at the site of the borehole at each successive lowstand. This trend is confirmed by foraminifera assemblages showing an evolution of the depositional environment from inner shelf to mid-outer shelf conditions, followed by a progressive shoaling, during MIS 2, caused by the increased sediment flux from the Po River lowstand drainage system.

[48] The Adriatic margin shows differentiated tectonic styles from north to south, depending on the different thicknesses of the subducting lithosphere. A high subsidence rate, on the order of 1 mm/yr, characterizes the northernmost part of the basin, in marked contrast with the uplift (~0.4 mm/yr) of the Apulian region in the south. The central Adriatic basin, where the borehole PRAD1.2 is located, appears to subside at 0.3 mm/yr and can be considered as a transition area between the high subsidence values of the northern Adriatic and the uplift of the south. This rate is only partially compensated by the sediment flux from the catchment and explains the overall backstepping of the Pleistocene regressive sequences along the western margin of the central Adriatic, mimicking the stratigraphic pattern typical of a young passive continental margin.

Appendix A

A1. Decompaction

[49] Following *Athy* [1930] and *Sclater and Christie* [1980], the porosity-depth relation for normally pressured sediments follows an exponential law (Figure A1):

$$\Phi = \Phi_0 \cdot e^{-cz}, \tag{A1}$$

with the following decompaction parameters: Φ_0 is initial porosity, c is porosity coefficient ($[c] = m^{-1}$), and z is depth of interest ($[z] = m$).

[50] The c coefficient is calculated by fitting the porosity value obtained by the sonic log performed parallel to the drilling of the borehole PRAD1.2. In order to minimize the error, two values of c are taken into account by using two different exponential fitting of the porosity values: one from 0 to 25 m and one from 25 to 71.2 m (Figure A1). This simplification is commonly adopted even where discrete intervals show inversions in their porosity with depth.

[51] The *second step* is to calculate the decompacted thickness of each unit. A unit of thickness T_N is buried at a depth d_N. We want to know the thickness of the unit (T_0) at some earlier time, when the unit was buried only to a depth of d_0 (Figure A2). The basic assumptions are that the porosity decreases exponentially with depth and the volume of rock grains within the unit does not change:

$$\int_{d_0}^{d_0+T_0} (1-\Phi)dz = \int_{d_N}^{d_N+T_N} (1-\Phi)dz. \tag{A2}$$

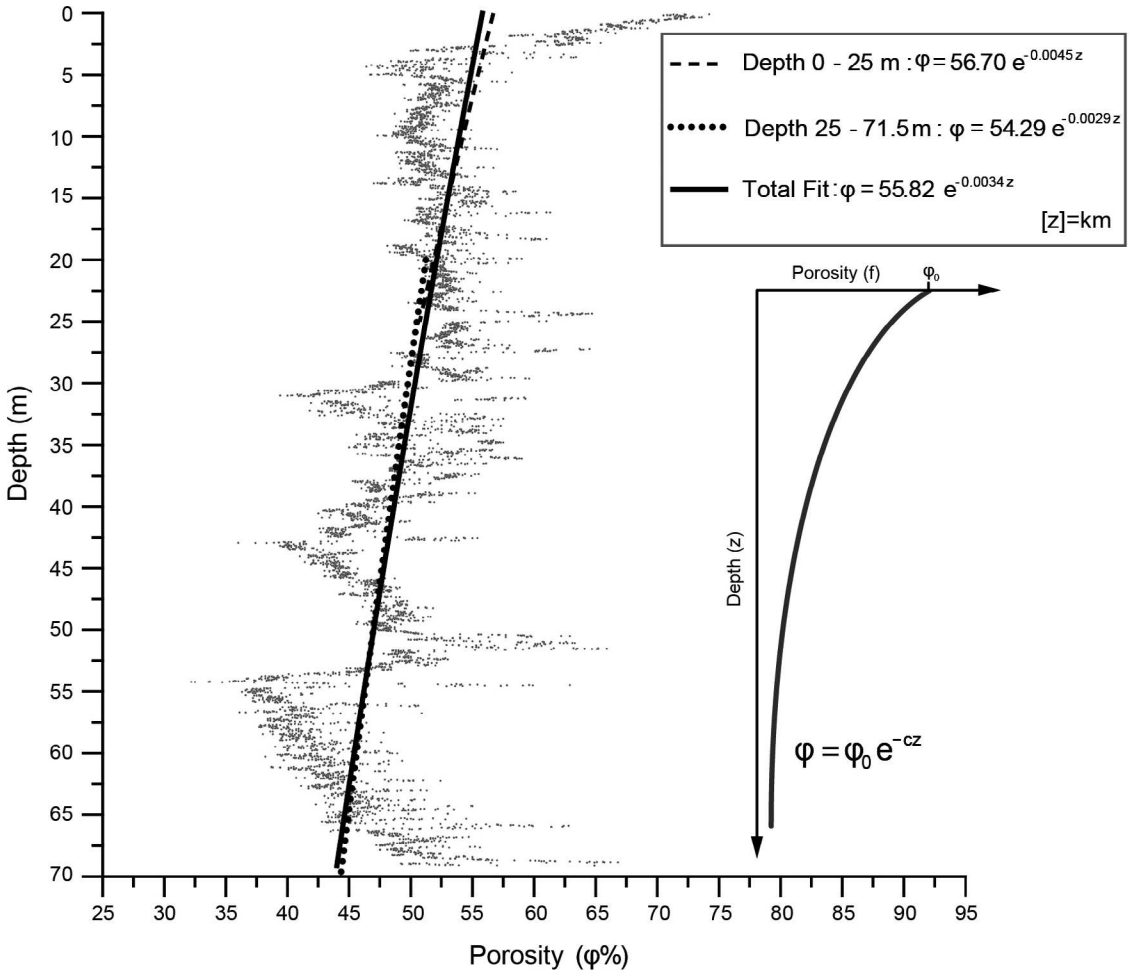

Figure A1. PRAD1.2 porosity-depth values obtained indirectly from gamma-density log calculated using a multisensor core logger (Geotek). The legend shows three compaction curves used to extrapolate the decompacted porosity and the bulk density. The solid line fits the entire borehole data. In order to minimize the error, two different compaction curves (dashed and dotted lines) are used for two intervals: 0–25 m depth and 25 m to the bottom of the borehole. The compaction coefficient (c) reflects the compaction behavior: the higher the c value, the faster the sediment is compacted. The diagram on the right shows theoretical porosity versus depth.

These two integrals can be evaluated analytically, knowing that

$$\Phi_N = \Phi_0 \exp(-cz). \tag{A3}$$

$$\begin{aligned}\int_{d_0}^{d_0+T_0}(1-\Phi)dz &= \int_{d_0}^{d_0+T_0}(1-\Phi_0\cdot e^{-cz})dz \\ &= \int_{d_0}^{d_0+T_0} dz - \Phi_0\int_{d_0}^{d_0+T_0}(e^{-cz})dz \\ &= [z]_{d_0}^{d_0+T_0} + \frac{\Phi_0}{c}[e^{-cz}]_{d_0}^{d_0+T_0} \\ &= T_0 + \frac{\Phi_0}{c}e^{-cd_0}\cdot\left(e^{-cT_0}-1\right).\end{aligned} \tag{A4}$$

By applying the same method for the right side of the equation, we obtain

$$T_0 + \frac{\Phi_0}{c}e^{-cd_0}\cdot\left(e^{-cT_0}-1\right) = T_N + \frac{\Phi_0}{c}e^{-cd_N}\cdot\left(e^{-cT_N}-1\right). \tag{A5}$$

It is impossible to solve equation (A5) directly for T_0; this is an example of transcendental equation. The best approximate solution can be obtained by isolating T_0 and assuming a value for it, and then calculating a new value for T_0. This process is repeated until T_0 stops changing from one step to the next. The resulting value is the solution.

[52] Isolating T_0 from equation (A5) gives

$$T_0 = -\frac{\Phi_0}{c}e^{-cd_0}\cdot\left(e^{-cT_0}-1\right) + T_N + \frac{\Phi_0}{c}e^{-cd_N}\cdot\left(e^{-cT_N}-1\right), \tag{A6}$$

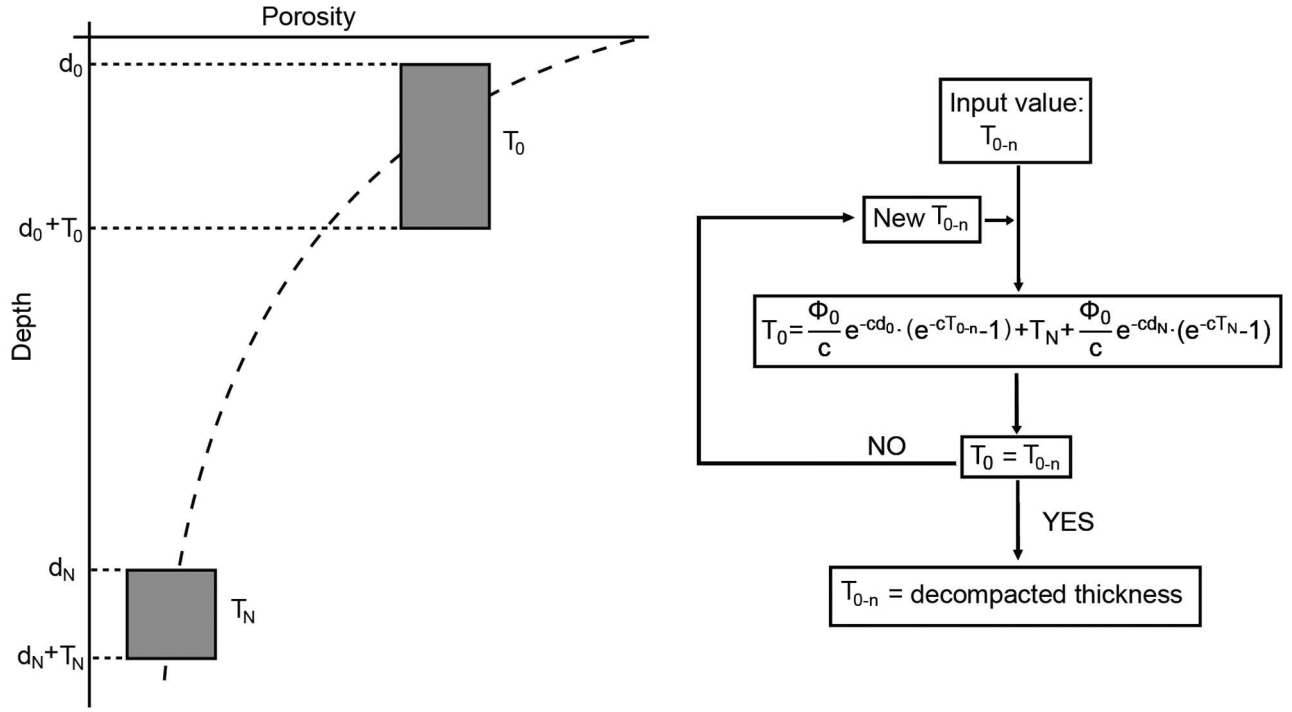

Figure A2. (left) Diagram showing the decompaction procedure. The upper and lower boundaries of each sedimentary unit (gray boxes) are introduced in the equations. (right) Algorithm to evaluate the decompacted depth; for each cycle, the algorithm tends toward the final decompacted value until the result stops changing.

where T_0 is thickness after decompaction ($[T_0]$ = m), T_N is initial thickness ($[T_N]$ = m), d_0 is new burial depth ($[d_0]$ = m), d_N is burial depth ($[d_N]$ = m), Φ_0 is initial porosity, and c is porosity constant ($[c] = m^{-1}$).

[53] A reasonable estimate for T_0 is the modern thickness, measured in the borehole. By introducing this value on the right side of equation (A6), we obtain the first value of decompacted thickness. The process has to be repeated until T_0 converges to a stable value, following the algorithm defined in Figure A2. Table A1 and Figure 5 show the decompacted depths.

A2. Isostasy

[54] In the classical scheme of Airy isostasy [*Airy*, 1855], changes in topographic relief or seafloor elevation are compensated locally by changes in crustal thickness. An Airy compensation assumes a lithosphere with zero lateral strength: if a surface load is applied, the crust behaves as a series of vertical-sided prisms, where shear stresses cannot be transmitted from one prism to the adjacent ones.

[55] The weight of a column of sediment of uniform section is directly proportional to the bulk density, that is the

Table A1. Decompaction Process[a]

Unit Name	Age (kyr)															
	340	331	315	263	248	225	184	143	125	68	61	57.5	27.3	17.5	7.2	0
U-10/11	13.368	19.81	21.783	25.043	29.716	32.521	38.195	41.94	44.173	53.709	54.899	55.445	60.461	66.162	70.415	71.2
U-10	0	6.72	8.776	12.171	17.033	19.949	25.842	29.728	32.043	41.919	43.151	43.716	48.907	54.792	59.189	60
U-9	0	0	2.101	5.57	10.536	13.513	19.525	23.487	25.846	35.905	37.159	37.734	43.019	49.002	53.476	54.2
U-8/2	0	0	0	3.492	8.491	11.487	17.537	21.523	23.888	34.006	35.267	35.845	41.16	47.174	51.672	52.5
U-8/1	0	0	0	0	5.056	8.085	14.201	18.229	20.618	30.836	32.109	32.692	38.058	44.125	48.665	49.5
T-III	0	0	0	0	0	3.079	9.294	13.385	15.811	26.18	27.471	28.062	33.505	39.652	44.254	45.1
U-7	0	0	0	0	0	0	6.277	10.407	12.856	23.32	24.623	25.219	30.71	36.907	41.458	42.4
U-6	0	0	0	0	0	0	0	4.215	6.713	17.379	18.706	19.313	24.907	31.21	35.934	36.8
T-II	0	0	0	0	0	0	0	0	2.532	13.34	14.684	15.299	20.965	27.342	32.124	33
U-5	0	0	0	0	0	0	0	0	0	10.895	12.249	12.868	18.578	25	29.818	30.7
U-4/2	0	0	0	0	0	0	0	0	0	0	1.429	2.081	8.095	14.84	19.89	20.8
U-4/1	0	0	0	0	0	0	0	0	0	0	0	0.656	6.713	13.503	18.585	19.5
U-3	0	0	0	0	0	0	0	0	0	0	0	0	6.076	12.886	17.983	18.9
U-2	0	0	0	0	0	0	0	0	0	0	0	0	0	7.015	12.258	13.2
T-I	0	0	0	0	0	0	0	0	0	0	0	0	0	0	5.427	6.4
U-1	0	0	0	0	0	0	0	0	0	0	0	0	0	0	0	1

[a]The first column from right represents the present-day configuration of the borehole: the value corresponds to the depth of the bottom of each unit. The last value of each column represents the thickness (decompacted) of each unit at the time of deposition (see Appendix A).

Table A2. Porosity Values Used in the Decompaction Process[a]

Unit Name	Age (kyr)															
	340	331	315	263	248	225	184	143	125	68	61	57.5	27.3	17.5	7.2	0
U-10/11	0.534	0.524	0.521	0.516	0.509	0.505	0.496	0.491	0.488	0.474	0.472	0.472	0.465	0.457	0.451	0.450
U-10	0	0.539	0.536	0.531	0.523	0.519	0.510	0.504	0.501	0.486	0.485	0.484	0.477	0.468	0.462	0.461
U-9	0	0	0.543	0.537	0.530	0.525	0.516	0.510	0.507	0.492	0.490	0.489	0.482	0.474	0.467	0.466
U-8/2	0	0	0	0.542	0.534	0.529	0.520	0.514	0.510	0.496	0.494	0.493	0.485	0.477	0.471	0.470
U-8/1	0	0	0	0	0.541	0.536	0.526	0.520	0.517	0.501	0.499	0.499	0.491	0.482	0.476	0.475
T-III	0	0	0	0	0	0.542	0.532	0.526	0.522	0.507	0.505	0.504	0.496	0.487	0.481	0.480
U-7	0	0	0	0	0	0	0.540	0.533	0.529	0.513	0.511	0.510	0.502	0.493	0.487	0.485
U-6	0	0	0	0	0	0	0	0.541	0.537	0.521	0.519	0.518	0.509	0.500	0.493	0.492
T-II	0	0	0	0	0	0	0	0	0.543	0.526	0.524	0.523	0.514	0.505	0.498	0.496
U-5	0	0	0	0	0	0	0	0	0	0.536	0.534	0.533	0.524	0.514	0.507	0.505
U-4/2	0	0	0	0	0	0	0	0	0	0	0.565	0.563	0.548	0.532	0.521	0.518
U-4/1	0	0	0	0	0	0	0	0	0	0	0	0.566	0.551	0.535	0.523	0.521
U-3	0	0	0	0	0	0	0	0	0	0	0	0	0.559	0.542	0.530	0.528
U-2	0	0	0	0	0	0	0	0	0	0	0	0	0	0.558	0.545	0.543
T-I	0	0	0	0	0	0	0	0	0	0	0	0	0	0	0.560	0.56
U-1	0	0	0	0	0	0	0	0	0	0	0	0	0	0	0	0.57

[a]The last values of each column represent the porosity of the sedimentary unit at the time of deposition. The reconstructed porosity is then used to obtain the bulk density (see Table A3 and Appendix A).

density of a volume of material calculated taking into account the relationship between the volume of pores, saturated with salt water, and the volume occupied by sediment. The value of bulk density must be calculated each time the most recent unit is removed from the sediment column in the process of decompaction, taking into account changes in porosity occurring at each step. To know how the average bulk porosity of each sediment layer varies in time [*Angevine et al.*, 1990] and, consequently, to calculate the porosity of each sediment unit at its new depth, we need to solve the following, where y_1 and y_2 are the new burial depths:

$$\Phi = \frac{\Phi_0}{c}\frac{\exp(-cy_1) - \exp(-cy_2)}{y_2 - y_1}. \tag{A7}$$

Table A2 shows the results.

[56] The bulk density (ρ_b) depends on the porosity and the density of sediment grains (ρ_s). The density of the sediment grains of each unit of the modern sediment section is obtained by taking the mean value from the PRAD1.2 sonic log (Table 1). The bulk density (Table A3) can be evaluated using

$$\rho_b = \Phi\rho_w + (1 - \Phi)\rho_s, \tag{A8}$$

and the bulk density of the entire sedimentary column ($\overline{\rho}_b$) made of n units is

$$\overline{\rho}_b = \sum_i \left\{ \frac{\Phi_i\rho_w + (1 - \Phi_i)\rho_{s(i)}}{S^*} \right\} \cdot T_i^*, \tag{A9}$$

where Φ_i is the porosity of the ith Unit at the time t, $\rho_{s(i)}$ is the grain density of the same Unit ($[\rho_{s(i)}]$ = kg/m^3), T_i* is the thickness of the ith Unit ($[T_i^*]$ = m), and S* is the total thickness of the decompacted sedimentary column at the time t ($[S^*]$ = m).

[57] Once we obtain the bulk density of the sediment column in each of the stages of deposition, we can apply the Airy correction for surface loads:

$$Z = S \cdot \left(\frac{\rho_a - \overline{\rho}_b}{\rho_a - \rho_w} \right), \tag{A10}$$

where Z is depth of the basin after Airy compensation ([Z] = m), S is thickness of the removed sediment section ([S] = m), ρ_a is density of the underlying material, under the sediment section ($[\rho_a]$ = 3330 kg/m^3), $\overline{\rho}_b$ is bulk density of the sedimentary column ($[\overline{\rho}_b]$ = kg/m^3), and ρ_w is density of salt water ($[\rho_w]$ = 1030 kg/m^3).

Appendix B

[58] Foraminifera distribution has been and still is one of the most used proxy to evaluate variations in paleodepth of past depositional environment. Nevertheless, advantages

Table A3. Bulk Density of Each Unit Obtained From Decompacted Porosity Values[a]

Unit Name	Decompacted Total Thickness (m)	Bulk Density (kg/m^3)
U-1	71.2	1444.7
T-I	70.415	1446.3
U-2	66.162	1448
U-3	60.461	1447.7
U-4/1	55.445	1448.5
U-4/2	54.899	1448.7
U-5	53.709	1449
T-II	44.173	1449.6
U-6	41.94	1449.3
U-7	38.195	1446
T-III	32.521	1441.5
U-8/1	29.716	1439.5
U-8/2	25.043	1435.3
U-9	21.783	1428.4
U-10	19.81	1423.5
U-10/11	13.368	1411.6

[a]See Appendix A.

and disadvantages of this method have been highlighted by recent studies of the ecological requirements of foraminifera. Water depth cannot be per se the only limiting factor for the life of benthic foraminifera [*Van der Zwaan et al.*, 1999]; food availability (flux) and oxygen content are considered among the factors more limiting benthic foraminifera distribution (see *Jorissen* [1999] for a review). Individual species are never good paleodepth markers, even if it is possible to distinguish species typical of deep waters and others of shelf environment.

[59] In this study, the paleobathymetry estimate has been obtained evaluating the composition of the benthic foraminifera assemblage (see Tables 3 and 5; from *Piva* [2007] and *Piva et al.* [2008b]), and ascribing to each assemblage the geomorphologic context (i.e., shelf, slope) along with the bathymetric range occupied by the assemblages and based on (local) models of distribution of the modern benthic foraminifera in the Adriatic Sea [*Jorissen*, 1988, 1987; *Van der Zwaan and Jorissen*, 1991; *Barmawidjaja et al.*, 1992; *De Stigter et al.*, 1998; *Morigi et al.*, 2005] and Mediterranean [*De Rijk et al.*, 1999]. However, the application of local bathymetric zonations has some limitations, as the absolute numerical estimates of depth are dependent on local flux variation [*Van der Zwaan et al.*, 1999]. In Tables 3 and 5 the benthic foraminifera assemblages are expressed by three ranks of abundance from which the bathymetric range has been obtained following the subsequent classification: in bold italics are reported the most abundant taxa (>20%), in underlined italics the common taxa (5–10%) and in italics the taxa with abundances between 1 and 5%. Moreover, it is necessary to consider that PRAD1–2 spans approximately the last 400 kyr and in many intervals the assemblages, present during glacials and interglacials, are dominated by taxa presently living neither in the Adriatic nor in the Mediterranean (for instance *Sigmoilina sellii* in MIS 2, *Islandiella islandica* and *Elphidium excavatum* forma *clavata* in MIS 6, 8 and 10). The bathymetric range for these species had therefore to be obtained from the extra-Mediterranean literature [*Miller et al.*, 1982; *Linke and Lutze*, 1993; *Jennings et al.*, 2004; *Murray*, 2006].

[60] To get a relatively more quantitative paleowater depth estimate, we also applied the formula developed by *Van der Zwaan et al.* [1990]. This method relies on the idea that planktonic and benthic foraminifera are both dependent on flux and that this dependency will be eliminated using the ratio between the two. The proposed formula is D = ln (a + b %P), with D = depth, a = 3.58718, b = 0.03534; %P = P/P + (B-infaunal), where P = number of planktic foraminifera specimens and B = number of benthic foraminifera specimens. The "a" and "b" values implies that if P = 100 the estimated paleobathymetry is 1250 m, while if P = 0 D is 36 m. Moreover, this method assumes negligible the dissolution of the tests and reworked specimens should not be counted and used for this purpose. As shown in the formula, the benthic term must be corrected for the presence of genera with infaunal habitat, such as *Bulimina*, *Globobulimina*, *Bolivina*, *Uvigerina* and *Fursenkoina*.

[61] In the first method described, the reconstructed bathymetric range does not depend on planktic foraminifera abundance; the method was applied to double-check the values obtained following *Van der Zwaan et al.* [1990], and, at places, to estimate paleodepth in intervals where *Van der Zwaan et al.*'s [1990] formula proved not applicable (for instance in environments shallower than 40 m and during sapropel events.).

[62] **Acknowledgments.** This study was supported by the EU project PROMESS1 (EVR1-2001-41), funded within the 5th Framework Programme. Antonio Cattaneo thanks ISMAR-CNR for financial support during a 6-month sabbatical leave in Bologna. We are grateful to Alessandro Amorosi and an anonymous reviewer for reviewing the manuscript and providing useful comments and suggestions. We also thank Eugenio Carminati for his help and interesting discussions on this subject and Marco Ligi, Valentina Ferrante, Marzia Rovere, and Elisabetta Campiani for their support on seismic processing and mapping. This is CNR- ISMAR Bologna contribution 1649.

References

Airy, G. B. (1855), On the computation of the effect of the attraction of mountain masses, *Philos. Trans. R. Soc. London*, *145*, 101–104, doi:10.1098/rstl.1855.0003.

Allen, P. A., and J. R. Allen (1990), *Basin Analysis, Principles and Applications*, 451 pp., Blackwell Sci., Cambridge, U.K.

Amorosi, A., M. L. Colalongo, F. Fusco, G. Pasini, and F. Fiorini (1999), Glacio-eustatic control of continental–shallow marine cyclicity from Late Quaternary deposits of the southeastern Po Plain, northern Italy, *Quat. Res.*, *52*, 1–13, doi:10.1006/qres.1999.2049.

Amorosi, A., M. L. Colalongo, F. Fiorini, F. Fusco, G. Pasini, S. C. Vaiani, and G. Sarti (2004), Palaeogeographic and palaeoclimatic evolution of the Po Plain from 150-ky core records, *Global Planet. Change*, *40*, 55–78, doi:10.1016/S0921-8181(03)00098-5.

Angevine, C. L., P. L. Heller, and C. Paola (1990), *Quantitative Sedimentary Basin Modeling*, *Educ. Course Notes*, vol. 32, 247 pp., Am. Assoc. of Pet. Geol., Tulsa, Okla.

Antonioli, F., et al. (2009), Holocene relative sea-level changes and vertical movements along the Italian and Istrian coastlines, *Quat. Int.*, *206*, 102–133, doi:10.1016/j.quaint.2008.11.008.

Asioli, A. (1996), High resolution foraminifera biostratigraphy in the Central Adriatic basin during the last deglaciation: A contribution to the PALICLAS Project, in *Palaeoenvironmental Analysis of Italian Crater Lake and Adriatic Sediments*, edited by F. Oldfield and P. Guilizzoni, *Mem. Ist. Ital. Idrobiol.*, *55*, 197–218.

Asioli, A., F. Trincardi, J. J. Lowe, D. Ariztegui, L. Langone, and F. Oldfield (2001), Sub-millennial scale climatic oscillations in the central Adriatic during the Lateglacial: Palaeoceanographic implications, *Quat. Sci. Rev.*, *20*, 1201–1221, doi:10.1016/S0277-3791(00)00147-5.

Athy, L. F. (1930), Density, porosity, and compaction of sedimentary rocks, *Am. Assoc. Pet. Geol. Bull.*, *14*, 1–24.

Bard, E., B. Hamelin, and R. G. Fairbanks (1990), U-Th ages obtained by mass spectrometry in corals from Barbados: Sea level during the past 130,000 years, *Nature*, *346*, 456–458, doi:10.1038/346456a0.

Barmawidjaja, D. M., F. J. Jorissen, S. Puskaric, and G. J. Van der Zwaan (1992), Microhabitats selection by benthic foraminifera in the northern Adriatic Sea, *J. Foraminiferal Res.*, *22*(4), 297–317, doi:10.2113/gsjfr.22.4.297.

Bassinot, F. C., L. D. Labeyrie, E. Vincent, X. Quidelleur, N. J. Shackleton, and Y. Lancelot (1994), The astronomical theory of climate and the age of the Brunhes Matuyama magnetic reversal, *Earth Planet. Sci. Lett.*, *126*, 91–108, doi:10.1016/0012-821X(94)90244-5.

Berger, A., and M. F. Loutre (1991), Insolation values for the climate of the last 10 million years, *Quat. Sci. Rev.*, *10*, 297–317, doi:10.1016/0277-3791(91)90033-Q.

Carminati, E., C. Doglioni, and D. Scrocca (2003), Apennines subduction-related subsidence of Venice (Italy), *Geophys. Res. Lett.*, *30*(13), 1717, doi:10.1029/2003GL017001.

Carminati, E., L. Corda, G. Mariotti, and M. Brandano (2007), Tectonic control on the architecture of a Miocene carbonate ramp in the central Apennines (Italy): Insights from facies and backstripping analyses, *Sediment. Geol.*, *198*, 233–253, doi:10.1016/j.sedgeo.2006.12.005.

Cattaneo, A., and F. Trincardi (1999), The late-Quaternary transgressive record in the Adriatic epicontinental sea: Basin widening and facies partitioning, in *Isolated Shallow Marine Sand Bodies: Sequence Stratigraphic Analysis and Sedimentologic Interpretation*, edited by K. Bergman and J. Snedden, *Spec. Publ. SEPM Soc. Sediment. Geol.*, *64*, 127–146.

Cattaneo, A., A. Correggiari, L. Langone, and F. Trincardi (2003), The late-Holocene Gargano subaqueous delta, Adriatic shelf: Sediment pathways and supply fluctuations, *Mar. Geol.*, *193*, 61–91, doi:10.1016/S0025-3227(02)00614-X.

Cattaneo, A., F. Trincardi, A. Asioli, and A. Correggiari (2007), The western Adriatic Shelf Clinoform: Energy-limited bottomset, *Cont. Shelf Res.*, *27*, 506–525, doi:10.1016/j.csr.2006.11.013.

Chappell, J., and N. J. Shackleton (1986), Oxygen isotopes and sea level, *Nature*, *324*, 137–140, doi:10.1038/324137a0.

Colantoni, P., A. Asioli, A. M. Borsetti, L. Capotondi, and C. Vergnaud-Grazzini (1989), Subsidenza tardo-pleistocenica ed olocenica nel medio Adriatico evidenziata dalla geofisica e da ricostruzioni paleoambientali, *Mem. Soc. Geol. Ital.*, *42*, 209–220.

De Rijk, S., S. R. Troelstra, and E. J. Rohling (1999), Benthic foraminiferal distribution in the Mediterranean Sea, *J. Foraminiferal Res.*, *29*, 93–103.

De Stigter, H. C., F. J. Jorissen, and G. J. Van der Zwaan (1998), Bathymetric distribution and microhabitat partitioning of live (Rose Bengal stained) benthic foraminifera along a shelf to deep sea transect in the southern Adriatic Sea, *J. Foraminiferal Res.*, *28*, 40–65.

Doglioni, C., F. Mongelli, and P. Pieri (1994), The Puglia uplift (SE Italy): An anomaly in the foreland of the Apenninic subduction due to buckling of a thick continental lithosphere, *Tectonics*, *13*, 1309–1321, doi:10.1029/94TC01501.

Ferranti, L., et al. (2006), Markers of the last interglacial sea-level high stand along the coast of Italy: Tectonic implications, *Quat. Int.*, *145–146*, 30–54, doi:10.1016/j.quaint.2005.07.009.

Jennings, A. E., N. J. Weiner, G. Helgadottir, and J. T. Andrews (2004), Modern foraminiferal faunas of the Southwestern to Northern Iceland shelf: Oceanographic and environmental controls, *J. Foraminiferal Res.*, *34*(3), 180–207, doi:10.2113/34.3.180.

Jordan, T. E., and P. B. Flemings (1991), Large-scale stratigraphic architecture, eustatic variation, and unsteady tectonism: A theoretical evaluation, *J. Geophys. Res.*, *96*, 6681–6699, doi:10.1029/90JB01399.

Jorissen, F. J. (1987), The distribution of benthic foraminifera in the Adriatic Sea, *Mar. Micropaleontol.*, *12*, 21–48, doi:10.1016/0377-8398(87)90012-0.

Jorissen, F. J. (1988), Benthic foraminifera from the Adriatic Sea: Principles of phenotypic variation, *Utrecht Micropaleontol. Bull. 37*, 174 pp., Utrecht, Netherlands.

Jorissen, F. J. (1999), Benthic foraminiferal microhabitats below the sediment-water interface, in *Modern Foraminifera*, edited by B. K. Sen Gupta, pp. 161–180, Kluwer Acad., Dordrecht, Netherlands.

Jouet, G., S. Berné, M. Rabineau, M. A. Bassetti, P. Bernier, B. Dennielou, F. J. Sierro, J.-A. Flores, and M. Taviani (2006), Shoreface migrations at the shelf edge and sea-level changes around the Last Glacial Maximum (Gulf of Lions, NW Mediterranean), *Mar. Geol.*, *234*, 21–42, doi:10.1016/j.margeo.2006.09.012.

Kent, D. V., D. Rio, F. Massari, G. Kukla, and L. Lanci (2002), Emergence of Venice in the Pleistocene, *Quat. Sci. Rev.*, *21*, 1719–1727, doi:10.1016/S0277-3791(01)00153-6.

Laj, C., C. Kissel, and A. P. Roberts (2006), Geomagnetic field behavior during the Iceland Basin and Laschamp geomagnetic excursions: A simple transitional field geometry?, *Geochem. Geophys. Geosyst.*, *7*, Q03004, doi:10.1029/2005GC001122.

Lambeck, K., F. Antonioli, A. Purcell, and S. Silenzi (2004), Sea-level change along the Italian coast for the past 10,000 yr, *Quat. Sci. Rev.*, *23*, 1567–1598, doi:10.1016/j.quascirev.2004.02.009.

Lea, D. W., P. A. Martin, D. K. Pak, and H. J. Spero (2002), Reconstructing a 350 kyr history of sea level using planktonic Mg/Ca and oxygen isotopic records from a Cocos Ridge core, *Quat. Sci. Rev.*, *21*, 283–293, doi:10.1016/S0277-3791(01)00081-6.

Linke, P., and G. F. Lutze (1993), Microhabitat preferences of benthic foraminifera: A static concept or a dynamic adaptation to optimize food acquisition?, *Mar. Micropaleontol.*, *20*, 215–234, doi:10.1016/0377-8398(93)90034-U.

Lisiecki, L. E., and M. E. Raymo (2005), A Pliocene-Pleistocene stack of 57 globally distributed benthic $d^{18}O$ records, *Paleoceanography*, *20*, PA1003, doi:10.1029/2004PA001071.

Lourens, L. J. (2004), Revised tuning of Ocean Drilling Program Site 964 and KC01B (Mediterranean) and implications for the $d^{18}O$, tephra, calcareous nannofossil, and geomagnetic reversal chronologies of the past 1.1 Myr, *Paleoceanography*, *19*, PA3010, doi:10.1029/2003PA000997.

Martinson, D. G., N. G. Pisias, J. D. Hays, J. Imbrie, T. C. Moore, and N. J. Shackleton (1987), Age dating and the orbital theory of the ice ages: Development of a high resolution 0 to 300,000-year chronostratigraphy, *Quat. Res.*, *27*, 1–29, doi:10.1016/0033-5894(87)90046-9.

Massari, F., D. Rio, R. Serandrei Barbero, A. Asioli, L. Capraro, E. Fornaciari, and P. P. Vergerio (2004), The environment of Venice area in the past two million years, *Palaeogeogr. Palaeoclimatol. Palaeoecol.*, *202*, 273–308, doi:10.1016/S0031-0182(03)00640-0.

Meese, D. A., A. J. Gow, R. B. Alley, G. A. Zielinsky, P. M. Grootes, M. Ram, K. C. Taylor, P. A. Mayewski, and J. F. Bolzan (1997), The Greenland Ice Sheet Project 2 depth-age scale: Methods and results, *J. Geophys. Res.*, *102*, 26,411–26,423, doi:10.1029/97JC00269.

Miller, A. L., D. B. Scott, and F. S. Medioli (1982), *Elphidium excavatum* (Terquem): Ecophenotypic versus subspecific variation, *J. Foraminiferal Res.*, *12*(2), 116–144, doi:10.2113/gsjfr.12.2.116.

Morigi, C., F. J. Jorissen, S. Fraticelli, B. J. Horton, M. Principi, A. Sabbatini, L. Capotondi, P. V. Curzi, and A. Negri (2005), Benthic foraminiferal evidence for the formation of the Holocene mud-belt and bathymetrical evolution in the central Adriatic Sea, *Mar. Micropaleontol.*, *57*, 25–49, doi:10.1016/j.marmicro.2005.06.001.

Murray, J. (2006), *Ecology and Applications of Benthic Foraminifera*, Cambridge University Press, New York.

Patacca, E., and P. Scandone (2004), The Plio-Pleistocene thrust belt: Foredeep system in the southern Apennines and Sicily, in *Geology of Italy: Special Volume of the Italian Geological Society for the IGC 32 Florence 2004*, edited by V. Crescenti et al., pp. 93–129, Società Geologica Italiana, Rome, Italy.

Pieri, M., and G. Groppi (1981), Subsurface geological structure of the Po plain, Italy, *Publ. 414*, 23 pp., P. F. Geodin., Cons. Naz. delle Ric., Rome.

Piva, A. (2007), Stratigrafia ad alta risoluzione dei depositi Quaternari in Adriatico centrale e meridionale: Impatto di cambiamenti climatici a scala sub-Milankoviana sulla circolazione in Mediterraneo, Ph.D. thesis, Univ. of Bologna, Bologna, Italy.

Piva, A., A. Asioli, R. R. Schneider, F. Trincardi, N. Andersen, E. Colmenero-Hidalgo, B. Dennielou, J.-A. Flores, and L. Vigliotti (2008a), Climatic cycles as expressed in sediments of the PROMESS1 borehole PRAD1.2, central Adriatic, for the last 370 ka: 1. Integrated stratigraphy, *Geochem. Geophys. Geosyst.*, *9*, Q01R01, doi:10.1029/2007GC001713.

Piva, A., A. Asioli, N. Andersen, J. O. Grimalt, R. R. Schneider, and F. Trincardi (2008b), Climatic cycles as expressed in sediments of the PROMESS1 borehole PRAD1.2, central Adriatic, for the last 370 ka: 2. Paleoenvironmental evolution, *Geochem. Geophys. Geosyst.*, *9*, Q03R02, doi:10.1029/2007GC001785.

Posamentier, H. W., and G. P. Allen (1993), Siliciclastic sequence stratigraphic patterns in foreland, ramp-type basins, *Geology*, *21*, 455–458, doi:10.1130/0091-7613(1993)021<0455:SSSPIF>2.3.CO;2.

Rabineau, M., S. Berné, J.-L. Olivet, D. Aslanian, F. Guillocheau, and P. Joseph (2006), Paleo sea levels reconsidered from direct observation of paleoshoreline position during Glacial Maxima (for the last 500,00 yr), *Earth Planet. Sci. Lett.*, *252*, 119–137, doi:10.1016/j.epsl.2006.09.033.

Ridente, D., and F. Trincardi (2002), Eustatic and tectonic control on deposition and lateral variability of Quaternary regressive sequences in the Adriatic basin (Italy), *Mar. Geol.*, *184*, 273–293, doi:10.1016/S0025-3227(01)00296-1.

Ridente, D., and F. Trincardi (2006), Active foreland deformation evidenced by shallow folds and faults affecting late Quaternary shelf-slope deposits (Adriatic Sea, Italy), *Basin Res.*, *18*(2), 171–188, doi:10.1111/j.1365-2117.2006.00289.x.

Ridente, D., F. Trincardi, A. Piva, A. Asioli, and A. Cattaneo (2008), Sedimentary response to climate and sea level changes during the past 400 ka from borehole PRAD1.2 (Adriatic margin), *Geochem. Geophys. Geosyst.*, *9*, Q09R04, doi:10.1029/2007GC001783.

Ridente, D., F. Trincardi, A. Piva, and A. Asioli (2009), The combined effect of sea level and supply during Milankovitch cyclicity: Evidence from shallow-marine $\delta^{18}O$ records and sequence architecture (Adriatic margin), *Geology*, *37*, 1003–1006, doi:10.1130/G25730A.1.

Rohling, E. J., M. Fenton, F. J. Jorissen, P. Bertrand, G. Ganssen, and J. P. Caulet (1998), Magnitudes of sea level lowstands of past 500,000 years, *Nature*, *394*, 162–165, doi:10.1038/28134.

Royden, L. E., E. Patacca, and P. Scandone (1987), Segmentation and configuration of subducted lithosphere in Italy: An important control on thrust-belt and foredeep-basin evolution, *Geology*, *15*, 714–717, doi:10.1130/0091-7613(1987)15<714:SACOSL>2.0.CO;2.

Sclater, J. G., and P. A. F. Christie (1980), Continental stretching: An explanation of the post-mid-Cretaceous subsidence of the central North Sea basin, *J. Geophys. Res.*, *85*, 3711–3739, doi:10.1029/JB085iB07p03711.

Scrocca, D. (2006), Thrust front segmentation induced by differential slab retreat in the Apennines (Italy), *Terra Nova*, *18*, 154–161, doi:10.1111/j.1365-3121.2006.00675.x.

Shackleton, N. J. (1987), Oxygen isotopes, ice volume and sea level, *Quat. Sci. Rev.*, *6*, 183–190, doi:10.1016/0277-3791(87)90003-5.

Skene, K. I., D. J. W. Piper, A. E. Aksu, and J. P. M. Syvitski (1998), Evaluation of the global oxygen isotope curve as a proxy for Quaternary sea level by modeling of delta progradation, *J. Sediment. Res.*, *68*, 1077–1092.

Sleep, N. H. (1971), Thermal effects of the formation of Atlantic continental margins by continental break up, *Geophys. J. R. Astron. Soc.*, *24*, 325–350.

Steckler, M. S. (1999), High resolution sequence stratigraphic modeling: 1. The interplay of sedimentation, erosion and subsidence, in *Numerical Experiments in Stratigraphy: Recent Advances in Stratigraphic and Computer Simulations*, edited by J. Harbaugh et al., *Mem. 62*, pp. 139–149, Soc. of Econ. Paleontol. and Mineral., Tulsa, Okla.

Steckler, M. S., and A. B. Watts (1978), Subsidence of the Atlantic-type continental margin off New York, *Earth Planet. Sci. Lett.*, *41*, 1–13, doi:10.1016/0012-821X(78)90036-5.

Sydow, J., and H. H. Roberts (1994), Stratigraphic framework of a late Pleistocene shelf-edge delta, Northeast Gulf of Mexico, *AAPG Bull.*, *78*, 1276–1312.

Tesson, M., C. Labaune, and B. Gensous (2005), Small rivers contribution to the Quaternary evolution of a Mediterranean littoral system: The western gulf of Lion, France, *Mar. Geol.*, *222–223*, 313–334, doi:10.1016/j.margeo.2005.06.021.

Thorne, J. A., and D. J. P. Swift (1991), Sedimentation on continental margins, VI: A regime model for depositional sequences, their component systems tracts, and bounding surfaces, in *Shelf Sand and Sandstone Bodies*, edited by D. J. P. Swift et al., *Spec. Publ. Int. Assoc. Sedimentol.*, *14*, 189–255.

Tosi, L., P. Teatini, L. Carbognin, and J. Frankenfield (2007), A new project to monitor land subsidence in the northern Venice coastland (Italy), *Environ. Geol.*, *52*, 889–898, doi:10.1007/s00254-006-0530-8.

Trincardi, F., and A. Correggiari (2000), Quaternary forced regression deposits in the Adriatic basin and the record of composite sea-level cycles, in *Depositional Response to Forced Regression*, edited by D. Hunt and R. Gawthorpe, *Geol. Soc. Spec. Publ.*, *172*, 245–269.

Vail, P. R., R. Mitchum Jr., R. Todd, J. Widmier, S. Thompson III, J. Sangree, J. Bubb, and W. Hatlelid (1977), Seismic stratigraphy and global changes of sea-level, in *Seismic Stratigraphy*, edited by C. E. Payton, pp. 49–212, Am. Assoc. Petrol. Geol., Tulsa, Okla.

Van der Zwaan, G. J., and F. J. Jorissen (1991), Biofacial patterns in river-induced anoxia, in *Modern and Ancient Continental Shelf Anoxia*, edited by R. Tyson and T. Pearson, *Geol. Soc. Spec. Publ.*, *58*, 65–82.

Van der Zwaan, G. J., F. J. Jorissen, and H. C. de Stigter (1990), The depth dependency of planktonic/benthic foraminiferal ratio: Constraints and applications, *Mar. Geol.*, *95*, 1–16, doi:10.1016/0025-3227(90)90016-D.

Van der Zwaan, G. J., I. A. P. Duijnstee, M. den Dulk, S. R. Ernst, N. T. Jannink, and T. J. Kouwenhoven (1999), Benthic foraminifers: Proxies or problems? A review of paleoecological concepts, *Earth Sci. Rev.*, *46*, 213–236, doi:10.1016/S0012-8252(99)00011-2.

Van Hinte, J. E. (1978), Geohistory analysis: Application of micropaleontology in exploration geology, *AAPG Bull.*, *62*, 201–222.

Waltham, D., C. Taberner, and C. Docherty (2000), Error estimation in decompacted subsidence curves, *AAPG Bull.*, *84*, 1087–1094.

Watts, A. B., and W. B. F. Ryan (1976), Flexure of the lithosphere and continental margin basins, *Tectonophysics*, *36*, 25–44, doi:10.1016/0040-1951(76)90004-4.

A. Asioli, IGG, CNR, Via Matteotti 30, 35137 Padova, Italy.

A. Cattaneo, GM-LES, Ifremer, 29280 Plouzané, France.

V. Maselli, Dipartimento di Scienze della Terra e Geologico-Ambientali, Univerisità di Bologna, Piazza di Porta San Donato 1, 40126 Bologna, Italy. (vittorio.maselli@bo.ismar.cnr.it)

D. Ridente, IGAG, CNR, Piazzale Moro 5, 00185 Rome, Italy.

F. Trincardi, ISMAR, Istituto di Scienze Marine (CNR), Via Gobetti 101, 40129 Bologna, Italy.

CHAPTER IV

Maselli, V., E. Hutton, A. Kettner, J. Syvitski and F. Trincardi, High-frequency sea level and sediment supply fluctuations during Termination I: An integrated sequence-stratigraphy and modeling approach from the Adriatic Sea (*Marine Geology*, Accepted under revision).

High-frequency sea level and sediment supply fluctuations during Termination I: An integrated sequence-stratigraphy and modeling approach from the Adriatic Sea

Vittorio Maselli[1,*], Eric Hutton[2], Albert Kettner[2], James Syvitski[2] and Fabio Trincardi[3]

[1] ISMAR-CNR, Istituto di Scienze Marine, Via Gobetti 101, 40129, Bologna, Italy; University of Bologna, Dipartimento di Scienze della Terra e Geologico-Ambientali, Piazza di Porta San Donato 1, 40126, Bologna, Italy

[2] ISTAAR, Institute of Arctic and Alpine Research, University of Colorado at Boulder, 1560 30th Street, Campus Box 450, Boulder, CO 80309-0450, USA

[3] ISMAR-CNR, Istituto di Scienze Marine, Via Gobetti 101, 40129, Bologna, Italy

[*] Corresponding Author: Vittorio Maselli, E-mail: vittorio.maselli@bo.ismar.cnr.it; Phone: +39-051-639-8878.

Abstract

After the end of the Last Glacial Maximum (LGM), Termination I recorded one of the fastest and highest amplitude eustatic oscillations of the late Quaternary: in less then 15 kyr (between ca. 20 and 5.5 kyr BP) sea level rose about 120 meters, with, at least, two steps of increased rate of ice melting and eustatic rise, called Meltwater ulses 1A and 1B. The Transgressive sedimentary succession deposited during this interval on several mid-latitude continental margins, among which the central Adriatic margin, includes three distinct units, each deposited during a specific interval of the last sea level rise. In particular, the central Adriatic middle TST unit (mTST), composed by two prograding sedimentary wedges separated by an erosional surface, appears the most complex of the three TST units. The mTST unit formed during an interval of extreme climatic instability including the Bölling-Allerød and until the Younger Dryas - Holocene transition. Sequence stratigraphy analyses, integrated by core samples and ^{14}C age estimates,

indicate an enhanced sediment flux during the deposition of the mTST unit, as a consequence of the high-frequency climatic oscillations occurred. Modeling simulations with HydroTrend v3.0, a hydrological water balance and transport model, show high rates of sediment delivery within the interval between 13.8 and 11.5 kyr BP as a consequence of increased rates of rainfall and partial melting of the Alpine glaciers. Reconstructions of the sediment architecture using 2D Sedflux 1.0C, a basin-fill model, reproduce the complexity of the internal architecture of the middle TST unit driven primarily by sea level. The internal unconformity within the mTST unit can best be explained by introducing a minor sea level fall during the Younger Dryas. This conclusion is supported by the presence of an extensive barrier-island-lagoon system at -75 m below sea level, corresponding to the YD time interval and representing the best evidence of paleo-shoreline for this interval.

Keywords: Numerical Modeling, Sea level, Adriatic Sea, Transgressive sediments, Younger Dryas.

1. Introduction

The late Pleistocene-Holocene deglaciation was accompanied by intense climatic oscillations governed by changes in the summer insolation tuned by the Milankovian cyclicity and by higher frequency internal feedback processes in the land ocean interaction (Ruddiman and McIntyre, 1981; Bond et al., 1997). High northern latitude insolation, atmospheric CO_2, and tropical Pacific sea surface temperatures are considered the main mechanisms governing the growth of ice sheets and mountain glaciers, which reached their maximum extent ca. 26 kyr BP (Clark et al., 2009). During the Last Glacial Maximum (LGM), between 26 and 19 kyr, the north Atlantic polar front moved southward, reaching ca. 45° N, and sea level fell to its lowest position of about -120 meters (Ruddiman and McIntyre, 1981; Bard et al., 1996; Clark et al., 2009). The stability of ice caps has a strong relation with climatic cycles and in turn controls the climatic evolution by influencing the oceanic thermohaline circulation by introducing fresh water from ice and snow melt. The post LGM period, started about 19 kyr with an early sea level rise of 10-15 meters due to the melting of part of the northern hemisphere ice sheets (Clark et al., 2004), was punctuated by high-frequency climatic cycles, the most important of which was the Bölling-Allerød to Younger Dryas transition (Bond et al., 1992; Alley et al., 1993; Bond et al., 1997). Depending on this climatic complexity, sea level rise showed two rapid steps connected to two intervals of enhanced fresh water discharge, called Meltwater pulses 1A and 1B, starting at 14.2 and 11.3 kyr BP respectively (Fairbanks, 1989). During these phases sea level rose each time about 20 meters in less then 500 yr (Bard et al., 1990; Bard et al., 1996; Clark et al., 2002). Even if the magnitude, the timing and the potential source of the two Meltwater events are constrained, the cause of the Younger Dryas (YD) cold event and the extent of its impact on sea level changes and ice sheets stability are still debated (Carlson, 2010). The fast sea level rise occurred during Meltwater pulses 1A and 1B and the major climatic cooling of the YD event between them had a big influence also on the sediment deposition along continental margins (Cattaneo and Trincardi, 1999; Blanchon and

72 Shaw, 1995).

73 The transgressive sedimentary succession (Transgressive Systems Tract, TST) deposited
74 during the last sea level rise records the impact of these short-term climatic fluctuations on clastic
75 continental margins through the deposition of geometrically complex sedimentary bodies. High-
76 resolution sequence stratigraphic studies, integrated by core sampling and ^{14}C dates, show that the
77 Mediterranean continental margins are an ideal site to study these factors (Hernández-Molina et al.,
78 1994; Trincardi et al., 1996b; Cattaneo and Trincardi, 1999; Labaune et al., 2005; Berné et al.,
79 2007). We apply this approach to the central Adriatic margin to recognize the fingerprint of the
80 main sub-Milankovian climatic events that punctuated the late Quaternary Termination I, and to
81 disentangle the contribution of each process and its impact.

82 The central Adriatic late Pleistocene-Holocene transgressive deposit, formed between 19
83 kyr and 5.5 kyr BP and records the last sea level rise from -118 ± 2 m (Bard et al., 1996) to its
84 modern position (Trincardi et al., 1996a, 1996b). The internal geometry of the TST comprises 3
85 main units, bounded by regional erosion surfaces formed during intervals of decreased sediment
86 supply and accelerated sea level rise connected to the two Meltwater events (Cattaneo and
87 Trincardi, 1999); in particular the middle TST deposit, as equivalent deposits on other
88 Mediterranean margins (Hernández-Molina et al., 1994; Labaune et al., 2005; Berné et al., 2007),
89 records a phase of intense sediment supply and still-stand (or possibly a fall) sea level, related to the
90 Younger Dryas cold event. The results obtained from sequence stratigraphy analysis of the Adriatic
91 margin are then integrated by modeling simulations of the sediment discharge since the Last Glacial
92 Maximum to reproduce the internal architecture of the TST deposit and to understand the impact on
93 the margin stratigraphy of the two Meltwater pulses 1A and 1B and of the Younger Dryas cold
94 event. This goal was achieved using the two complementary models: HydroTrend v.3.0. and 2D-
95 Sedflux 1.0C (Syvitski and Hutton, 2001; Kettner and Syvitski, 2008a; Hutton and Syvitski, 2008).
96 The climate-driven hydrological model HydroTrend simulates the Po River sediment discharge
97 since the LGM (Kettner and Syvitski, 2008b) and works coupled with 2D-Sedflux, a two-

98 dimensional basin-filling model that generates stratigraphy and sediment architecture using a
99 collection of individual processes.
100
101 **2. Regional Setting**
102
103 The Adriatic Sea is a temperate semi-enclosed basin (elongated 800 km, in the NW-SE
104 direction and 200 km across) in the centre of the Mediterranean Sea. Bordered by three mountain
105 chains, the Alps to the north, the Apennine to the west and the Dinaric Mountain to the east, the
106 northern Adriatic Sea is part of the foreland domain between the Apennine and the Dinaric chains
107 (Royden et al., 1988). The western sector of the central and northern part is a Plio-Quaternary
108 foredeep basin originated during the formation of the Apennine chain and progressively migrated
109 eastward with the advance of the Apennine subduction. South of the Gargano promontory the
110 modern thrust front is located onshore and it is represented by the Bradanic trough (**Fig. 1**). The two
111 domains are separated by the Tremiti High (**Fig. 1**), which represents a right lateral transfer zone
112 between the two areas characterized by different lithospheric thickness and differential rollback
113 behaviors (Doglioni et al., 1994).
114 The modern Adriatic Sea is a mud-dominated system with the Po River, located in the
115 northwestern corner, representing the main sediment entry point. The basin can be divided into
116 three different sectors on the base of seafloor morphology. The northern area is characterized by a
117 shallow continental shelf, extending southward about 350 km from the gulf of Venice and gently
118 dipping of ca. 0.002°, representing the result of several southward progradations driven by sea level
119 cycles (Ridente et al., 2008). The central Adriatic Sea is a small remnant basin reaching 260 m
120 water depth (the Mid Adriatic Deep, MAD), confined to the north by the Po River delta, formed
121 during the last sea level lowstand, and to the south by the Gallignani-Pelagosa ridge. The MAD
122 provides one of the best high-resolution marine records of the entire Mediterranean Sea for the post
123 LGM interval: indeed, this region recorded most of the sub-millennial climatic oscillations

124 discovered in the Northern Hemisphere ice core stratigraphy (Asioli et al., 2001). On the continental
125 shelf adjacent to the MAD, the post-glacial interval records the same climatic oscillations through
126 the deposition of a thick and laterally variable deposit (Cattaneo and Trincardi, 1999).
127
128 **2.1. Po River Hydrology**
129
130 The modern Po River is a 673 km long river characterized by a relatively steep gradient,
131 upstream of its closure point (Pontelagoscuro, see **Figure 2**), located ca.100 km landward of the
132 delta mouth of *Po di Pila*. The watershed receives water and sediment from a 74500 km^2 drainage
133 area, of which more than 30800 km^2 are above 200 m in elevation, by more than 140 tributaries
134 (Correggiari et al., 2005). The suspended sediment delivered to the Adriatic basin by the modern Po
135 River and by the numerous Apennine rivers draining the eastern side of the Apennine chain north of
136 the Gargano promontory is about 42 $x10^6$ t/yr, of which ca. 15 $x10^6$ t/yr is provided by the Po River,
137 that is also the main source of fresh water: the average discharge measured at Pontelagoscuro (see
138 the map in **Figure 2**) in the time interval between 1918 and 2003 is about 1.525 $x10^3$ m^3/s, reaching
139 values of 12 $x10^3$ m^3/s during the main flood events (Nelson, 1970). The sediment delivered by the
140 Po River and the other Apennine rivers during the last 5.5 kyr, corresponding to the modern high
141 stand of sea level, is deposited in a continuous sedimentary body along the western side of the
142 Adriatic Sea, forced by the cyclonic circulation (Cattaneo et al., 2003; Cattaneo et al., 2007; **Fig. 2**).
143 In contrast, during the LGM the drainage system was more than twice as large, reaching
144 about 190000 km^2 (see **Fig. 2**). As highlighted by seismic profiles, during the LGM the "Mega" Po
145 River was the only source of fresh water and sediment load to the basin, collecting most of the
146 Apennine and Alpine rivers, as well as few minor rivers flowing from the western Dinaric front (De
147 Marchi, 1922; Cattaneo et al., 2003). The sediment carried by the Po River during the last glacial
148 period filled progressively the western side of the MAD, forming a lowstand sedimentary body
149 thicker than 200 m, in less then 15 kyr (Trincardi et al., 1996a).

3. METHODS

A dense grid of high-resolution CHIRP profiles allows the definition of the late Quaternary post LGM depositional sequence in the central Adriatic margin, and the recognition of its internal architecture on the basis of seismic reflector geometry and regional correlation. The seismic-stratigraphic interpretation was constrained by the reinterpretation of previous work on a large number of sediment cores through multi-proxy stratigraphic analyses (formanifera ecozonation, pollen spectra, magnetic susceptibility and stable isotopes), supported by ^{14}C age estimates and tephrostratigraphy (Asioli et al., 2001; Piva et al., 2008a, 2008b, 2008c; Bourne et al., 2010).

The geological interpretation derived from the integration of seismic-stratigraphic and core data was then compared with the results of modeling simulations obtained from two coupled models: HydroTrend v3.0 (Kettner and Syvitski, 2008a) used to quantify the sediment and water discharge for the last 21 kyr BP and 2D-Sedflux1.0.C to predict margin stratigraphy (Syvitski and Hutton, 2001).

4. HydroTrend v3.0

Hydrotrend 3.0 (Kettner and Syvitski, 2008a) is a numerical climate driven model that simulates water and sediment discharge, as suspended load and bedload, at a river mouth. Here it has been applied to simulate the sediment and water fluxes of the Po River during the last 21 kyr (Kettner and Syvitski, 2008b). Discharge predictions are based on multi-proxy input parameters describing the drainage-basin characteristics and the climate parameters and constrains. The drainage properties of the basin include river networks, cumulative hypsometric curves, reliefs and reservoir distributions, average basin temperature, precipitation and evapotraspiration, elevation of the glacier equilibrium line altitude (ELA), soil properties and hydraulic conductivity. Some of the

parameters listen above are assumed constant throughout the simulation to average present day values (as soil properties, hydraulic conductivity and evapotraspiration), not being possible to estimate during past times.

The water discharge at the river mouth (Q_T) is function of 5 different parameters (precipitation, basin location, temperature, elevation and soil properties) that can be summarize in the following equation (for a detailed description of the variables and relative dimensions used in this paper see **Table 1**):

$$Q_T = Q_{rain} + Q_{ice} + Q_{nival} \pm Q_{gr} - Q_{evap}$$

The parameters Q_{nival} and Q_{ice} have an important role in the Po River hydrology because the Alpine glaciers strongly influence the hydrological balance during glacial time and subsequent warming phases. The glacier equilibrium line altitude, in combination with hypsometric information is used to quantify the glacier area, with the assumption that 33% of the glacier is below ELA and represents the ablation zone, while the 66% above ELA is the accumulation zone; glacier volume is then obtained from glacier area using an exponential relation (Kettner and Syvitski, 2008a).

The total average suspended sediment discharge can be defined as the sum of average suspended sediment controlled by climatic and basin properties plus an additional values which accounts for sediment generated by glaciers:

$$\overline{Qs_T} = \overline{Qs_d} + \overline{Qs_g}$$

The long-tern average suspended load can be obtained using three different models (for a detailed description of each model see Kettner and Syvitski, 2008a). For the Adriatic area either the *QRT* or the *QART* model better simulate climate scenarios that are strongly influenced by changes in precipitation (Kettner and Syvitski, 2008b). In this study the *QRT* model was chosen to simulate the suspended sediment load, which is defined as:

$$\overline{Qs_d} = (1 - TE)\alpha_6 \overline{Q}^{\alpha_7} R^{\alpha_8} e^{k_2 \overline{T}}$$

200 *TE* is the trapping efficiency rate of reservoirs; this parameter plays an important role in the
201 sediment flux of the Po River as the drainage area is characterized by 5 water bodies (Lugano,
202 Como, Iseo, Maggiore and Garda Lakes) formed by moraine dams during Holocene glacial retreat.
203 The daily simulation of suspended sediment load is obtained in HydroTrend using the stochastic
204 model "*PSI*" of Morehead et al. (2003).
205 The last parameter to take into account in the total sediment flux to the basin is the bedload.
206 In HydroTrend the delta plain slope characteristics and the daily average water discharge are the
207 main parameters affecting the bedload transport, and are related in the following equation:

208 $$Q_b = \left(\frac{\rho_s}{\rho_s - \rho}\right) \cdot \frac{\rho g Q^{\beta} S e_b}{g \tan \lambda} \quad \text{when } u \geq u_{cr}$$

209

210 **4.1. HydroTrend Input parameters**

211

212 The drainage area of the Po River has been strongly influenced by the eustatic fluctuations
213 from the LGM onwards. During the LGM sea level was about 120 m below present level (Bard et
214 al., 1996) and so all the north Adriatic shelf was exposed forming an extensive alluvial plain from
215 the modern Po River delta to the north side of the MAD (see **Figure 2**). The paleo-drainage area of
216 the Po River during glacial condition has been reconstructed considering the modern bathymetry,
217 dropping the sea level of about 120 meters, and merging the result with surface elevation data: the
218 drainage area increases from 74500 km^2 of modern extension to about 190000 km^2 during LGM
219 (**Fig. 2**).
220 The Late Pleistocene to Holocene sea level rise has been modelled in 23 time steps, in order
221 to have the best resolution during phases of faster sea level rise such as the Meltwater pulses. The
222 sea level curve applied for this simulation (**Fig. 3**) is obtained by fitting eustatic curves from
223 different authors (Fairbanks, 1989; Chappell and Polach, 1991; Bard et al., 1996). An additional
224 new theoretical eustatic curve was introduced, which accounts for a possible minor sea level fall (of

about two meters) during the Younger Dryas cold event to reproduce the internal geometry of the middle unit of the central Adriatic TST.

The monthly climate statistics for the glacial period are estimated using the Community Climate Model-1 (Kutzbach et al., 1998). The modelled climate statistics as well as the ELA for LGM are combined with modern climate data and ELA estimates and interpolated for the last 21 kyr using a normalize ^{18}O GRIP curve to force the changes through time (Kettner and Syvitski, 2008b). The use of GRIP ice core as a forcing factor of the model is plausible, despite the large spatial distance between Greenland and the Adriatic Sea, because of the proved correlation with isotopic and bio-stratigraphic data from the central Adriatic (e.g. PRAD1.2 borehole, Piva et al. 2008a, 2008b). **Figure 3** shows the yearly averaged precipitation, temperature and ELA values during the last 21 kyr (Kettner and Syvitski, 2008b). The Late glacial (21 – 17 kyr) was characterized by an average temperature of 13.9 +/- 1 °C, and average annual precipitation of 0.8 +/-0.07 meters of water, and can be considered the coldest and driest period of the last 21 kyr. The Bölling-Allerød interval (14.7 – 12.8 kyr BP) is a period of very unstable climatic conditions. The onset of the Bölling records a rapid shift toward warmer and wetter climate in respect to the previous Oldest Dryas: the potential ELA was rapidly increasing, changing from 2500 m to 3000 m in less then 300 yr, and peaks in temperature of more than 19 °C and in precipitation of 1.35 m/yr can be recorded. The Bölling-Allerød transition is marked by the Meltwater pulse 1A, which has a big impact on the drainage area of the Po River, and by the short cold interval of the Older Dryas. The Allerød is still a period of warm climatic conditions, characterized by average temperature of 16.5 +/- 1.1 °C and by the shifting of the ELA toward lower elevation, but also records a phase of climatic deterioration, culminating with the YD event. The onset of the Younger Dyas (ca. 12.8 kyr BP) records an abrupt shift toward colder and dryer climatic conditions, reaching values comparable to those of Late glacial interval: 14.2 +/- 1.3 °C average temperatures and 0.8 +/- 0.008 m/yr of precipitation. The end of the YD interval was characterized by two centuries of very unstable climatic conditions: during this interval the ELA changes from 2400 to 3000 meters, the

temperature maxima from 13 to 17.5 °C and the precipitations from 0.8 to 1 m/yr, punctuated by high intensity annual storm events. The interval covered by the HST, 5.5 kyr to present-day, was characterized by higher temperature and precipitation values, and by more stable climatic conditions.

5. 2D-Sedflux 1.0C

2D-Sedflux is a 2-dimensional basin-fill model that predicts basin stratigraphy considering evolving boundary conditions (sea floor bathymetry, sea level and coastline position, sediment flux) to create sedimentary body architecture (Syvitski and Hutton, 2001; Hutton and Syvitski 2008). Sediments are delivered to the basin through a single river; an input file characterizes the river mouth dynamics and the kind of sediment: each grain size is characterized by grain diameter, bulk density, diffusion coefficient and removal rate.

The river mouth dynamics are described by water discharge Q_0, mean suspended load Qs_0 and bedload Q_b transport. The water discharge Q_0 includes three hydraulic parameters that are necessary to describe the initial boundary conditions for surface plumes:

$$Q_0 = u_0 b_0 h_0$$

The hydraulic components are: u_0 river flow velocity, b_0 channel width and h_0 channel depth.

The suspend load carried by the river into the basin is function of the ith grain size intervals (Cs_i):

$$Qs_0 = Q_0 \sum_{i=1}^{n} Cs_i$$

The bedload transport is obtained from the relationship developed by Bagnold (1966) and is function of the water-sediment density contrast, of the slope of the riverbed and of the discharge. The river's suspended sediment load is distributed as a surface plume or as a hyperpycnal flow, depending on the density contrast between river and basin water, while the river bedload can be

276 spread over specified distance, favoured by failure processes or turbidity currents. The suspended
277 sediment is advected by the river-induced velocity field, diffused by the fluid turbulence and
278 deposited from the plum by a first order removal rate, depending on the grain size (Syvitski and
279 Alcott, 1993).

280 The governing equation is the steady 2-dimensional advection-diffusion equation:

281 $$\frac{\partial uI}{\partial x}+\frac{\partial vI}{\partial y}+\lambda I=\frac{\partial}{\partial x}\left(K\frac{\partial I}{\partial x}\right)+\frac{\partial}{\partial y}\left(K\frac{\partial I}{\partial y}\right)$$

282 where:

283 x and y are the axial and lateral directions, u and v are the axial and lateral velocity, I is the
284 sediment inventory of the plume, λ is the first order removal rate constant for each grain size, K is
285 the sediment diffusivity. The sediment deposited from the plume can be resuspended by many
286 processes that are assimilated to be a single diffusive process, controlled by a diffusion constant,
287 which falls off exponentially with increasing water depth and reflects the maximum energy of the
288 coastal process.

289 The sediment load accumulating on the shelf and the water load due to changes in sea level
290 imply isostatic subsidence of the Earth's surface. Subsidence can be modelled using an elastic beam
291 that is allowed to flex: a more rigid beam records a broader and shallower deflection compared to a
292 less rigid beam characterized by deeper and narrower deflection. The rigidity of the lithosphere can
293 be estimated using the effective elastic thickness (Watts, 1992):

294 $$E_T=\sqrt[3]{\frac{12(1-\eta^2)D}{\sigma}},$$

295 with $\}^2$ Poisson's ratio and σ Young's modulus and D flexural rigidity. For the central
296 Adriatic margin the values are obtained in Royden (1988):

297 E_T= 10 km, D = 7.2 x10^{21} Nm and σ/(1-η^2) = 8.7 x10^{10} N/m^2.

298 In Sedflux the subsidence of a sedimentary basin is modelled using two different
299 approaches: one referring to the isostatic compensation for sediment and water load changes and

one due to tectonics, modelled specifying the subsidence rates at various positions and times. The elastic flexure approach requires four basic assumption: the lithosphere is assumed to have a linear elastic rheology, the deflection needs to be small, the lithosphere is thin compared to the horizontal dimension and planar sections within the plate are assumed to remain planar after deflection.

For a single vertical load applied, the displacements are given by:

$$w(x) = \frac{p(x)\alpha^3}{8D}\exp\left(-\frac{|x|}{\alpha}\right)\left(\cos\left(-\frac{|x|}{\alpha}\right)+\sin\left(-\frac{|x|}{\alpha}\right)\right) \quad \text{with } \alpha = \sqrt[4]{\frac{4D}{\rho_m g}}.$$

$w(x)$ is the vertical displacement of the crust referring to an horizontal position, ρ_m is the density of the overlying sediments and D is the flexural rigidity of the Earth's crust. Because of the assumption of the linearity of the system, the resulting displacement due to multiple vertical loads is simply the sum of the displacements due to each individual load.

The last process to be taken into account in the basin fill modeling is the sediment compaction. The porosity of a sedimentary column is a function of the grain size and of the sediment load. In Sedflux the sediment is able to compact to a minimum value only through mechanical process, as shown by the following relationship:

$$\frac{\partial\phi}{\partial\sigma} = -c\left(\phi - \phi_0\right)$$

where σ is the load, ϕ is the porosity, c is an empirical constant and ϕ_0 is the final porosity at its minimum value.

5.1. Sedflux Input parameters

Sedflux requires 7 input files, as described in Syvitski and Hutton (2001). The first file contains the model parameters such as time duration of the model, spatial resolution and basin geometry, the characteristic of the sediment, and all the constants used for sediment transport. The

second file contains the initial bathymetry, which is obtained by seismic profiles ST05 and ST06, (see **Figure 4**) mapping the modern depth of the unconformity (ES1) connected to the last sea level fall (Trincardi et al. 1996a; Cattaneo and Trincardi, 1999; Clark et al., 2009). Before starting the simulations, the bathymetric profile has to be restored at the time of the Last Glacial Maximum by a 2D flexural model (Kubo et al., 2006), in order to account for the sediment load of the Transgressive and Highstand deposits, estimate the effect of the water load due to the sea level rise and construct a more realistic paleo-morphology (**Fig. 4**). The third input file specifies the information to simulate a surface sediment plum, as a function of the concentration of the sediment in the basin and seawater density. The fourth input file includes the river discharge values, which are obtained from the HydroTrend simulation of the Po River discharge during the last 21, assumed to be the only source of sediment during the LGM period. The size of sediment used for the simulation of HydroTrend is specified also in Sedflux as the fifth input file. The sediment is composed of 4 different grain sizes. The sixth input file defines the sea level curve. The last input file specifies the tectonic driving force: subsidence or uplift rates are specified for various times and at different horizontal positions.

6. Results

6.1. Stratigraphy of late-Quaternary TST deposits in the Central Adriatic

The late Pleistocene-Holocene transgressive deposits (Transgressive Systems Tract or TST) deposited during a phase of rapid but not monotonic sea level rise between ca. 19 to 5.5 kyr BP (Bard, 1996; Asioli, 1996; Cattaneo and Trincardi, 1999). On the north Adriatic shelf, the late-Quaternary TST is composed of patchy barrier island and incised valleys systems (**Fig. 1**); in the central Adriatic, the TST is composed by a composite sedimentary body thicker than 25 meters and mainly pelitic, laying between a regional unconformity (surface ES1), below, and the maximum

flooding surface (mfs), above, that can be divided in three units separated by two regional surfaces (S1 and S2, see **Figure 4** and **Figure 5**; Cattaneo and Trincardi, 1999).

The complex internal geometry of the central Adriatic TST reflects the interaction between sea level rise, lateral changes in sediment accumulation delivery and the interaction between marine circulation and preexisting sea floor morphology. Each unit records distinct phases of the last sea level rise: the basal unit records the sea level rise between -120 and -95 meters, the middle unit between -95 and -60 meters, and the upper unit between -60 meters and the position of the shoreline reached at the time of maximum marine ingression, 5.5 kyr BP (Cattaneo and Trincardi, 1999).

Seismostratigraphic correlations indicate that the lower TST unit (LTST), comprised between the surfaces ES1 and S1, includes two distinct depocenters, located respectively southwest of the MAD and around the Tremiti High (see **Figure 5**). Dated samples along the central Adriatic shelf (cores PAL94-8 and PAL94-9) and correlations from the deepest part of the basin (core CM92-43) indicate that the LTST unit recorded the early phases of the last sea level rise, between ca. 17 kyr and 14.5 kyr (Cattaneo and Trincardi, 1999). During this interval the basin was characterized by cold water, as suggested by the presence of *G. bulloides* and *G. quinqueloba*, and influenced by fresh water inputs, as testified by the presence of *A. perlucida* in core PAL94-8, likely recording the location of the Po River and other Apennine deltas closer to the MAD (Asioli, 1996). The middle TST unit (mTST) accumulated on the inner-mid shelf, forming a prograding wedge thicker than 10 meters, and in the MAD, forming a continuous unit of marine mud. Stratigraphic correlations with core CM92-43, and the recognition of tephra C-2 and Y1 in core PAL94-8 (Calanchi et al., 1998), indicate that surface S1 was older than 14.5 kyr BP (Cattaneo and Trincardi, 1999).

The upper TST unit (uTST), confined between surface S2 and the mfs, records the last phases of the sea level rise. This unit is composed of marine muddy sediments and shows two main depocenters, both onlapping landward: one is located landward of the present day shoreline, the second is instead a marine onlap found in about -90 m against depositional reliefs generated by the

underlying middle TST deposit. The upper TST unit is composed of marine mud, rich in planktic foraminifera with assemblages typical of the outer shelf to upper slope environment. Dated samples show that the upper TST unit covers the period between the end of the Meltwater 1B (ca. 11.5 – 11.1 kyr BP, Bard et al., 1996) and the maximum marine ingression, ca 5.5 kyr BP (See **Figure 5** and **6**).

6.2. Stratigraphy of the middle TST unit

The middle unit of the Transgressive Systems Tract is confined by two regional surfaces (S1 and S2). Along the shelf the mTST unit consists of three main depocenters elongated parallel to the coast, reflecting local deltaic entry points and alongshore-oceanographic currents (Cattaneo and Trincardi, 1999; **Fig. 5**). In both areas the mTST unit, formed by a 10-15 m thick deposit in the inner-middle shelf pinching out basinward, includes etherolitic facies with sharp-based sandy layers and displays seaward dipping internal reflectors, separated into two prograding bodies (named mTST-1 and mTST-2 sub-unit from the lower) by an internal unconformity (surface Si, **Figure 5** and **6**). The mTST-1 sub-unit is composed by very low angle basinward dipping reflectors, with a direction of progradation oblique to the coast, and truncated at their top by unconformity Si, that extends down to -87 m depth below sea surface. The mTST-2 sub-unit, more than 8 m thick, is located more landward than mTST-1 sub-unit and consists of higher angle downlapping reflectors, prograding beyond the limit reached by mTST-1 sub-unit, and is eroded at the top by surface S2; this surface is erosive down to -90 m depth below sea surface. The mTST unit was cored in 5 sites: on the shelf, by borehole PRAD2-4 (inner shelf), cores RF95-13 and RF95-14 (middle shelf), cores PAL94-8, PAL94-9 (outer shelf to upper slope), and by core CM92-43 in the MAD (**Fig. 4** and **6**). Cores RF95-14 and RF95-15 penetrated the top of the mTST-2 sub-unit: dated ^{14}C sample on the RF95-14, two meters below surface S2, gives an age of 12337-11750 cal BP. Benthic foraminifera and mollusk content indicate that the sampled unit deposited in less than 30 m water depth. Another

^{14}C age estimate, available from borehole PRAD2-4, 27.5m below sea floor, is 11095-10687 cal BP (**Fig. 4**). Further chronological constraints come from cores PAL94-8 and PAL94-9, retrieved from the outer shelf, that reached the distal equivalent of the mTST unit (**Fig. 6**): in both cores this unit is replaced by a coarser layer corresponding to the merged S1+S2 unconformity (PAL94-9) and by a thin interval (less than two meters) of reworked material and mixed foraminifera assemblages (PAL94-8).

The tripartite Transgressive systems tract architecture, and in particular its composite middle TST unit, have a time-equivalent marine stratigraphic record in the MAD basin, where detailed stratigraphic analyses were conducted (core CM92-43, Asioli et al., 1999; 2001). Shelf to basin seismic stratigraphic analyses, integrated by core transects, indicate that the TST forms two complementary records on the inner-mid shelf and in the basin, respectively (**Fig. 6**). Foraminifera and pollen spectra analyses, integrated by δ^{18}O curves derived from both planktic (*Globigerina bulloides*) and benthic (*Bulimina margina*) foraminifera species (Asioli et al., 1999), document a rapid warming of surface water at ca. 14.6 kyr BP (peak abundance of *Globigerinoides* ex gr. *ruber*, among foraminifera) followed by an oscillatory cooling trend documented by a decline of all foraminifera and pollen indicators of warm climatic conditions (Asioli et al., 2001). A pronounced excursion in δ^{18}O on *G. bulloides* toward lighter values, at ca. 13.5 kyr BP during the Allerød, records an increase of freshwater discharge and influx of fluvially derived material. This short interval of increased freshwater discharge reflects the melting of Alpine and Apennine glaciers following the warming of the Bölling interval (Asioli et al., 2001), and may explain the evidence of an increased sediment delivery during the deposition of the mTST-1 sub-unit.

The cooling trend culminates with the Younger Dryas event, during which the warm species of *G.* ex gr. *ruber* is replaced by cold-water species (*G. bulloides* in **Figure 6**) and the pollen record shows a parallel turnover (decrease of *Quercus* and an increase of *Artemisia* in **Figure 6**), indicating cold and dry climatic conditions confirmed by the heaviest values of the *G. bulloides* δ^{18}O. The Younger Dryas event terminated abruptly ca. 11.5 kyr BP, as highlighted by the rapid

428 shift toward lighter values of the $\delta^{18}O$ and the abundance decline of *G. bulloides*, replaced by *G.* ex
429 gr. *ruber*, and corresponding to surface S2, atop the progradational deposits seen on the continental
430 shelf.

431 The greatest complexity of the mTST unit is reached in the area between the Tremiti High
432 and the Gargano promontory (see **Figure 7** and **8**). Also here the mTST unit consists of two
433 different units, separated by the internal unconformity Si. The mTST-1 sub-unit is formed by
434 laterally continuous shingled reflectors truncated, at their top, by surface Si (Cattaneo and
435 Trincardi, 1999). At depths between -90 and -85 meters below sea surface, a field of asymmetric
436 dunes, more then two meters high, correlates to surface S2. Landward of the dunes, a thick coarser
437 sandy unit (mTST-2 sub-unit) extends toward a shallower position, less then -80 meters, and
438 culminates with a complex sedimentary body, characterized by small scale erosions and bi-
439 directional downlapping reflectors interpreted as bay-head or flood-tidal deltas (Boyd et al., 1992;
440 Dalrymple et al., 1992; see **Figure 8**). Reflector S2 was sampled south of the Tremiti High in -82
441 meters of water depth: in the four cores (RF93-65, RF93-67, RF93-69, YD97-1, see **Figure 7**)
442 reflector S2 coincides with a reworked sandy layer with pebbles and cobbles, characterized by
443 shallow water fauna (*Bittium sp*., *Chamelea Gallina*, *Hydrobia sp*., *Jujubinus sp*., *Ammonia*
444 *beccarii*) mixed with species indicative of much deeper environments (*Timoclea ovata*,
445 *Parvicardium minimum*, *Plagiocardium papillosum*, *Miliolidae spp.*). Seismo-stratigraphical
446 correlation indicates that the sampled layer corresponds to reflector S2 of seismic line RF209 (see
447 **Figure 8**).

448 The stacking pattern of the entire TST, formed by three backstepping units, and the internal
449 composite reflector geometry of the mTST unit indicate an unsteady sediment flux that can be
450 correlated to the main climatic events punctuating the last ca. 20 kyr. The erosive nature of the three
451 surfaces S1, S2 and Si, can be indirectly related to intervals of reduced sediment flux and enhanced
452 marine reworking (Cattaneo and Trincardi, 1999). Shelf to basin seismic correlations, 16 ^{14}C dates
453 in core CM92-43 accompanied by other sparse dates from shelf cores, micropaleontologic

454 ecozonations, pollen spectra and tephra stratigraphy (Asioli 1996; Trincardi et al., 1996; Catteneo
455 and Trincardi, 1999) indicate that: 1) the TST records a lowered sediment flux compared to glacial
456 and modern times, 2) compared to the rest of the TST, the middle TST unit corresponds, however,
457 to an interval of enhanced sediment flux recording the Bölling-Allerød and Younger Dryas events,
458 3) the lowest rates of sedimentation correspond to the formation of surfaces S1, S2 and Si; the first
459 two surfaces are connected to Meltwater events 1A and 1B while the latter may reflect a minor sea
460 level fall.
461
462 **6.3. Modeling Results**
463
464 The sea level rise recorded during the last 21 Kyr had a big impact on the amount of
465 sediment and water delivered by the Po River to the Adriatic Sea (Kettner and Syvitski, 2008b).
466 Forced by sea level, the drainage basin decreased more than two times, changing from ca. 190000
467 km^2 to 74500 km^2, and consequently the total water discharge of the Po River decreased (Q_T in
468 **Figure 9**). Another important factor controlling the water discharge is the melting of ice and snow
469 from the catchment. The model simulates several melting phases starting from the LGM (Q_{ice} in
470 **Figure 9**), the most important of which are those recorded at the onset of the Bölling warm period
471 and at the end of the Younger Dryas, that have had a big impact on the total discharge and sediment
472 bedload (see the peak of Q_b in **Figure** 10). The onset of the Bölling, marked by a peak in Alpine ice
473 melting (Porter and Orombelli, 1982), was followed by a prolonged phase of enhanced water
474 discharge due to increased precipitation, as reproduced in the warm and wet climate modelled by
475 the CCM-1 model (Kutzbach et al., 1998; Kettner and Syvitski, 2008b). In order to simulate the
476 sediment and water discharge during the Younger Dryas (and then using the results to simulate
477 margin stratigraphy with 2D-Sedflux) we run two different simulations, one using the fit of the
478 published sea level curves and the other introducing a theoretical sea level curve which accounts for
479 a protracted sea level still-stand and a short-term fall during the YD (see red line in **Figure 3**). The

480 result is that the "sea level modified run", leading also to a short-term broadening of the drainage
481 basin area, records a phase of enhanced sediment and water delivery at the onset of the YD (red
482 lines in **Figure 9** and **10**), marked by higher-amplitude peak discharge (see red line of Q_{peak} n
483 **Figure 10**), in contrast with lower values of sediment and water discharge obtained with the first
484 simulation. A peak in water and sediment discharge, mostly related to the melting of the snow and
485 ice that accumulated during the YD, marks the end of this climatic event (see **Figure 3** and **9**).
486 These two outputs generated with HydroTrend simulations are then integrated in 2D-
487 Sedflux forcing the model with the two different sea level curves. In particular, the modelled
488 margin stratigraphy using the "sea level modified run" shows the most realistic results because it
489 allows a better reconstruction of the complexity of the mTST unit seen on the seismic profiles. In
490 detail (see **Figure 11**) the time section shows a basal onlapping unit, ending landward at ca -90
491 meter depth, corresponding to the basal TST, formed by mud to silty-mud material showing
492 increasing grain size landward, the unconformity at the base and the two-stages progradational
493 events within mTST unit. The upper part of the simulation also portrays well the sedimentary
494 deposits during the late stages of the sea level rise and the next late Holocene highstand (**Fig. 11**).
495
496 **7. Discussion**
497
498 The late Quaternary records one of the most complex climatic intervals of the entire geologic
499 history. During this interval the climatic instability, forced by changing insolation parameters, led to
500 a major eustatic fluctuation, with a sea level rise of about 120 meters in less than 15 kyr (Bard et al.,
501 1996). As highlighted by several authors, this rise was not monotonic, but instead punctuated by
502 short (sub-millennial) events of extremely enhanced melting of the ice caps, leading to abrupt steps
503 in sea level rise, like the Meltwater pulses 1A and 1B (Fairbanks, 1989).
504 Most reconstructions of the sea level history derive from the study of multiple, direct or
505 indirect, sea level indicators: coral reefs (Chappell and Polach, 1991; Bard et al., 1996), stable-

506 isotope records from benthonic foraminifera (Shackleton, 1987; Siddall et al., 2003), organic matter
507 associated to mangrove deposits (Hanebuth et al., 2000), as well as modeling simulations (Lambeck
508 and Chappell, 2001; Siddall et al., 2010). As sea level changes govern the deposition of clastic
509 sedimentary successions along continental margins, several authors tried to reconstruct the
510 magnitude of sea level oscillations by studying drowned shoreline deposits and the associated
511 unconformities (Skene et al., 1998). The geometry, position and age of clastic sedimentary deposits
512 on continental shelves can therefore be used as an indicator of past changes in sea level once local
513 tectonic components are taken into account.

514 The Adriatic Sea, among other mid-latitude continental margins (Boyd et al., 1992;
515 Dalrymple et al., 1992, Hernández-Molina et al., 1994; Anderson et al., 1995; Blanchon and Shaw,
516 1995; Abdulah et al., 2004; Anderson et al., 2004; Labaune et al., 2005; Osterberg, 2006; Berné et
517 al., 2007), presents a composite TST deposit, which records the impact of sea level and sediment-
518 supply oscillations on sub-millennial scales during the late Quaternary and in particular during the
519 interval encompassing the Bölling, Allerød and Younger Dryas events. Along the central Adriatic
520 margin, supply fluctuations occurred at very high frequency, resulting in a tripartite TST: while the
521 three units composing the transgressive sedimentary body record intervals of enhanced sediment
522 flux, reaching the highest values during the deposition of the middle unit, the regional
523 unconformities bounding the TST reflect short-term decreases in sediment flux and enhanced
524 strength of marine processes corresponding to the two Meltwater Pulses (**Fig. 12**). The reason of the
525 drop in sediment delivery during the Meltwater pulses is likely related to major changes in the river
526 equilibrium profile forced by rapid sea level rise, so that the bedload was trapped in alluvial plains
527 through channel aggradation and flood plain construction (Cattaneo and Trincardi, 1999).

528 The mTST unit records complex climatic events between the MWP 1A and 1B: the Bölling-
529 Allerød transition and the Younger Dryas cold event. Overall the mTST unit indicates a phase of
530 high sediment flux, separated by a short-term decline coinciding with the formation of surface Si
531 (**Fig. 12**). The central Adriatic mTST unit is formed by two sedimentary wedges, showing a dual

532 character: while the costal onlap migrates landward, as typical of any transgressive setting, this
533 sedimentary body consists of basinward downlapping strata typical of a progradational succession,
534 indicating that sediment supply was able to compete with the continuous formation of new
535 accommodation space. The mTST-1 sub-unit, confined between erosional surfaces S1 and Si,
536 records the Older Dryas to Allerød transition: model results suggest that during this interval an
537 enhanced sediment flux can be related to high values of precipitation. The deposition of the mTST-
538 2 sub-unit, instead, appears related to dryer conditions with respect to the previous wet interval as
539 suggested by the CCM-1 Climatic model (Kutzbach et al., 1998; Kettner and Syvitski, 2008b).
540 During the Younger Dryas an increase in sediment flux was likely connected to a decline in
541 vegetation cover due to the establishment of sub glacial arid conditions. The climatic instability
542 recorded during this interval determined a reduction in soil vegetation cover, leading to increased
543 denudation rates of high altitude areas and soil erosion. Moreover, as the results of HydroTrend
544 simulations indicate, this progradation can be related to increased rates of water and sediment
545 discharge connected to the partial melting of the Alpine glaciers, that grew during the YD.

546 In the area between the Tremiti High and the Gargano promontory, the mTST-2 sub-unit can
547 be interpreted as a complex barrier-island-lagoon system, with bay-head or flood-tidal delta
548 deposits eroded at the top by surface S2 (**Fig. 12**). This shoreline deposits is the best indicator of the
549 sea level position attained during the Younger Dryas at about -75 m at the end of the Younger
550 Dryas. Interestingly, this result is in good agreement with the modeling simulation of Siddall et al.
551 (2010).

552 The results of sequence stratigraphy are then integrated with numerical simulations: the water
553 and sediment discharge during the last 21 kyr is obtained with HydroTrend v.3.0 (Kettner and
554 Syvitski, 2008b), a climate-driven hydrological water balance and transport model, and the internal
555 architecture of the Late Pleistocene-Holocene deposits is modelled with 2D Sedflux, a stratigraphic
556 simulation model (Syvitski and Hutton, 2001).

557 Modeling simulations show that the middle TST unit is a consequence of increased sediment
558 discharge in the interval between the B/A and the YD and the composite internal geometry is
559 primarily related to sea level: a sea level fall during the sub glacial condition reached in the YD is
560 the best explanation for the two steps prograding mTST unit and for its internal unconformity Si.
561 Moreover, sediment discharge simulated with HydroTrend indicates that there are two peaks in
562 sediment flux during the Allerød and at the end of the YD, separated by a drop in sedimentation.
563 This result is in good agreement with a total independent result, as the same drop in sedimentation
564 rate can be observed in core CM92-43.
565 The solutions generated with Sedflux using different HydroTrend input files show that the
566 model is able to reproduce the formation of a middle TST unit characterized by up to 15 meters
567 thick deposits, with shingled internal reflectors. Moreover the simulations show that the complexity
568 of the margin stratigraphy is primarily related to the two Meltwater pulses, but also that a two step
569 prograding middle TST unit can be generated only introducing a phase still stand or a minor, but
570 significant, fall in sea level during the Younger Dryas.
571
572 **8. Conclusion**
573
574 Sea level oscillations, together with sediment flux fluctuations, are the main mechanisms
575 governing sedimentation along continental margins during the Quaternary. The late Pleistocene-
576 Holocene sea level rise, reconstructed by several authors using various paleo-shoreline indicators,
577 occurred in less then 15 kyr and was characterized by at least two intervals of more accelerated sea
578 level rise, each connected to two periods of enhanced ice melting. The study of the central Adriatic
579 margin offers new evidence of the impact of high-frequency climatic and eustatic oscillations on a
580 sub-Milankovian time scale, particularly during the Bölling-Allerød to Younger Dryas transition. A
581 similar complexity characterizes the transgressive sedimentary succession along other mid-latitude
582 clastic continental margins.

583 In the central Adriatic Sea and elsewhere in the Mediterranean, the Transgressive Systems
584 Tract consists of a tripartite deposit, confirming the step-wise nature of the sea level rise,
585 punctuated by the two Meltwater pulses 1A and 1B. Our modeling results, combined with new
586 seismo-stratigraphic investigations on the Adriatic TST, suggest that the increased stratigraphic
587 complexity within the middle TST unit, recording the B/A and YD events; can best be explained by
588 sea level oscillations, including a minor but significant sea level fall during the Younger Dryas
589 event. The stratigraphy of the TST units is further complicated by the occurrence, during this
590 interval, of climate-driven supply fluctuations. The results obtained by the analysis of seismic
591 profiles, integrated by sediment core analysis, ^{14}C dating and modeling simulations, reveal new
592 insights into the process-response relations governing the deposition of the central Adriatic late-
593 Quaternary TST. In detail, the deposition of the middle TST unit, bounded by two erosional
594 surfaces generated during the main Meltwater pulses of the last Termination, recorded an interval of
595 enhanced sediment flux including the Bölling-Allerød and Younger Dryas intervals. Modeling
596 simulations indicate that the thick prograding deposit of the mTST unit derived from enhanced
597 sediment flux due to a reduction in soil cover vegetation during the YD cold event. Moreover, the
598 modeling of sediment architecture indicates that it is possible to generate the observed complexity
599 of the mTST unit by forcing sea level to fall during the Younger Dryas. This conclusion is
600 consistent with the evidence of a Younger Dryas shoreline deposit at ca. -75 m depth in the area
601 between the Tremiti High and the Gargano Promontory and with the presence of an extensive
602 erosional unconformity within the mTST unit.
603

References

Abdulah, K.C., Anderson, J.B., Snow, J.N., Holford-Jack. L., 2004. The Late Quaternary Brazos and Colorado deltas, offshore Texas, USA - Their evolution and the factors that controlled their deposition, in: Anderson, J.B., Fillon, R.H. (Eds.), Late Quaternary Stratigraphic Evolution of the Northern Gulf of Mexico Margin. SEPM (Society for Sedimentary Geology) Special Publication, Tulsa, pp. 237-269.

Alley, R.B., Meese, D.A., Shuman, C.A., Gow, A.J., Taylor, K.C., Grootes, P.M., White, J.W.C., Ram, M., Waddington, E.D., Mayewski, P.A., Zielinski, G.A., 1993. Abrupt increase in Greenland snow accumulation at the end of the Younger Dryas event. Nature 362, 527-529.

Anderson, J.B., Abdulah, K.C., Sarzalejo, S., Siringan F., Thomas, M.A., 1995. Late Quaternary sedimentation and high-resolution sequence stratigraphy of the Texas shelf, in: de Batist, M., Jacobs, P., (Eds.), Geology of Siliciclastic Shelf Seas. Geological Society Special Publication, London, pp. 155-169.

Anderson, J.B.,Rodriguez, A., Abdulah, K.C., Fillon, R.H., Banfield, L.A., McKeown H.A., Wellner, J.S., 2004. in: Anderson, J.B., Fillon, R.H. (Eds.), Late Quaternary Stratigraphic Evolution of the Northern Gulf of Mexico Margin. SEPM (Society for Sedimentary Geology) Special Publication, Tulsa, pp. 1-23.

Asioli, A., 1996. High-resolution foraminifera biostratigraphy in the central Adriatic basin during the last deglaciation: a contribution to the PALICLAS project. Memorie Istituto Italiano Idrobiologia 55, 197-217.

Asioli, A., Trincardi, F., Lowe, J.J., Oldfield, F., 1999. Short-term climate changes during the last Glacial-Holocene transition: comparison between the Mediterranean and North Atlantic records. Journal of Quaternary Science 4, 3732-3781.

Asioli, A., Trincardi, F., Lowe, J.J., Ariztegui, D., Langone, L., Oldfield, F., 2001. Sub-millennial scale climatic oscillations in the central Adriatic during the Lateglacial: palaeoceanographic implications. Quaternary Science Reviews 20, 1201-1221.

Bagnold, R.A., 1966. An approach to the sediment transport problem from general physics. U.S.G.S. Professional Paper 422-I, pp. 37.

Bard, E., Hamelin, B., Fairbanks, R.G., 1990. U–Th ages obtained by mass spectrometry in corals from Barbados: sea level during the past 130,000 years. Nature 346, 456-458.

Bard, E., Hamelin, B., Arnold, M., Montaggioni, L., Cabioch, G., Faure, G., Rougerie, F., 1996. Deglacial sea-level record from Tahiti corals and the timing of global Meltwater discharge. Nature 382, 241-244.

638 Berné, S., Jouet, G., Bassetti, M.A., Dennielou, B., Taviani, M., 2007. Late Glacial Preboreal sea-
639 level rise recorded by the Rhône deltaic system (NW Mediterranean). Marine Geology 245,
640 65-88.
641 Blanchon, P., Shaw, J., 1995. Reef drowning during the last deglaciation: Evidence for catastrophic
642 sea-level rise and ice-sheet collapse. Geology 23, 4-8.
643 Bond, G., Heinrich, H., Broecker, W., Labeyrie, L., McManus, J., Andrews, J., Huon, S., Jantschik,
644 R., Clasen, S., Simet, C., Tedesco, K., Klas, M., Bonani, G., Ivy, S., 1992. Evidence for
645 massive discharges of icebergs into the North Atlantic Ocean during the last glacial period.
646 Nature 360, 245-249.
647 Bond, G., Showers, W., Cheseby, M., Lotti, R., Almasi, P., deMenocal, P., Priore, P., Cullen, H.,
648 Hajdas, I., Bonani, G., 1997. A Pervasive Millennial-Scale Cycle in North Atlantic
649 Holocene and Glacial Climates. Science 278, 1257-1266.
650 Bourne, A.J., Lowe, J.J., Trincardi, F., Asioli, A., Blockley, S.P.E., Wulf, S., Matthews, I.P., Piva,
651 A., Vigliotti, L., 2010. Distal tephra record for the last ca. 105.000 years from core PRAD1-
652 2 in the central Adriatic Sea: implications for marine tephrostratigraphy. Quaternary Science
653 Reviews, 1-16, in press.
654 Boyd, R., Dalrymple, R.W., Zaitlin, A., 1992. Classification of clastic depositional environments.
655 Sedimentary Geology 80, 139-150.
656 Calanchi, N., Cattaneo, A., Dinelli, E., Gasparotto G., Lucchini, F., 1998. Tephra layers in Late
657 Quaternary sediments of the Central Adriatic Sea. Marine Geology 149, 191-209.
658 Cattaneo, A., Trincardi, F., 1999. The late-Quaternary transgressive record in the Adriatic
659 epicontinental sea: Basin widening and facies partitioning, in: Bergman, K., Snedden, J.
660 (Eds.), Isolated Shallow Marine Sand Bodies: Sequence Stratigraphic Analysis and
661 Sedimentologic Interpretation. SEPM (Society for Sedimentary Geology) Special
662 Publication, Tulsa, pp. 127-146.
663 Cattaneo, A., Correggiari, A., Langone, L., Trincardi, F., 2003. The late-Holocene Gargano
664 subaqueous delta, Adriatic shelf: Sediment pathways and supply fluctuations. Marine
665 Geology 193, 61-91.
666 Cattaneo, A., Trincardi, F., Asioli, A., Correggiari, A., 2007. The Western Adriatic shelf clinoform:
667 energy-limited bottomset. Continental Shelf Research 27, 506-525.
668 Carlson, A.E., 2010, What caused the Younger Dryas cold event? Geology 38, 383-384.
669 Chappell, J., Polach, H., 1991. Post glacial sea level rise from coral record at Huon Peninsula,
670 Papua New Guinea. Nature 349, 147-149.

671 Clark, P.U., Mitrovica, J.X., Milne, G.A., Turon, J.L., Siani, G., 2002. Sea level fingerprint as a
672 direct test for the source of global Meltwater Pulse 1A. Science 295, 2438-2441.
673 Clark, P.U., Marshall, A., McCabe, A.M., Mix, A.C., Weaver, A.J., 2004. Rapid rise of sea level
674 19000 years ago and its Global implications. Science 304, 1141-1144.
675 Clark, P.U., Dyke, A.S., Shakun, J.D., Carlson, A.E., Clark, J., Wohlfarth, B., Mitrovica, J.X.,
676 Hostetler, S.W., McCabe, A.M., 2009. The last Glacial Maximum. Science 324, 720-714.
677 Correggiari A., Cattaneo, A., Trincardi, F., 2005. The modern Po Delta system: Lobe switching and
678 asymmetric prodelta growth. Marine Geology 222-223, 49-74.
679 Dalrymple, R.W., Zaitlin, A., Boyd, R., 1992. Estuarine facies models: conceptual basis and
680 stratigraphic implications. Journal of Sedimentary Petrology 62, 1130-1146.
681 De Marchi, L., 1922. Variazioni di livello dell'Adriatico in corrispondenza delle espansioni glaciali.
682 Atti della Academia Scientifica Veneta-Trentino-Istriana 12-13, 3-15.
683 Doglioni, C., Mongelli, F., Pieri, P., 1994. The Puglia uplift (SE Italy): An anomaly in the foreland
684 of the Apenninic subduction due to buckling of a thick continental lithosphere. Tectonics 13,
685 1309-1321.
686 Fairbanks, R.G., 1989. A 17.000-yr glacio-eustatic sea level record: influence of glacial melting
687 rates on the Younger Dryas event and deep-ocean circulation. Nature 342, 637-642.
688 Hanebuth, T., Stattegger, P.K., Grootes, M., 2000. Rapid flooding of the Sunda shelf: A late-Glacial
689 Sea-level record. Science 288, 1033-1035.
690 Hernández-Molina, F.J., Somoza, L., Rey, J., Pomar, L., 1994. Late Pleistocene-Holocene
691 sediments on the Spanish continental shelves: Model for very high resolution sequence
692 stratigraphy. Marine Geology 120, 129-174.
693 Hutton, E.W.H., Syvitski, J.P.M., 2008. Sedflux 2.0: An advanced process-response model that
694 generate three-dimensional stratigraphy. Computer & Geosciences 34, 1319-1337.
695 Kettner, A.J., Syvitski, J.P.M., 2008a. HydroTrend v.3.0: A climate-driven hydrological transport
696 model that simulates discharge and sediment load leaving a river system. Computers &
697 Geosciences 34, 1170-1183.
698 Kettner, A.J., Syvitski, J.P.M., 2008b. Predicting discharge and sediment flux of the Po River, Italy
699 since the Last Glacial Maximum. Spec. Publ. Int. Assoc. Sedimentol. 40, 171-189.
700 Kubo, Y., Syvitski, J.P.M., Hutton, E.W.H., Kettner, A.J., 2006. Inverse modeling of post Last
701 Glacial Maximum transgressive sedimentation using 2D-Sedflux: Application to the
702 northern Adriatic Sea. Marine Geology 234, 233-243.
703 Kutzbach, J., Gallimore, R., Harrison, S., Behling, P., Selin, R., Laarif, F., 1998. Climate and biome
704 simulations for the past 21,000 years. Quaternary Science Reviews 17, 319-330.

705 Labaune, C., Jouet, G., Bernè, S., Gensous, B., Tesson, M., Delpeint, A., 2005. Seismic stratigraphy
706 of the Deglacial deposits of the Rhône prodelta and of the adjacent shelf. Marine Geology
707 222-223, 299-311.
708 Lambeck, K., Chappell, J., 2001. Sea level change through the Last Glacial cycle. Science 292,
709 679-686.
710 Morehead, M.D., Syvitski, J.P.M., Hutton, E.W.H., Peckham, S.D., 2003. Modeling the temporal
711 variability in the flux of sediment from ungauged river basins. Global and Planetary Change
712 39, 95-110.
713 Nelson, B.W., 1970. Hydrography, sediment dispersal, and recent historical development of the Po
714 River delta, Italy, in: Morgan, J.P. (Eds.), Deltaic sedimentation; Modern and Ancient.
715 SEPM (Society for Sedimentary Geology) Special Publication, Tulsa, pp. 152-184.
716 Osterberg, E.C., 2006. Late Quaternary (marine isotope stages 6-1) seismic sequence stratigraphic
717 evolution of the Otago continental shelf, New Zeland. Marine Geology 229, 159-178.
718 Peinson, G.E., 1992. Transgressive barrier-island and estuarine systems, in: Walker, R.G., James,
719 N.P. (Eds.), Facies Models: Response to Sea Level Changes. Geological Association of
720 Canada, pp. 179-194.
721 Piva, A., Asioli, A., Schneider, R.R., Trincardi, F., Andersen, N., Colmenero-Hidalgo, E.,
722 Dennielou, B., Flores, J.-A., Vigliotti, L., 2008a. Climatic cycles as expressed in sediments
723 of the PROMESS1 borehole PRAD1.2, central Adriatic, for the last 370 ka: 1. Integrated
724 stratigraphy. Geochem. Geophys. Geosyst. 9, Q01R01, doi:10.1029/2007GC001713.
725 Piva, A., Asioli, A., Andersen, N., Grimalt, J.O., Schneider, R.R., Trincardi, F., 2008b. Climatic
726 cycles as expressed in sediments of the PROMESS1 borehole PRAD1.2, central Adriatic,
727 for the last 370 ka: 2. Paleoenvironmental evolution. Geochem. Geophys. Geosyst. 9,
728 Q03R02, doi:10.1029/2007GC001785.
729 Piva, A., Asioli, A., Trincardi, F., Schneider, R.R., Vigliotti, L., 2008c. Late-Holocene climate
730 variability in the Adriatic Sea (Central Mediterranean). The Holocene 18, 153-167.
731 Porter, S.C., Orombelli, G., 1982. Lateglacial ice advances in the western Italian Alps. Boreas 11,
732 125-140.
733 Ridente, D., Trincardi, F., Piva, A., Asioli, A., Cattaneo, A., 2008. Sedimentary response to climate
734 and sea level changes during the past 400 ka from borehole PRAD1.2 (Adriatic margin).
735 Geochem. Geophys. Geosyst. 9, 1-20.
736 Royden, L., 1988. Flexural behavior of the continental lithosphere in Italy: Constrains imposed by
737 gravity and deflection data. Journal of Geophysical Research 93, 7747-7766.

738 Ruddiman, W.F., McIntyre, A., 1981. The North Atlantic Ocean during the Last Deglaciation.
739 Palaeogeography, Palaeoclimatology, Palaeoecology 35, 145-214.
740 Shackleton, N.J., 1987. Oxygen isotopes, ice volume and sea level. Quaternary Science Reviews 6,
741 183-190.
742 Skene, K.I, Piper, D.J.W., Aksu, A.E., Syvitski, J.P.M., 1998. Evaluation of the global oxygen
743 isotope curve as a proxy for Quaternary sea level by modeling of delta progradation. Journal
744 of Sedimentary Research 68, 1077-1092.
745 Siddall, M., Rohling, E.J., Almogi-Labin, A., Hemleben, Ch., Meischner, D., Schmelzer, L.,
746 Smeed, D.A., 2003. Sea-level fluctuations during the last glacial cycle. Nature 423, 853-858.
747 Siddall, M., Kaplan, M.R., Schaefer, J.M., Putnam, A., Kelly, M.A., Goehring, B., 2010. Changing
748 influence of Antarctic and Greenlandic temperature records on sea-level over the last glacial
749 cycle. Quaternary Science Reviews 29, 410-423.
750 Syvitski, J.P.M., Alcott, J.M., 1993. GRAIN2: predictions of particle size seaward of river mouths.
751 Computer & Geosciences 19 (3), 399-446.
752 Syvitski, J.P.M., Hutton, E.W.H., 2001. 2D SEDFLUX 1.0C: an advanced process-response
753 numerical model for the fill of sedimentary basins. Computer & Geosciences 27 (6), 731-
754 754.
755 Trincardi, F., Correggiari, A., Roveri, M., 1996a. Late Quaternary transgressive record and
756 deposition in a modern epicontinental shelf: the Adriatic semi-enclosed basin. Geo-Marine
757 Letters 14, 41-51.
758 Trincardi, F., Cattaneo, A., Asioli, A., Correggiari, A., Langone, L., 1996b. Stratigraphy of the
759 Late-Quaternary deposits in the central Adriatic basin and the record of short term climatic
760 events. Memorie Istituto Italiano Idrobiologia 55, 39-70.
761 Watts, A.B., 1992. The effective elastic thickness of the lithosphere and the evolution of foreland
762 basin. Basin Research 4, 169-178.
763

764 **Figure Captions**

765

766 Fig. 1

767 Digital elevation model of the Adriatic Sea with the structural elements: Mid Adriatic Deep,
768 a small remnant basin >250 meters deep; northern Adriatic Sea floor characterized by sandy
769 deposits of drowned barrier-island systems formed during the last sea level rise. The black box
770 indicates the study area. Right: slope angle map of the Adriatic shelf shallower than 300 m. The
771 green dashed line indicates the offlap break of the late Holocene deposits (Cattaneo et al., 2007).

772

773 Fig. 2

774 Modern drainage area of the Po River (Blue) and during the Last Glacial Maximum (Red),
775 reconstructed using present-day sea floor bathymetry (modified from Kettner and Syvitski, 2008b).
776 The light-blue lines represent a theoretical representation of the river network during glacial time.
777 All the rivers draining the catchment area are considered tributaries of a "Mega" lowstand Po River.
778 The small box shows the modern configuration of the Po River delta plain. The red dashed line
779 represents the landward limit reached by sea level at the time of the maximum marine ingression.
780 Right: comparison between lowstand and modern values of sediment discharge (Q_b: base load; Q_s:
781 suspended load) and water discharge (Q_T) calculated using HydroTrend (Kettner and Syvitski,
782 2008b).

783

784 Fig. 3

785 Input parameters used for the HydroTrend simulation of the last 21 kyr (modified from
786 Kettner and Syvitski, 2008b). Two different HydroTrend simulations have been ran in order to
787 reconstruct the discharge during the Younger Dryas event, considering two different sea level
788 curves: the red line is a theoretical sea level curve which accounts for a sea level fall during the YD.

As a consequence, the drainage area increases too (red line). The ELA is the Equilibrium Line Altitude.

Fig. 4

Line drawing of the seismic lines ST05 and ST06 (see location in the map), showing the internal subdivision of the transgressive deposits, and the location of borehole PRAD2-4. The input bathymetry for 2D-Sedflux simulations has been obtained through the mapping of the unconformity ES1. Before starting the simulations, the modern depth of ES1 has been restored to LGM time by removing the post LGM sediment and water load using a 2D flexural model, see text for detail.

Fig. 5

Central Adriatic stratigraphy along the seismic profile CSS700 and its interpretation: in blue the Transgressive systems tract (TST) and in green the Highstand systems tract (HST). The TST is divided into three units, separated by two regional surfaces, S1 and S2, each recording a specific interval of the sea level rise. The LTST unit, formed by a 10 meters thick muddy unit, is characterized by a chaotic seismic signature. The mTST unit, formed by two-step prograding units >10 m thick, shows low-angle basinward downlapping reflectors, separated by an internal surface of erosion, Si. Each step of progradation records an interval of enhanced sediment supply occurred during the Bölling-Allerød to Younger Drays transition. The upper TST unit onlaps the basinward limit of the mTST unit and records the last phases of the sea level rise. The maximum flooding surface (mfs) separates transgressive and highstand deposits, which form a continuous clinoform extending from the Po River delta toward the south Adriatic. Each map shows the thickness of the highstand deposits, of the transgressive deposits, and of the middle transgressive unit (modified from Cattaneo and Trincardi, 1999). The middle TST unit is characterized by three depocenters,

elongated parallel to margin, which reflects the interaction between sediment distribution, marine processes and sea floor morphology.

Fig. 6

Shelf to basin correlation of the middle TST (mTST) unit. On the shelf the mTST unit is more then 10 m thick and its top was reached by cores RF95-13 and RF95-14, and by the borehole PRAD2-4 (see Figure 4). Dated samples and tephra stratigraphy indicate that this unit deposited before Meltwater pulse 1B. The unit pinches-out basinward where the cores PAL94-9 and PAL-8 encountered a layer of reworked material corresponding to the amalgamated surface S1+S2. Toward the MAD the mTST unit expands into a thick unit of marine mud where core CM92-43 was retrieved demonstrating that the base of the mTST unit correlates to the Meltwater pulse 1A. The pollen spectra and foraminifera associations in core CM92-43 record a cooling trend starting during the B/A and culminating with the YD cold event (modified from Asioli et al., 2001). The small red arrow in the *G. bulloides* $\delta^{18}O$ curve highlights an increase of freshwater discharge and influx of fluvially derived material, which possibly reflects the melting of Alpine and Apennine glaciers (Asioli et al., 2001).

Fig. 7

Cross correlation of seismic profiles COS154, COS156 and AMC243 (between the Tremiti High and the Gargano Promontory) where the four cores reached a layer of reworked coarse material, characterized by very shallow water fauna assemblages. Seismic correlations indicate that this layer corresponds to surface S2 atop of the Younger Dryas interval. The black vertical line on profile COS154 is the tie point with seismic line RF209 of Figure 8.

Fig. 8

839 Seismic profile RF209 (see location in Figure 7) shows that the mTST-1 sub-unit is formed
840 by a thick deposit of basinward progradational reflectors, while the mTST-2 sub-unit has a more
841 complex internal architecture, showing bi-directional downlap and small scales internal erosional
842 surfaces beneath surface S2. The mTST-2 sub-unit is interpreted as a lagoonal system with bay-
843 head and flood-tidal deltas. In a distal position, ca. -82 meters of water depth, surface S2 is topped
844 by asymmetric sand dunes up to two meters thick.
845
846 Fig. 9
847 Water discharge obtained with HydroTrend simulations, divided in the contribution of snow
848 (Q_{nival}) and ice (Q_{ice}) melting, and rainfall (Q_{rain}). The red line shows the simulation in case of a
849 small sea level fall. The peak in ice melting at the end of the Younger Dryas (upper yellow stripe)
850 corresponds to a major melting phase of the Alpine glaciers.
851
852 Fig. 10
853 Sediment discharge obtained with HydroTrend simulations, divided in bedload (Q_b) and
854 suspended load (Q_s). Red line indicates the sea level modified results. The peak in bedload transport
855 at the end of the Younger Dryas (upper yellow stripe) reflects the partial melting of Alpine glaciers
856 (see the equivalent peak in Figure 9).
857
858 Fig. 11
859 Time section and Grain-size section of the central Adriatic margin stratigraphy modeled
860 with 2D Sedflux. The result of the simulation is obtained forcing the model with the "sea level
861 modified" curve and represents the best reproduction of the observed stratigraphy. Both sections
862 show the tripartite architecture of the transgressive record, with the middle TST unit characterized
863 by basinward downlapping geometry bounded by erosional surfaces and characterized by coarser
864 material. The black box refers to the line drawing of seismic line ST05 (see also Figure 4).

865

866 Fig. 12

867 Stratigraphy of the central Adriatic margin during the Younger Dryas event. Left: north of
868 the Tremiti High, the mTST unit is composed of two superposed submarine prograding bodies.
869 Right: south of the Tremiti High, the mTST unit is characterized by a barrier-island-lagoon system,
870 eroded at its top at the end of the Younger Dryas likely as a consequence of the Meltwater pulses
871 1B. Schematic paleo-environmental reconstruction are derived and modified from Peinson (1992).
872 Center: sedimentation rate obtained from the core CM92-43 compared to the sediment bedload
873 discharge modelled with HydroTrend. Both results show enhanced sediment flux during the
874 Bölling-Allerød to Younger Dryas transition; moreover the YD is characterized by a decrease in
875 sediment flux, centered at 12 kyr BP, where erosional surface Si formed inside of the middle TST
876 unit.

877

878 Table 1

879 Nomenclature.

Fig. 1

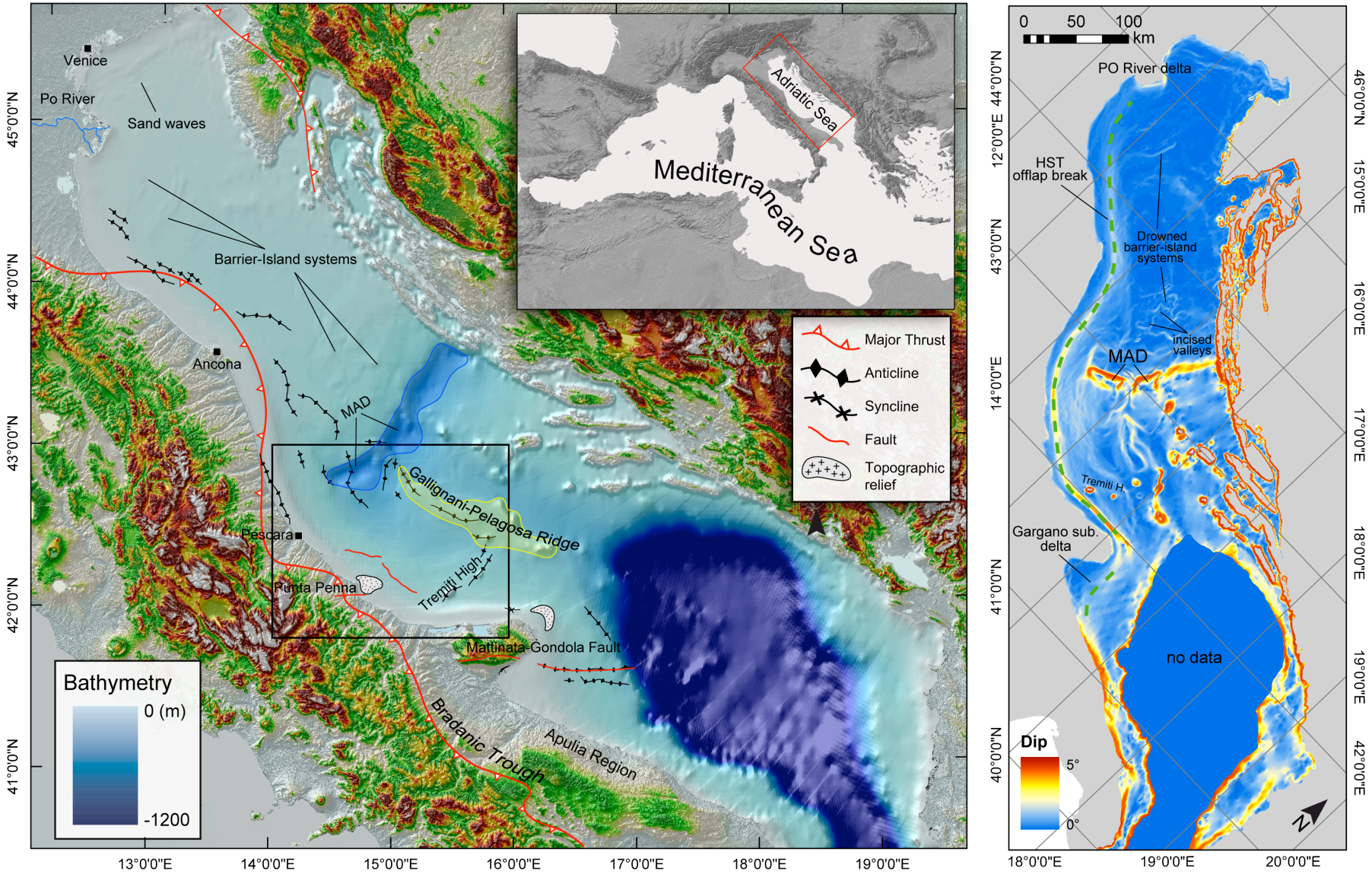
Venice
Po River
Sand waves
Barrier-Island systems
Ancona
MAD
Gallignani-Pelagosa Ridge
Pescara
Punta Penna
Tremiti High
Mattinata-Gondola Fault
Bradanic Trough
Apulia Region
Bathymetry
0 (m)
-1200
Mediterranean Sea
Adriatic Sea
Major Thrust
Anticline
Syncline
Fault
Topographic relief
45°0'0"N
44°0'0"N
43°0'0"N
42°0'0"N
41°0'0"N
13°0'0"E
14°0'0"E
15°0'0"E
16°0'0"E
17°0'0"E
18°0'0"E
19°0'0"E
0
50
100
km
PO River delta
HST
offlap break
Drowned
barrier-island
systems
incised
valleys
MAD
Tremiti H.
Gargano sub.
delta
no data
Dip
5°
0°
N
12°0'0"E
14°0'0"E
15°0'0"E
16°0'0"E
17°0'0"E
18°0'0"E
19°0'0"E
20°0'0"E
40°0'0"N
41°0'0"N
42°0'0"N
43°0'0"N
44°0'0"N
46°0'0"N

Fig. 2

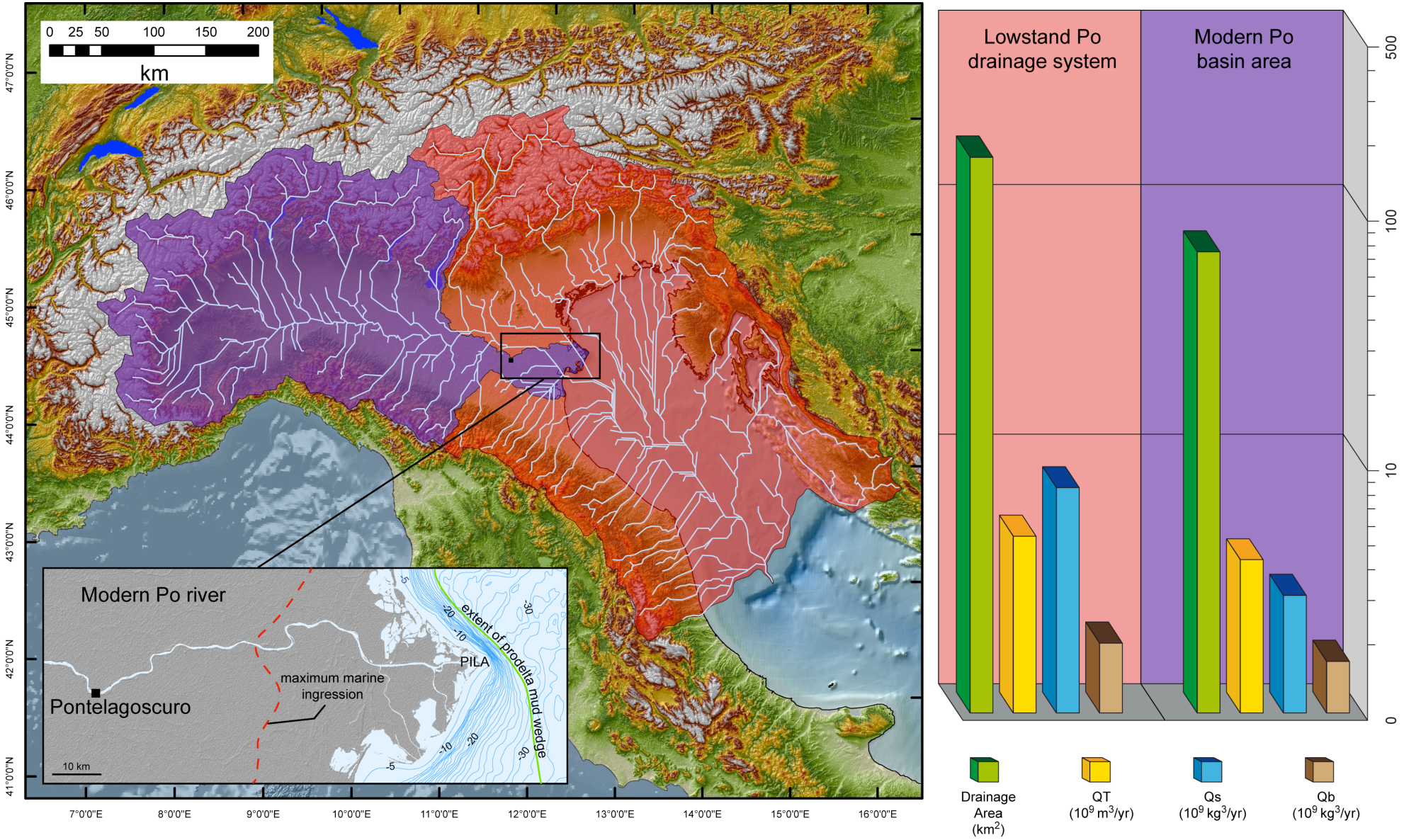
0 25 50 100 150 200
km
Modern Po river
Pontelagoscuro
maximum marine ingression
PILA
extent of prodelta mud wedge
10 km
-5
-10
-20
-30
47°0'0"N
46°0'0"N
45°0'0"N
44°0'0"N
43°0'0"N
42°0'0"N
41°0'0"N
7°0'0"E
8°0'0"E
9°0'0"E
10°0'0"E
11°0'0"E
12°0'0"E
13°0'0"E
14°0'0"E
15°0'0"E
16°0'0"E
Lowstand Po drainage system
Modern Po basin area
500
100
10
0
Drainage Area (km2)
QT (10^9 m^3/yr)
Qs (10^9 kg^3/yr)
Qb (10^9 kg^3/yr)

Fig. 3

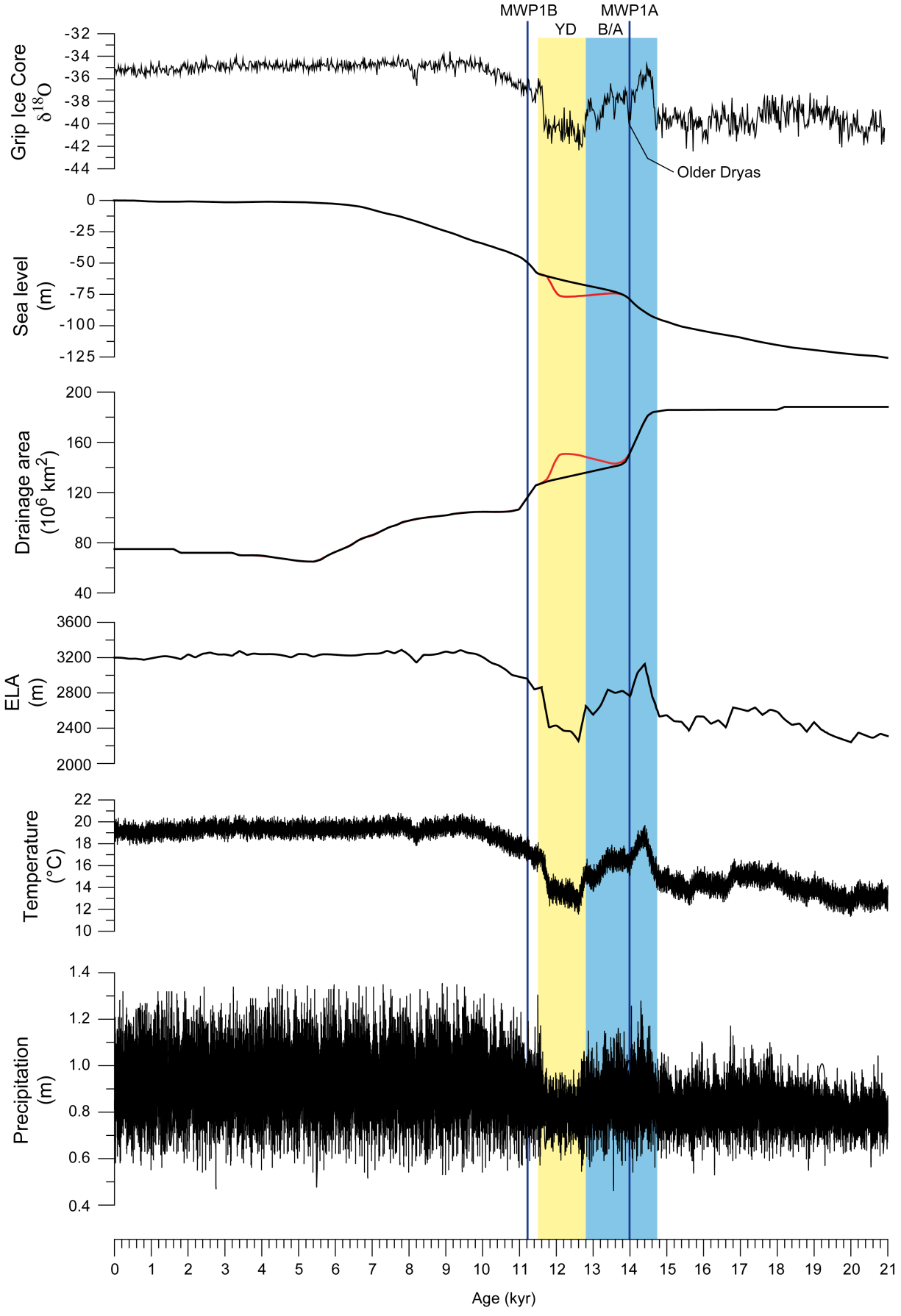
MWP1B
YD
B/A
MWP1A
Older Dryas
Grip Ice Core δ18O
-32
-34
-36
-38
-40
-42
-44
Sea level (m)
0
-25
-50
-75
-100
-125
Drainage area (10^6 km^2)
200
160
120
80
40
ELA (m)
3600
3200
2800
2400
2000
Temperature (°C)
22
20
18
16
14
12
10
Precipitation (m)
1.4
1.2
1.0
0.8
0.6
0.4
0
1
2
3
4
5
6
7
8
9
10
11
12
13
14
15
16
17
18
19
20
21
Age (kyr)

Fig. 4

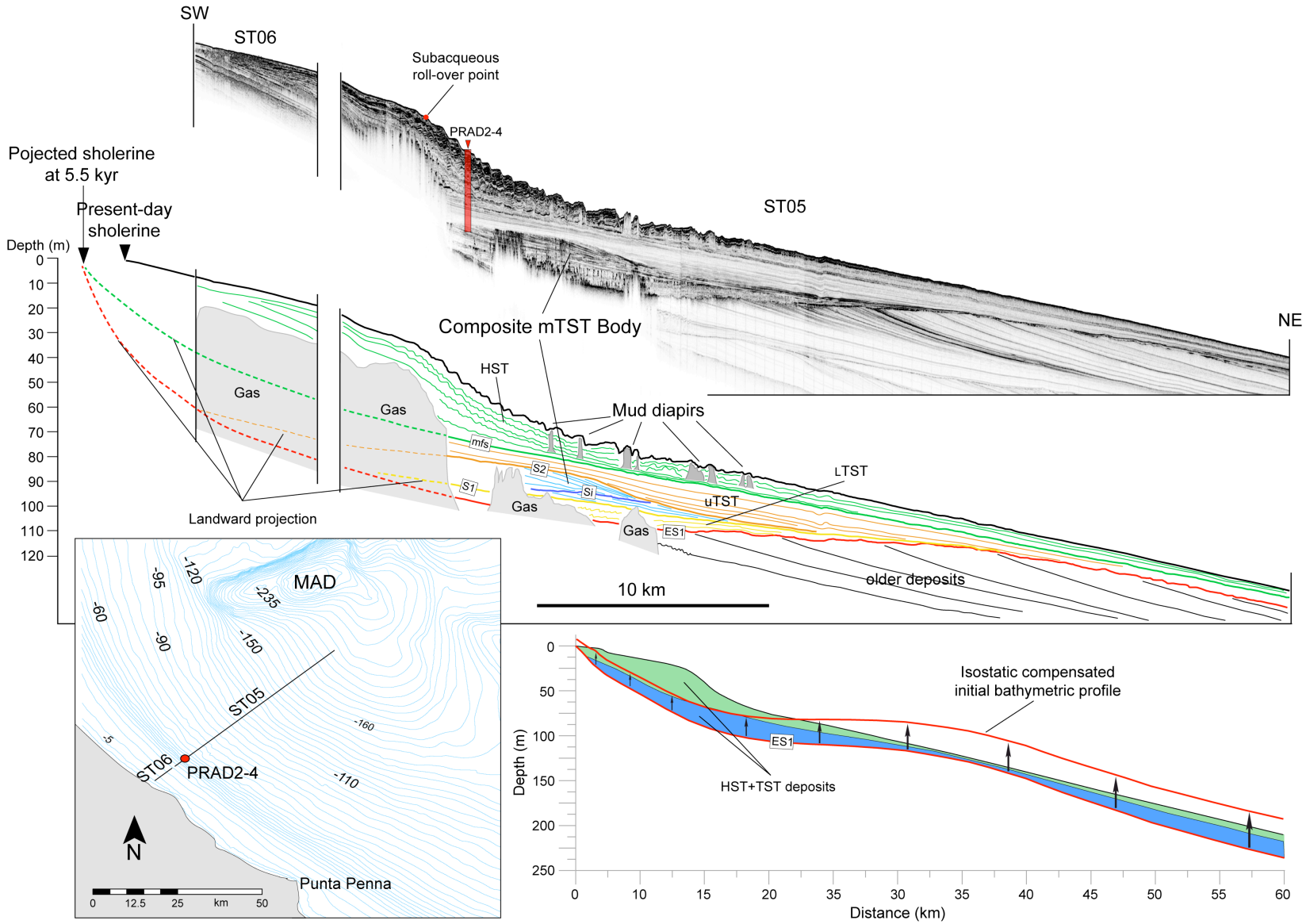
SW
ST06
Subacqueous
roll-over point
PRAD2-4
ST05
NE
Pojected sholerine
at 5.5 kyr
Present-day
sholerine
Depth (m)
0
10
20
30
40
50
60
70
80
90
100
110
120
Composite mTST Body
HST
Mud diapirs
Gas
Gas
mfs
S2
S1
Si
LTST
uTST
Gas
Gas
ES1
older deposits
Landward projection
10 km
MAD
-120
-95
-235
-60
-90
-150
ST05
-160
-5
ST06
PRAD2-4
-110
N
Punta Penna
0
12.5
25
km
50
Isostatic compensated
initial bathymetric profile
ES1
HST+TST deposits
Depth (m)
0
50
100
150
200
250
0
10
15
20
35
30
35
40
45
50
55
60
Distance (km)

Fig. 5

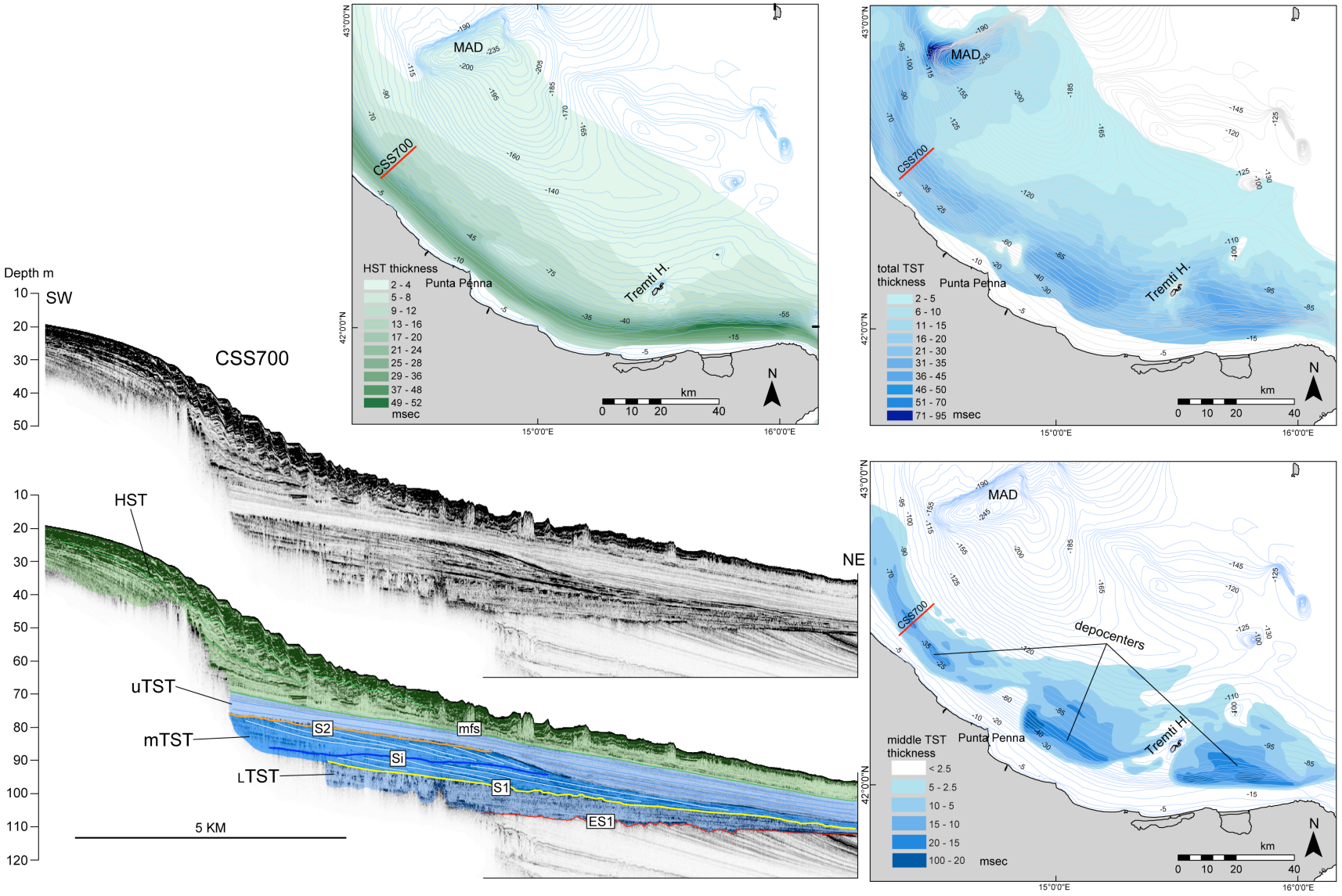
Depth m
SW
CSS700
NE
HST
uTST
mTST
LTST
S2
Si
S1
ES1
mfs
5 KM
MAD
Punta Penna
Tremti H.
HST thickness
2 - 4
5 - 8
9 - 12
13 - 16
17 - 20
21 - 24
25 - 28
29 - 36
37 - 48
49 - 52
msec
total TST thickness
2 - 5
6 - 10
11 - 15
16 - 20
21 - 30
31 - 35
36 - 45
46 - 50
51 - 70
71 - 95
msec
middle TST thickness
< 2.5
5 - 2.5
10 - 5
15 - 10
20 - 15
100 - 20
msec
depocenters
km
N
43°0'0"N
42°0'0"N
15°0'0"E
16°0'0"E

Fig. 6

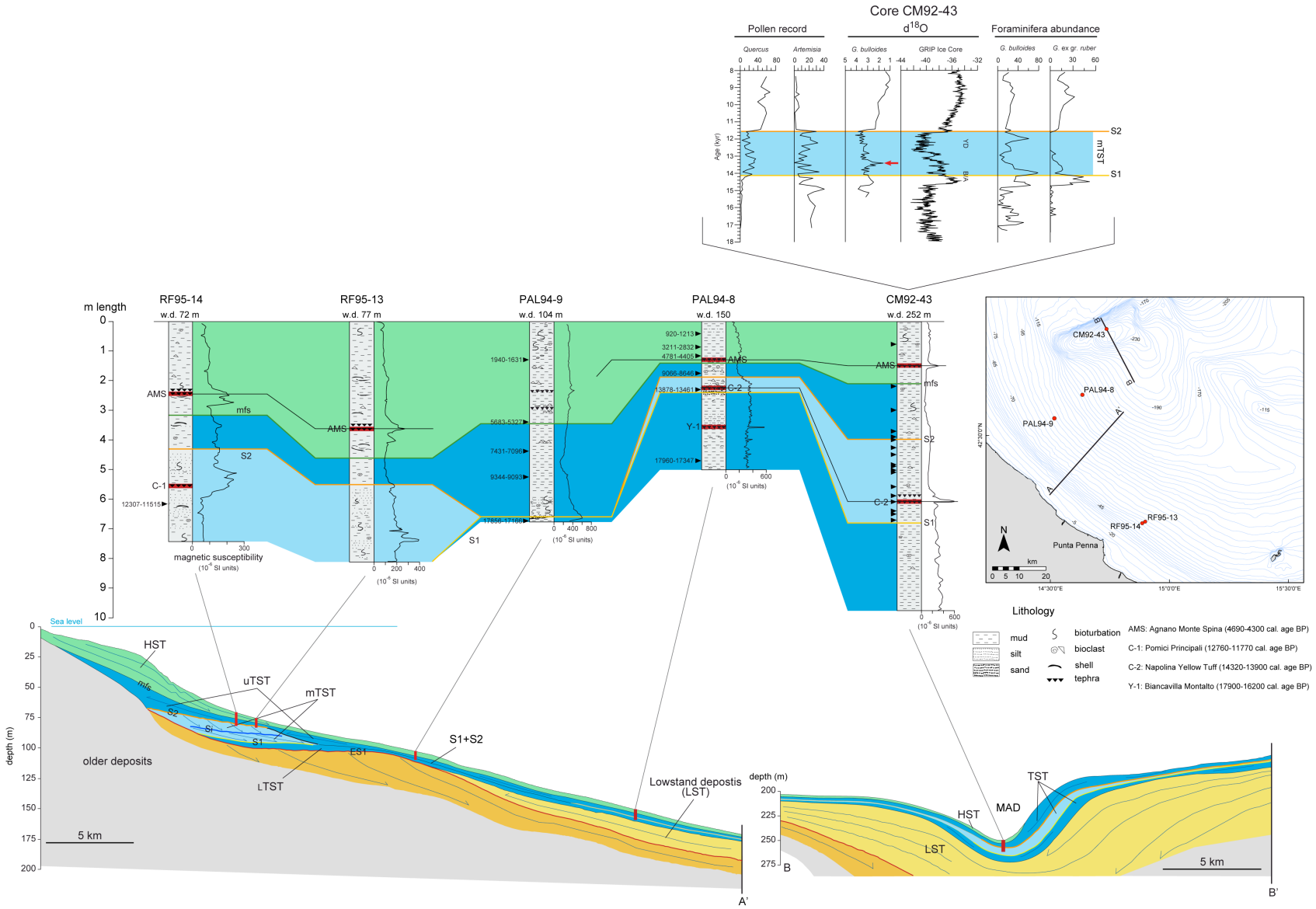
Core CM92-43
Pollen record
d18O
Foraminifera abundance
Quercus
Artemisia
G. bulloides
GRIP Ice Core
G. bulloides
G. ex gr. ruber
Age (kyr)
YD
B/A
S2
mTST
S1
m length
RF95-14
w.d. 72 m
RF95-13
w.d. 77 m
PAL94-9
w.d. 104 m
PAL94-8
w.d. 150
CM92-43
w.d. 252 m
AMS
mfs
S2
C-1
C-2
Y-1
S1
magnetic susceptibility
(10-6 SI units)
CM92-43
PAL94-8
PAL94-9
RF95-14
RF95-13
Punta Penna
N
km
Lithology
mud
silt
sand
bioturbation
bioclast
shell
tephra
AMS: Agnano Monte Spina (4690-4300 cal. age BP)
C-1: Pomici Principali (12760-11770 cal. age BP)
C-2: Napolina Yellow Tuff (14320-13900 cal. age BP)
Y-1: Biancavilla Montalto (17900-16200 cal. age BP)
Sea level
HST
mfs
uTST
mTST
S2
Si
S1
ES1
LTST
S1+S2
older deposits
Lowstand depostis
(LST)
depth (m)
5 km
A'
TST
MAD
HST
LST
B
B'

Fig. 7

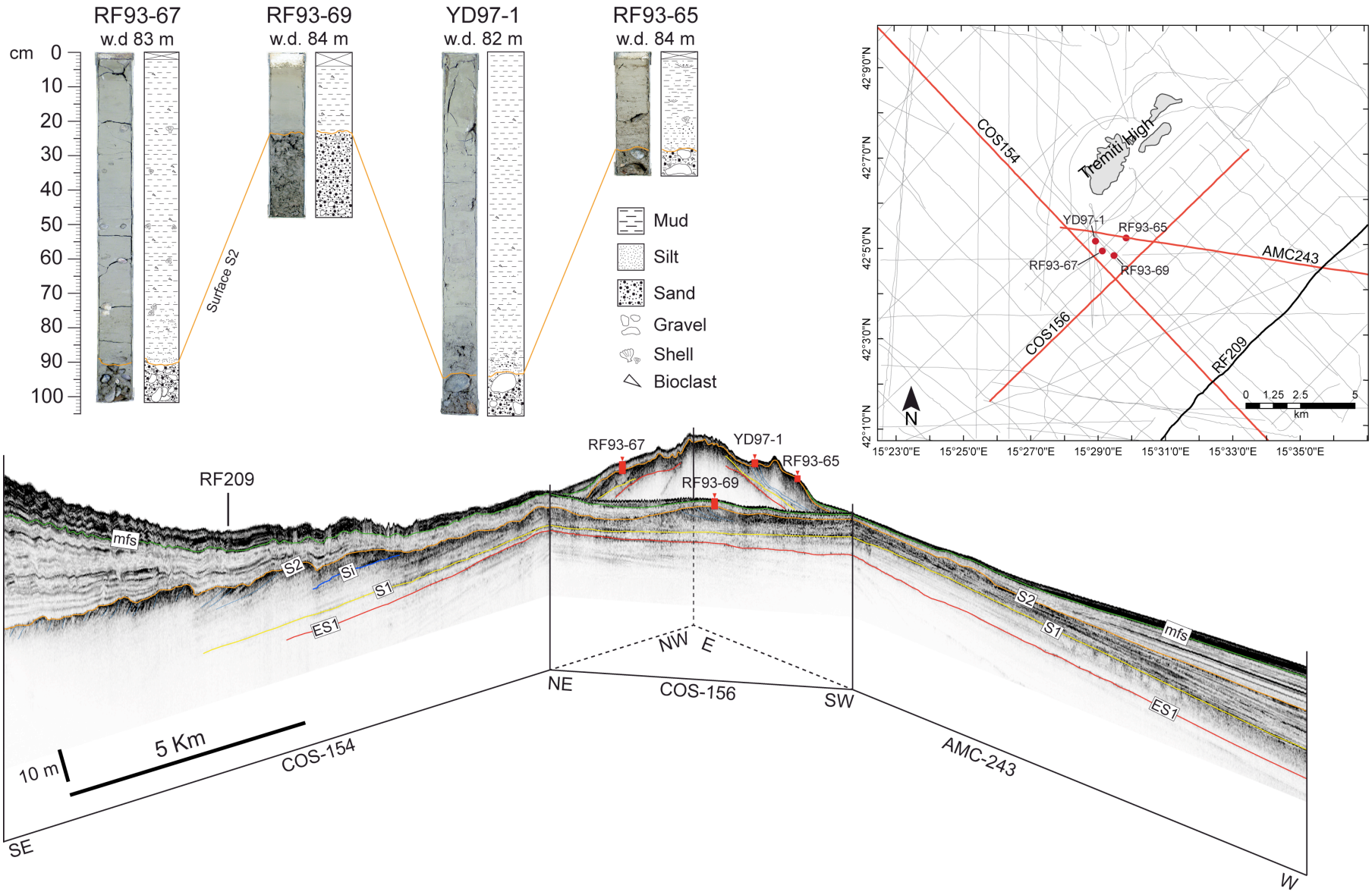
RF93-67
w.d 83 m
RF93-69
w.d. 84 m
YD97-1
w.d. 82 m
RF93-65
w.d. 84 m
cm 0
10
20
30
40
50
60
70
80
90
100
Surface S2
Mud
Silt
Sand
Gravel
Shell
Bioclast
COS154
Tremiti High
YD97-1
RF93-65
RF93-67
RF93-69
AMC243
COS156
RF209
N
0 1.25 2.5 5
km
42°9'0"N
42°7'0"N
42°5'0"N
42°3'0"N
42°1'0"N
15°23'0"E
15°25'0"E
15°27'0"E
15°29'0"E
15°31'0"E
15°33'0"E
15°35'0"E
RF93-67
YD97-1
RF93-65
RF93-69
RF209
mfs
S2
Si
S1
ES1
NW
E
NE
COS-156
SW
10 m
5 Km
COS-154
AMC-243
SE
W

Fig. 8

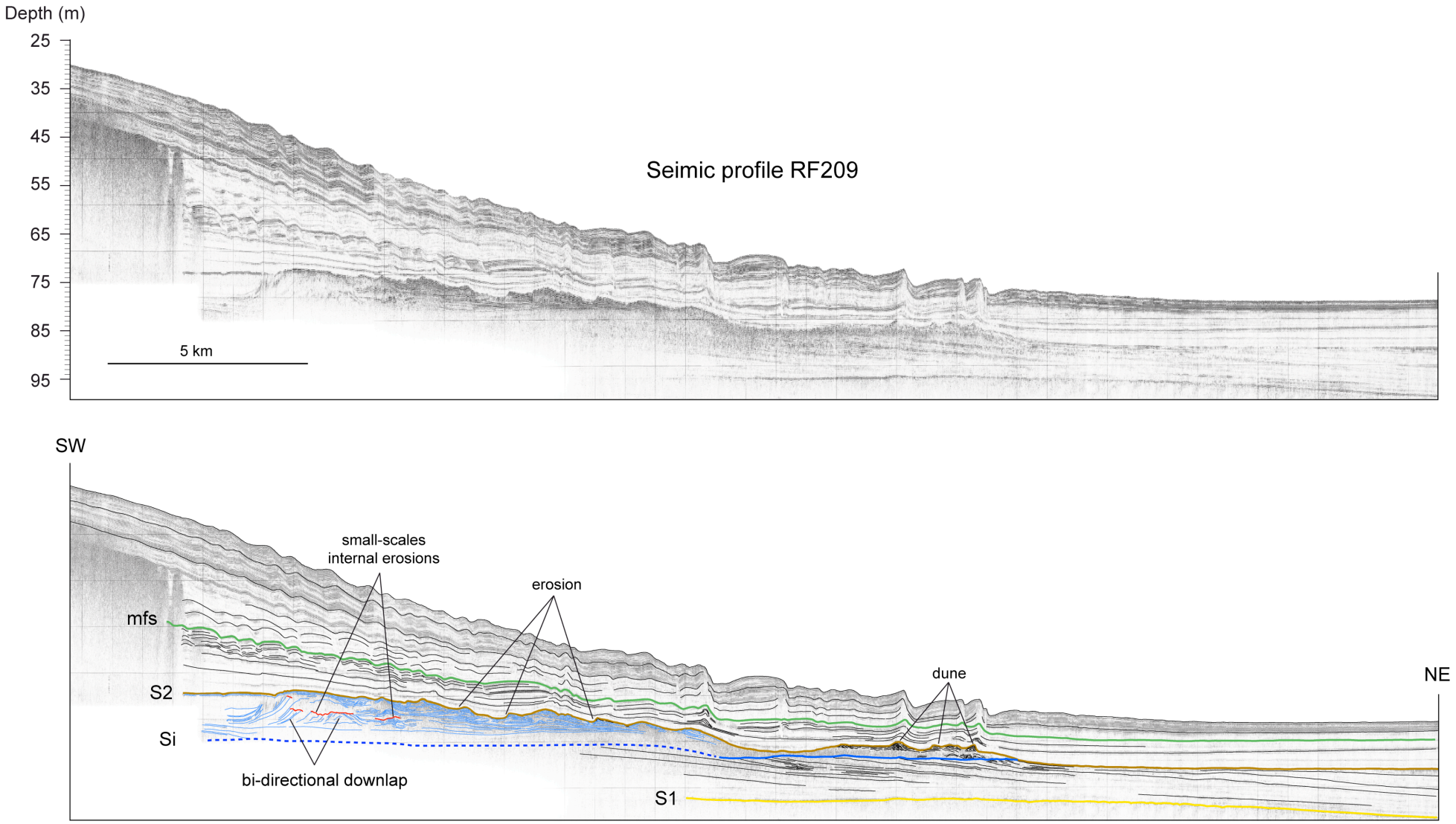
Depth (m)
25
35
45
55
65
75
85
95
Seimic profile RF209
5 km
SW
small-scales
internal erosions
erosion
mfs
S2
Si
dune
NE
bi-directional downlap
S1

Fig. 9

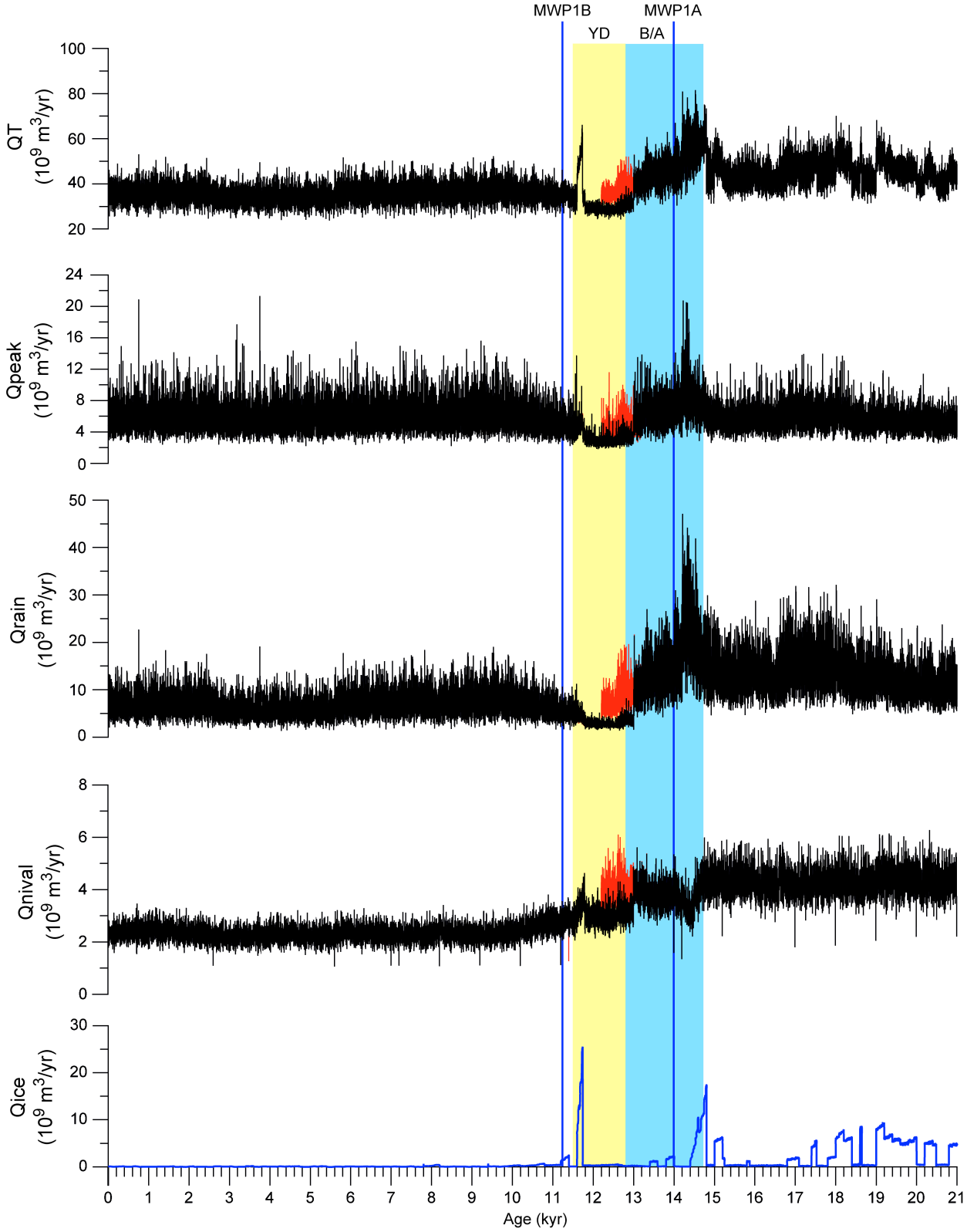
MWP1B
MWP1A
YD
B/A
QT
(10^9 m^3/yr)
Qpeak
(10^9 m^3/yr)
Qrain
(10^9 m^3/yr)
Qnival
(10^9 m^3/yr)
Qice
(10^9 m^3/yr)
Age (kyr)

Fig. 10

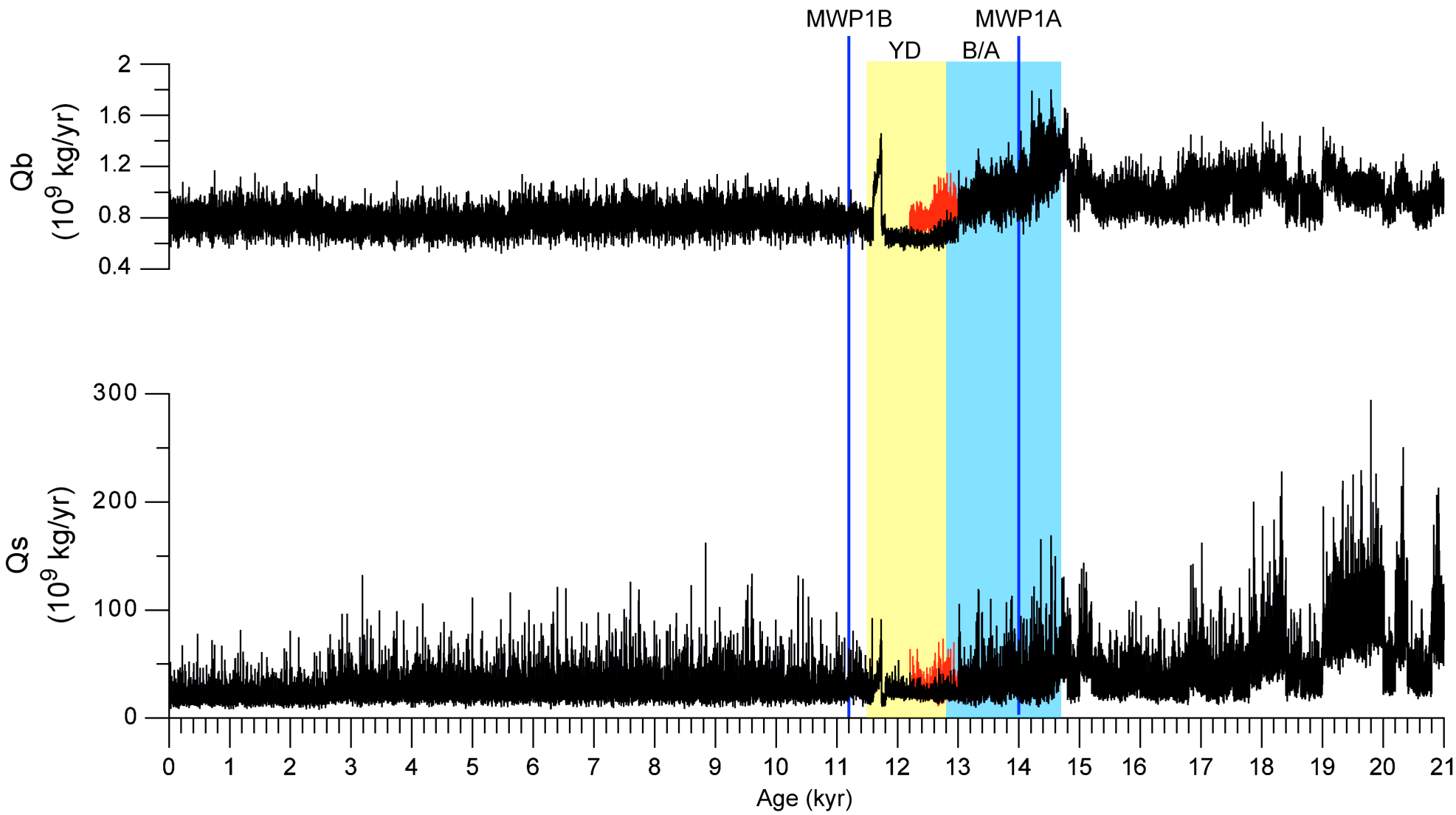
MWP1B
MWP1A
YD
B/A
Qb
(10^9 kg/yr)
2
1.6
1.2
0.8
0.4
Qs
(10^9 kg/yr)
300
200
100
0
0 1 2 3 4 5 6 7 8 9 10 11 12 13 14 15 16 17 18 19 20 21
Age (kyr)

Fig. 11

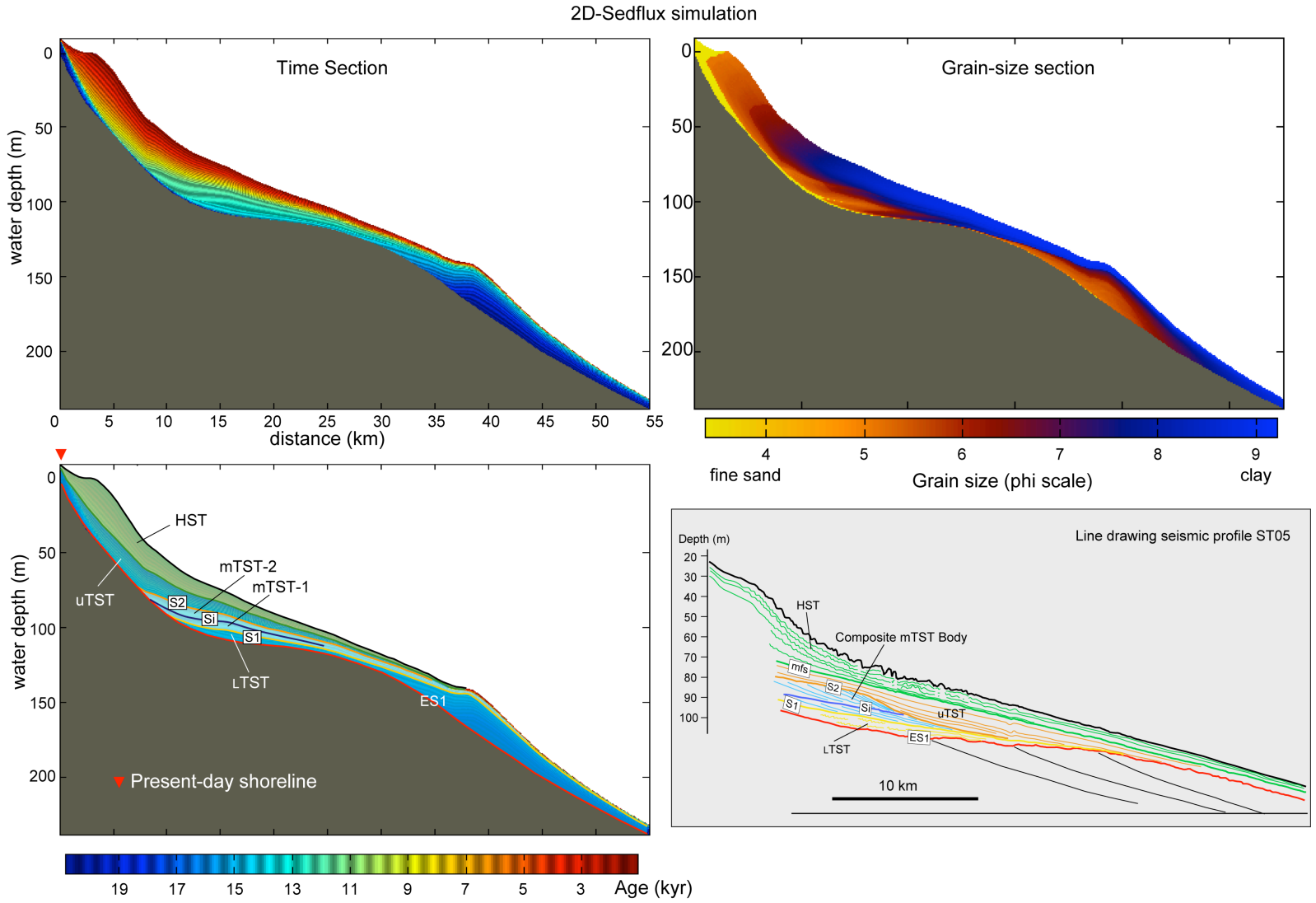
2D-Sedflux simulation
Time Section
water depth (m)
distance (km)
Grain-size section
fine sand
Grain size (phi scale)
clay
HST
mTST-2
mTST-1
uTST
S2
Si
S1
LTST
ES1
Present-day shoreline
Age (kyr)
Line drawing seismic profile ST05
Depth (m)
Composite mTST Body
mfs
10 km

Fig. 12

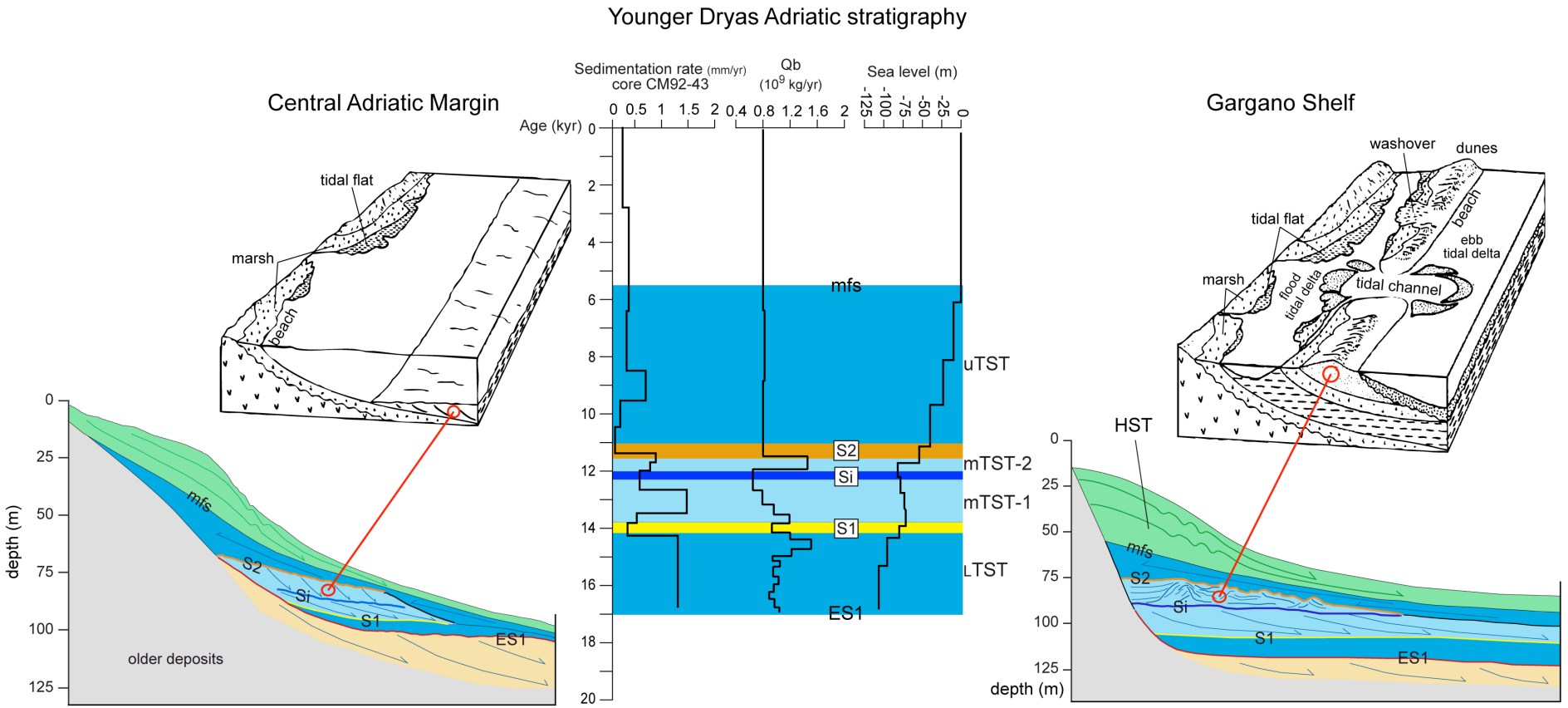
Younger Dryas Adriatic stratigraphy
Central Adriatic Margin
Gargano Shelf
Sedimentation rate (mm/yr)
core CM92-43
Qb
(10^9 kg/yr)
Sea level (m)
Age (kyr)
tidal flat
marsh
beach
washover
dunes
ebb
tidal delta
flood
tidal channel
mfs
S2
Si
S1
ES1
uTST
mTST-2
mTST-1
LTST
HST
older deposits
depth (m)

Tab. 1

e_b	Bedload efficiency (L^3/T)	Q_0	river discharge (L^3/T)
k_2	Global climate zone	u_0	mean river mouth flow velocity (L/T)
$\overline{Q}$	non-dimensional water discharge	b_0	channel width (L)
Q_T	Total water discharge (M/T)	h_0	channel depth (L)
Q_{rain}	Water discharge generated by rainfall (L^3T^{-1})	Qs_0	mean suspended sediment load leaving the river (M/T)
Q_{ice}	Water discharge generated by ice melt (L^3T^{-1})	Qb	bedload (M/T)
Q_{nival}	Water discharge generated by nival melt (L^3T^{-1})	Cs_i	concentration of the *i*th grain size (ML^{-3})
Q_{gr}	Water discharge generated by ground water (L^3T^{-1})	u	velocity in the x direction (L/T)
Q_{evap}	Water discharge loss by evapotraspiration (L^3T^{-1})	v	velocity in the y direction (L/T)
$\overline{Qs_t}$	total long-termo average suspended sediment discharge (MT^{-1})	λ	removal rate constant for a grain size (T^{-3})
$\overline{Qs_d}$	total suspended sediment discharge derived from glacial processes (MT^{-1})	x	distance in longitudinal direction (L)
$\overline{Qs_g}$	long-term total suspended sediment discharge (MT^{-1})	y	distance in lateral direction (L)
R	Maximum relief of river drainage basin from sea-level (L)	I	sediment inventory of the plume
S	Slope of the riverbed (L^{-1})	K	sediment diffussivity ($L^{-2}T^{-1}$)
$\overline{T}$	Basin wide average temperature (°C)	E_T	effective elastic thickness (L)
TE	Sediment trapping efficiency of reservoirs/lakes	ρ_m	density of the sediment (ML^{-3})
u	Stream velocity (L/T)	w	displacement of the crust due to sediment loading (L)
u_{cr}	Critical stream velocity (L/T)	c	empirical constant for compaction (LT^2M^{-1})
α_3-α_8	Global climate zone-based coefficients	ϕ	sediment porosity
λ	Limiting angle of repose of sediment grains lying on the river bed (°)	ϕ_0	porosity of sediment in its closest packed arrangement
ρ	Fluid desity (ML^{-3})	ρ_s	Grain density (ML^{-3})

CHAPTER V

The record of the last sea level rise in the northern Adriatic shelf. The Younger Dryas conundrum: Hypotheses and future investigations.

Introduction

In the last few decades the Adriatic Sea was intensively investigated in order to understand the impact of the Late Quaternary sea level fluctuations on the stratigraphic evolution of the basin (Trincardi et al., 1994; Amorosi et al., 1999; Ridente and Trincardi, 2002; Ridente et al., 2008), and to investigate the climatic oscillations of the central Mediterranean regions (Asioli et al., 2001; Amorosi et al., 2004; Piva et al., 2008a, b). Moreover, the central and, in particular, the northern Adriatic shelf, are ideal sites to quantify the magnitude and timing of the post-glacial sea level rise through the analysis of the Late Pleistocene-Holocene shallow marine transgressive deposits (Storms et al., 2008).

During the Last Glacial Maximum (LGM, ca. 18 kyr BP), when sea level reached its lowest position (of about -120 meters respect to present-day sea level elevation) after a long phase of slow sea level fall, the northern Adriatic shelf was almost completely in subaerial conditions, while the deepest part of the central Adriatic basin, the Mid Adriatic Deep (MAD), remained as a very small, shallow and semi-enclosed basin. Depending of the shelf morphology, the northern and central sector of the Adriatic Sea recorded the post-glacial sea level rise through the deposition of four correlative transgressive sedimentary bodies (Transgressive Systems Tract, TST; see Figure 5.1).

1 - Central Adriatic shelf

In central Adriatic margin, characterized by a ca. 50 km wide and 0.2° dip shelf, the transgressive record is composed a complex sedimentary succession more then 30 m thick, characterized by three depositional units in a backstepping configuration (Cattaneo and Trincardi, 1999). Moreover, as illustrated in Chapter 4, the middle TST unit, characterized by a prograding wedge deposited during the Younger Dryas cold event, recorded a period of high rate of sediment supply to the basin, and possibly a minor eustatic fall.

2 - South of the Tremity High

In the western Adriatic margin, confined between the Gargano Promontory and the Tremiti High, the Late Pleistocene-Holocene transgressive systems tract is still subdivided in a tripartite sedimentary body. In this area of the margin the prograding wedge corresponding to the middle TST unit is replaced by a complex barrier-island-lagoon system, confined at ca. -75 meters of water depth (see Chapter 4 for details).

3 - The Mid Adriatic Deep (MAD)

The MAD, located in the center of the Adriatic Sea and representing its deepest part with ca. 260 meters of water depth, is a small remnant basin that recorded a continuous marine sedimentation since glacial time, resulting in an undisturbed and expanded muddy succession. The sedimentary record of the MAD can be considered one of the best geological archive for paleo-environmental reconstructions in the Mediterranean Sea, as recorded all the climatic fluctuations during the last 20 kyr (Asioli et al., 2001; Piva et al., 2008a).

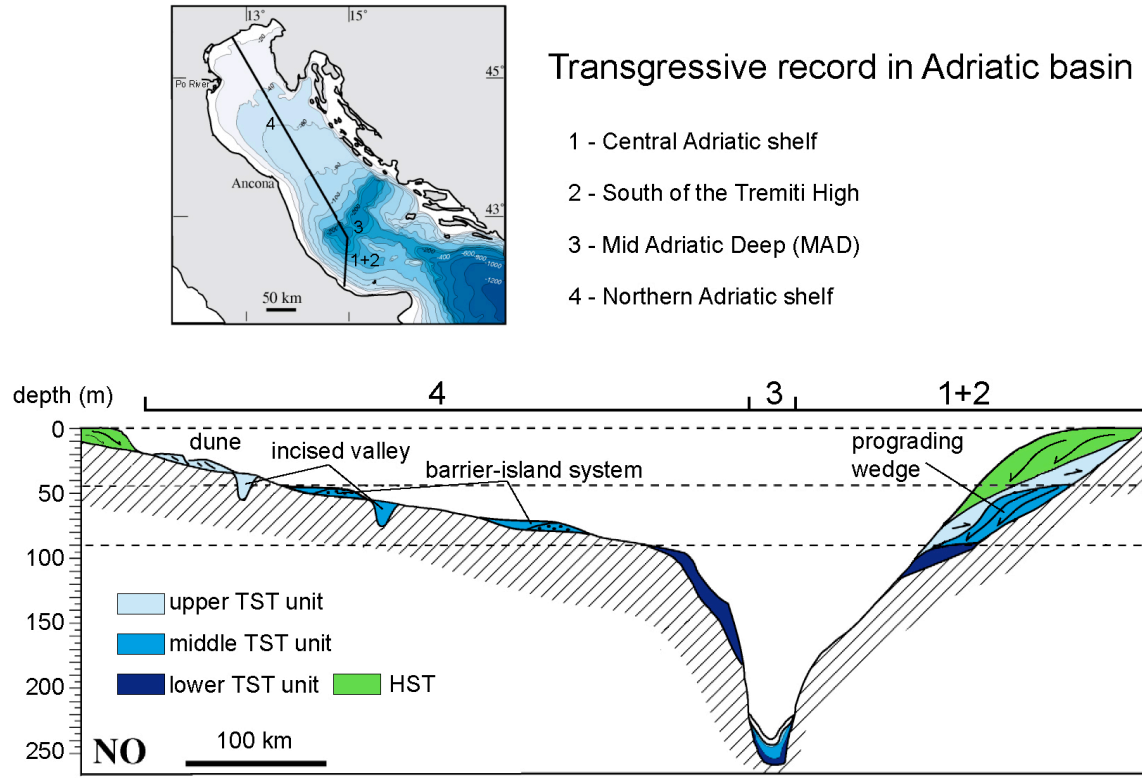

Figure 5.1 - Stratigraphic scheme of the Late Quaternary transgressive deposits along a section parallel to the axis of the Adriatic basin (modified from Trincardi et al., 1994; Cattaneo and Trincardi, 1999). The TST deposits along the central Adriatic margin are characterized by a muddy succession: its internal geometry and spatial distribution of the depocenters reflect the interaction between local tectonics, sediment supply and sea level fluctuations, marine circulation and preexisting sea floor morphologies. The MAD recorded the post LGM interval with a continuous deposition of marine mud (see Asioli et al., 2001). The transgressive record in the northern Adriatic shelf is characterized by sandy backstepping barrier-island systems with a patchy distribution, reflecting the step-wise nature of the post LGM sea level rise.

4 - The northern Adriatic shelf

During the LGM, the northern Adriatic shelf, a 350 km wide and 0.02° dip shelf, was almost completely exposed under subaerial conditions: at that time, a continuous alluvial plain incised by a "mega Po River" extended from the modern coastline toward the south, reaching the northern flank of the MAD. During the post-LGM sea level rise, the northern Adriatic shelf was progressively flooded, becoming an epicontinental shelf, mainly bottomed by the ravinement surface directly cutting continental deposits (Fig. 5.2).

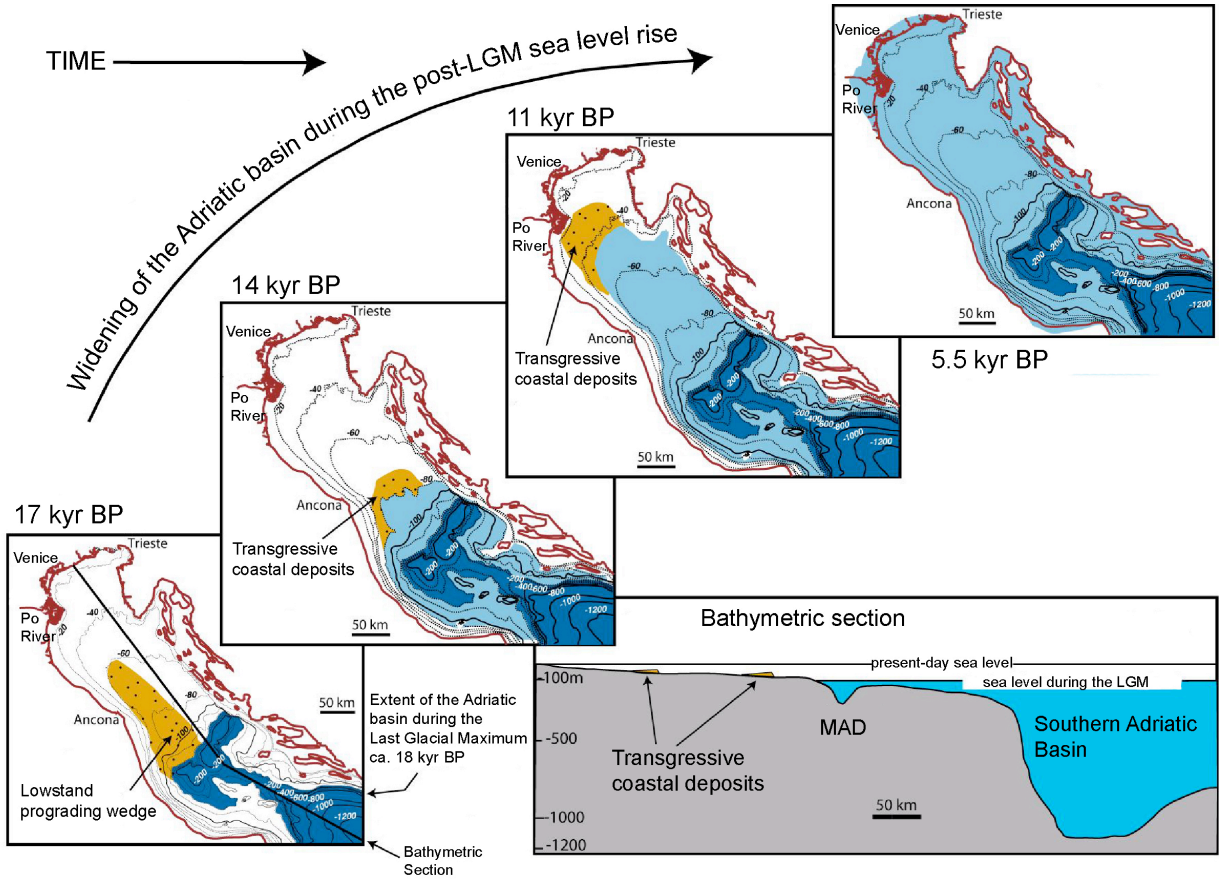

Figure 5.2 - Widening of the Adriatic basin forced by the post-glacial sea level rise (modified from Trincardi et al., 1994).

Although the post glacial eustatic rise was fast and widespread, it was however punctuated by short episodes of lowered rate of sea level rise, or, possibly, still-stand or even sea level fall. These steps in the eustatic trend were well recorded by patchy backstepping paralic deposits, including barrier-island, lagoon and incised-valley deposits, that were investigated in the last 15 yr by the ISMAR-CNR through a dense grid of seismic lines and sediment cores (Correggiari et al., 1996a, b; Correggiari et al., 1997; Storms et al., 2008).

Here I present the post-LGM sea level curve for the Adriatic basin, obtained by dating several shoreline indicators associated with the backstepping paralic deposits (i.e. lagoon peat

layers) of the northern Adriatic shelf, giving particular attention to two isolated areas, comprising the best preserved barrier-island deposits and recording the interval between the Meltwater Pulse 1A and the Younger Dryas cold event (Correggiari et al., 1996a).

The last sea level rise recorded in the northern Adriatic shelf

In the last few decades several Authors have tried to reconstruct the steps of the last sea level rise by the investigation of drowned coastal deposits (Hanebuth et al., 2000). The low-gradient continental shelf of the northern Adriatic Sea facilitates the preservation potential of paleo shoreline deposits, because a sea level rise of a few meters corresponds to a landward shift of several tens of kilometers of the shoreline. Moreover, the central sector of the northern Adriatic shelf was not reached by Late Holocene highstand deposits, forced against the mainland by the along-shore marine circulation flowing dominantly SE-ward (Cattaneo et al., 2007), and so can be easily investigated through high resolution seismic exploration and standard coring methods.

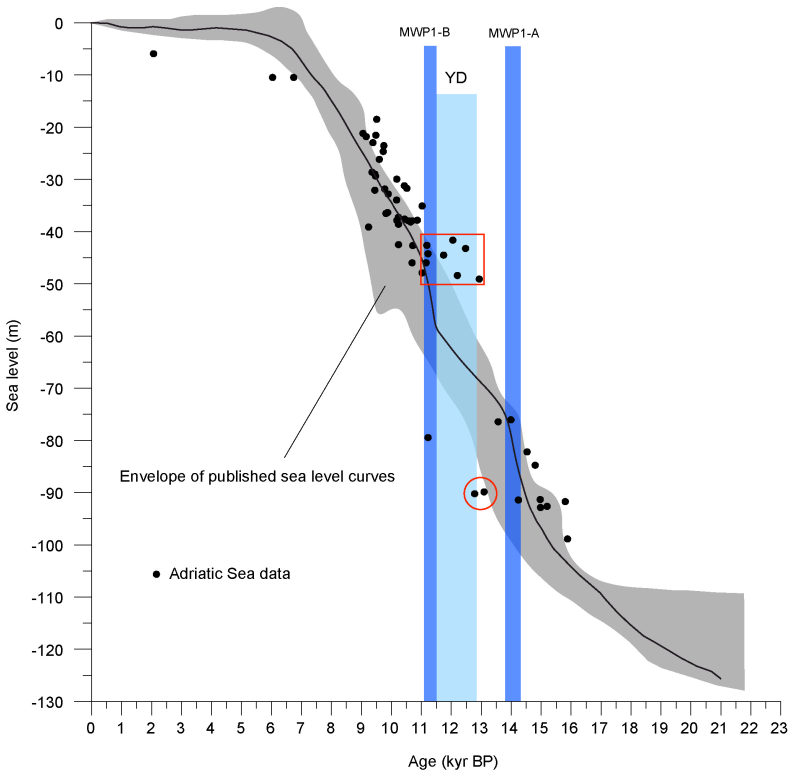

The last sea level rise has been reconstructed in the northern Adriatic shelf by dating several shoreline indicators: lagoon peat layers associated to barrier-island deposits or shells of mollusks living in water depth close to sea level (Fig. 5.3), as *Cerastoderma glaucum*. The sea level curve obtained shows a good fit with previous published sea level reconstructions (Correggiari et al., 1996a, b; 1997), albeit for the time interval between the two Meltwater Pulses, and in

Figure 5.3 - Comparison between published sea level curves (grey envelope, see Bard et al., 2010 and reference therein) and depth vs. age plot of calibrated ^{14}C dates from the northern Adriatic shelf (black dots). The square red box includes the ages obtained from the shallower deposit (Site A in Figure 5.4) while the red circle includes the ages obtained from the deeper paralic system (Site B in Figure 5.4). Timing of the Meltwater Pulses 1A and 1B (vertical blue bars) are derived from Bard et al., 1996. The light blue bar represents the Younger Dryas cold interval.

particular during the Younger Dryas cold reversal. At that time, two well define paralic sedimentary systems formed in the northern Adriatic shelf, at ca. -40 m and -90 m of water depth (see Figure 5.3).

The sedimentary record of the Younger Dryas

The transgressive deposits analyzed on several mid-latitude continental margins by using high resolution seismic methods and core sampling, indicate an enhanced sediment flux during the Younger Dryas, often ascribed to a still-stand or possibly a fall in sea level (Blanchon and Shaw, 1995; Abdulah et al., 2004; Anderson et al., 2004). Along other Mediterranean margins, the Younger Dryas interval within the TST is mainly characterized by two kinds of sedimentary deposits (although not univocally constrained chronologically): a thick prograding sedimentary wedge, characterized by basinward downlapping strata, or a drowned barrier-island sandy deposit (Hernández-Molina et al., 1994; Labaune et al., 2005; Bernè et al., 2007). As the prograding transgressive body characterizing the central Adriatic margin has been described and studied in Chapter 4, here the attention is focused on the analysis of drowned well preserved barrier-island deposits identified in the northern Adriatic shelf (see Figure 5.3).

The northern Adriatic YD record - SITE A

The northern Adriatic shelf, southeast of the modern Po River delta at ca. the -40 m isobath, is characterized by an elongated sand ridge, extending more then 30 km along the paleo-coastline (see Figure 5.4 and 5.5). The morphological expression of the sand ridge and the coarsening-upward trend deduced from sediment core analyses (Correggiari et al., 1996a; Correggiari et al., 1997), suggest that this sedimentary body is a drowned barrier island deposit. Schematic sections BB' and CC' in Figure 5.5 show that the barrier, formed by a sand ridge ca. 3 meters thick, is characterized by a steeper flank toward the south and is divided by two ravinement surfaces: the upper (named Rs in Figure 5.5) was possibly originated by wave reworking during transgression, and the lower was possibly related to migrating tidal channels (named tRs in Figure 5.5; Cattaneo et al., 2001). The overstepped barrier, see section CC' and the cross section DD', rests on a sub-horizontal platform, incised by small channels filled by pre-transgressive sediments. Several calibrated Radiocarbon ages, obtained by dating the peat layer at the base of the sand ridge (see black arrows in the schematic sections BB' and CC' in Figure 5.5), give and age ranging from 11.5 kyr BP to 13 kyr BP (Correggiari et al., 1996a; Storms et al, 2008).

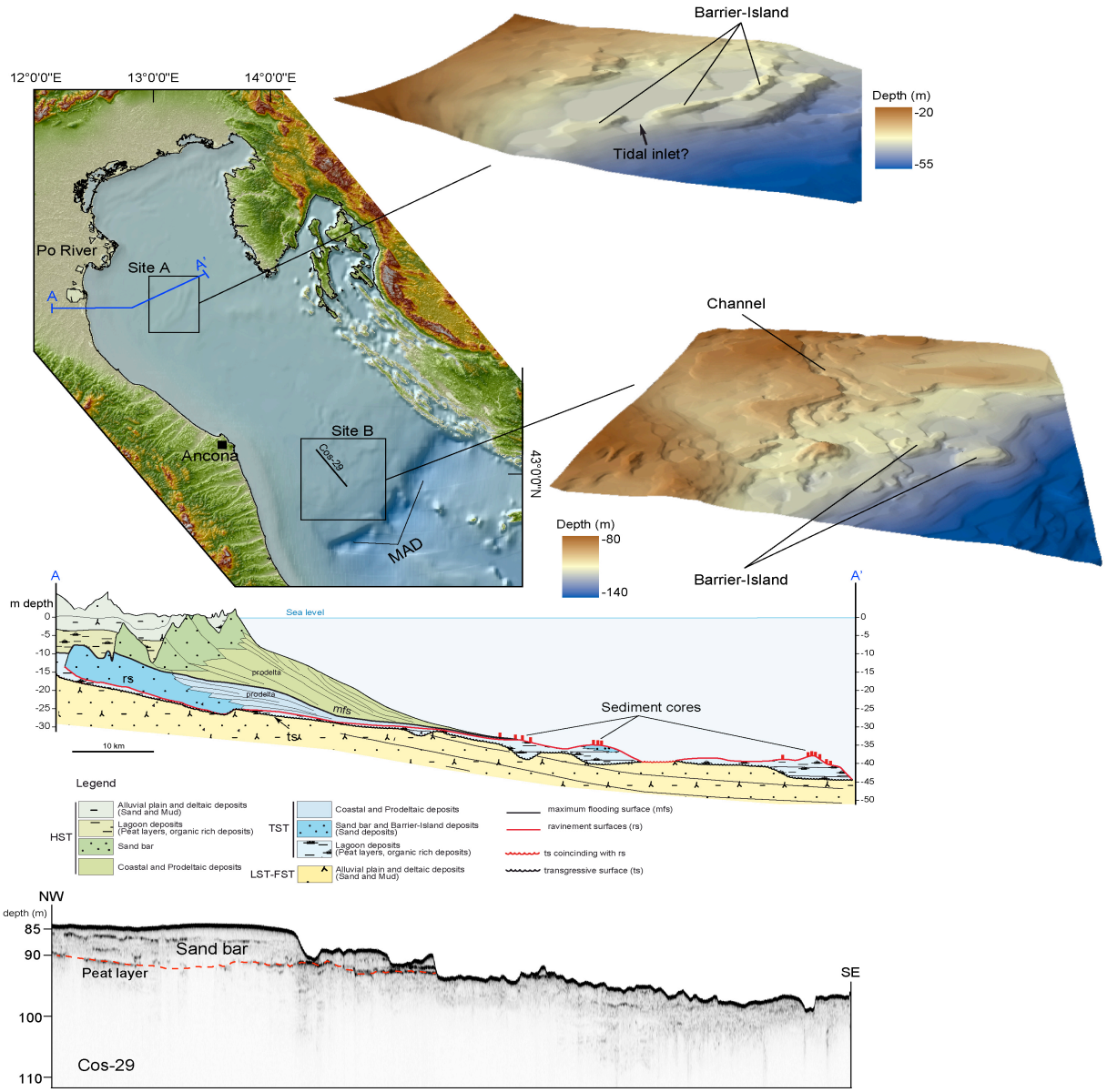

Figure 5.4 - Detailed 3D shaded morpho-bathymetric map showing the northern Adriatic best-preserved barrier-island deposits (square black boxes). Site A, offshore of Ravenna, is characterized by a more then 2 meters thick sand deposits, elongated more then 30 km in a NE-SW direction. Section AA', derived from a composite line drawing extending from the alluvial plain of Lamone river to offshore of the modern Po River delta (modified from Trincardi et al., in press, a), locates the preserved TST deposits relative to the distribution of the overlying HST deposits. Several of the cores, reported in section AA' as red vertical bars, reached the peat layer at the base of the barrier and give and age comprised between ca. 11.5 kyr and 13 kyr BP (Correggiari et al., 1996a). Site B, north of the MAD in ca. -90 meters of water depth offshore of Ancona, shows a complex morphology, derived from the marine reworking of transgressive barrier-island deposits (see seismic profile COS-29).

The northern Adriatic Sea, between -95 m and -80 m of water depth, is characterized by a relatively high gradient shelf, incised by a dense grid of sinuous channels, which are up then 20 km long, more then 10 meters deep, and separated by sand ridges (Cattaneo et al., 2001). A thin peat layer, correlated in high-resolution seismic profiles, rests conformably on the lowstand alluvial plain deposits and forms the base of the transgressive barrier deposits.

The peat layer (see red line in seismic profile I, Figure 5.6) is covered by 1-3 meters thick coarsening-upward sequence, usually associated with a transgressive backbarrier setting, suggesting that barrier island deposits were present during this phase of rapid sea level rise. The inferred age of the peat layer, sampled in several cores (see the map in Figure 5.6), range between 13 kyr BP and 14.5 kyr BP (Correggiari et al., 1996a). As illustrated in Figure 5.6, the base of some channels coincides with the peat layer (seismic profile II), whereas some other channels incise below the peat layer (seismic profile I). Moreover, seismic profiles suggest that most of the channels are not filled with sediment, exception made for a narrow (less the 500 meters) incised distributary channel more then 15 meters deep, completely filled by transgressive sediment (see seismic profile III in Figure 5.6), characterized by centimeter to millimetre-scale alternating silt and mud deposits from both marine and fluvial origin, and eroded at the top by a ravinement surface (see the core log AN97-34 in Figure 5.6). The modeling simulations described in Storms et al. (2008) suggest that the tidal amplification for the time interval corresponding to this phase of transgression (associated to the onset of MWP-1A) would provide a potential scenario for the estuarine infill of this channel.

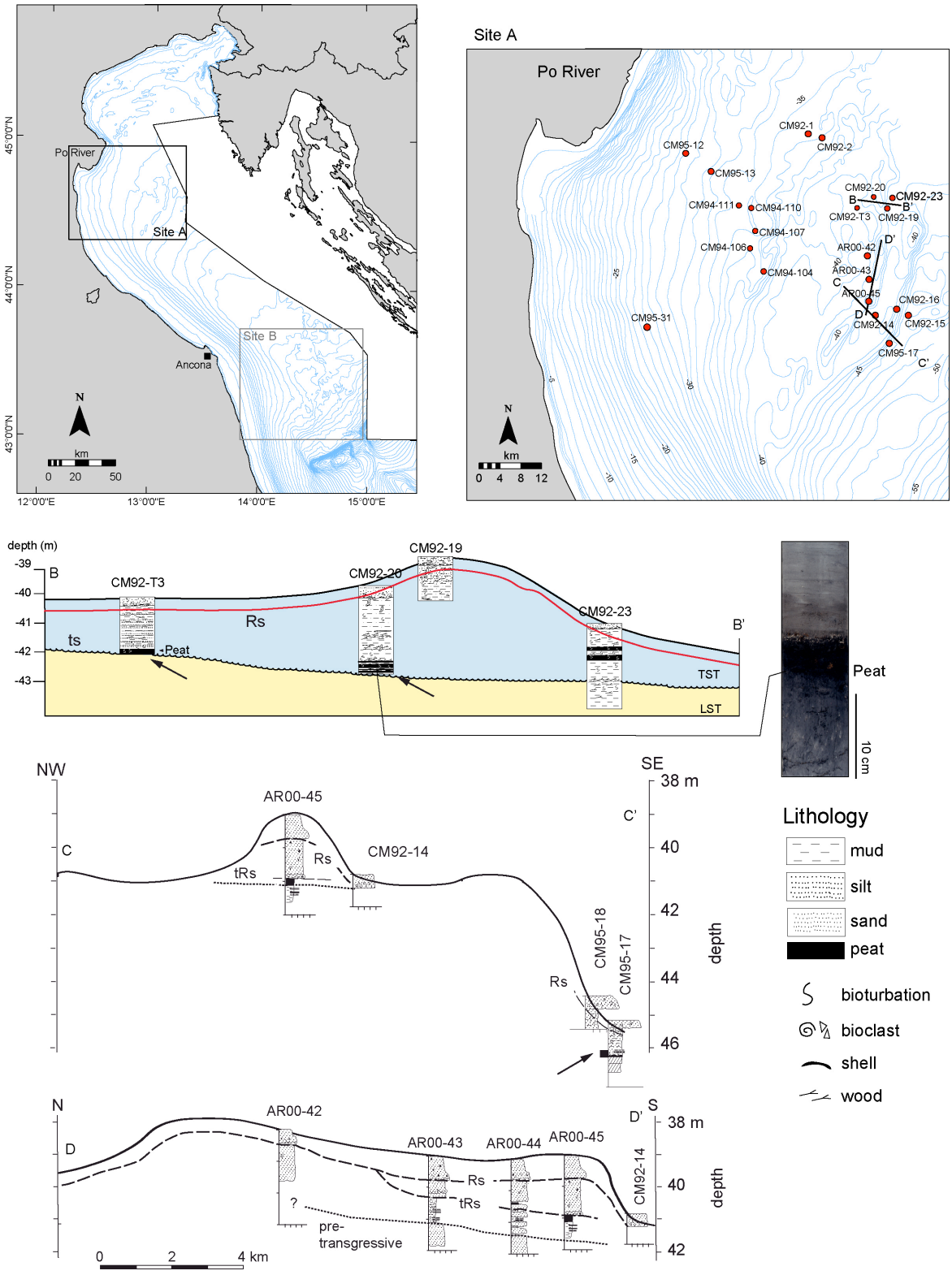

Figure 5.5 - Top left: Location of the shallowest barrier-island deposits (Site A, see black square); Top right: sediment cores reported on a detailed bathymetric map, which also shows the location of the three interpreted sections (BB', CC' and DD') reported in the lower part of the figure. Bottom: Section BB' shows a core correlation scheme across the northern sand bar deposit (modified from Trincardi and Argnani, 2001); Section CC' and DD' shows two schematic perpendicular sections across the overstepped barrier deposits (modified from Cattaneo et al., 2001). The black arrows in sections BB' and CC' represents the dated peat layer used for estimating the age of the barrier system and for reconstruct the sea level curve of Figure 5.3.

If the interpretations made are correct, in the interval between ca. 14 kyr BP and 11.5 kyr BP, roughly corresponding to onset of the Meltwater Pulse 1A and the end of the Younger Dryas cold reversal, the north Adriatic shelf is characterized by two distinct barrier-island deposits, one at ca. -40 mbsl, offshore of Ravenna (site A), and the other at ca. -90 mbsl, offshore of Ancona (site B). Several explanations and different models can be attempted to explain this conundrum, but, at this time, the problem is yet unsolved.

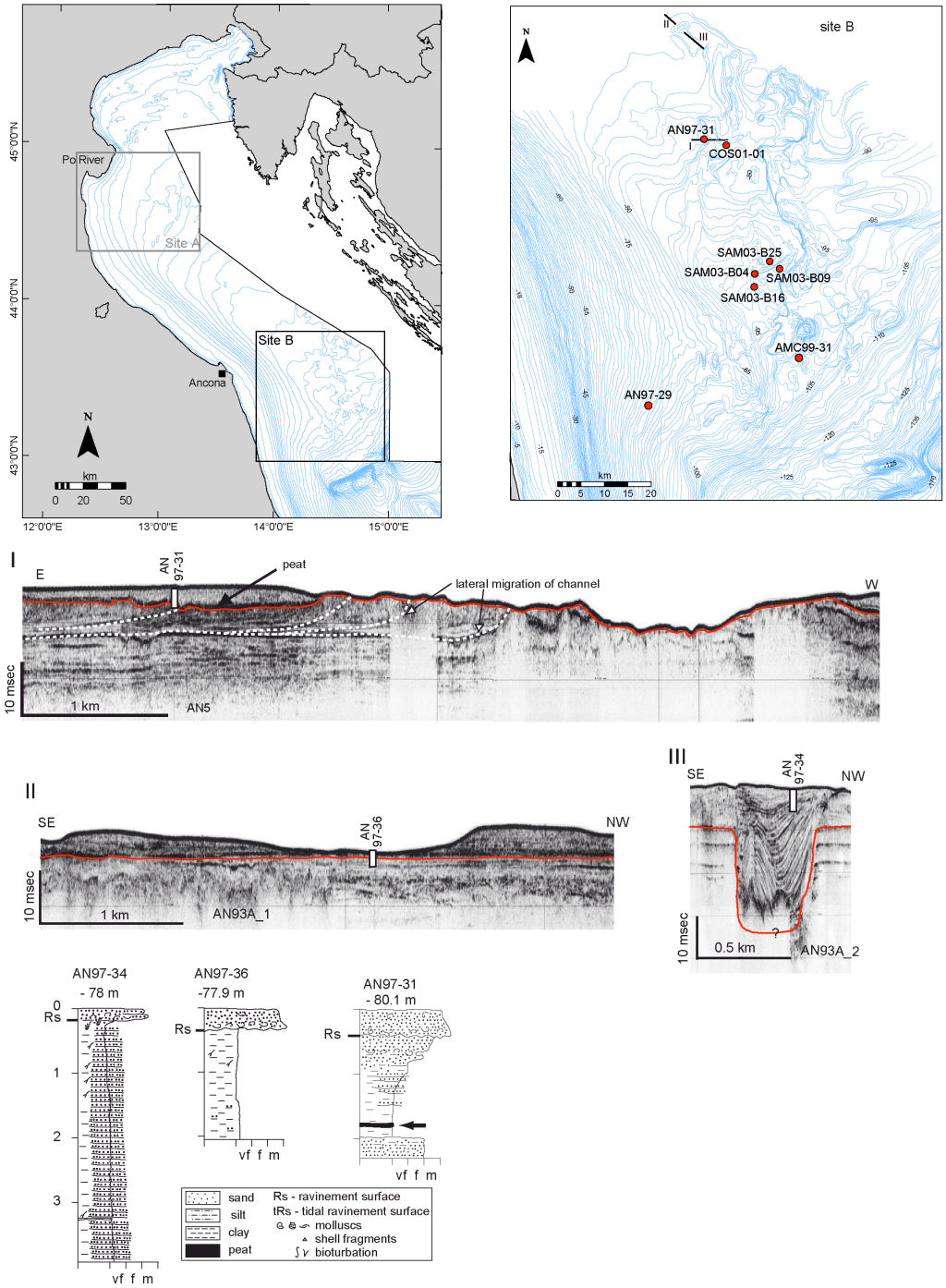

Figure 5.6 - Top left: Location of deepest transgressive barrier-island deposit (Site B, see black square). Top right: sediment cores reported on a detailed bathymetric map; back lines represent the three seismic profiles reported in the center of the figure. Center: Shallow seismic profiles of the deep isolated sediment body. The solid red line

separates the lowstand alluvial plain deposits (below) from the transgressive sediment. In profiles I and II the red line coincides with the sampled (and dated) peat layer. Bottom (modified from Correggiari et al., 1996a; and Storms et al., 2008): Schematic interpreted lithological data sampled within the sand bars (core AN97-31); within an empty channel (core AN97-36) and within a filled channel (core AN97-34).

The Younger Dryas conundrum

Here we present a set of possible alternate explanations:

1 - The two shoreline deposits reveal a very rapid and high magnitude sea level fluctuation in the interval comprised between the end of the Meltwater pulse 1A and the Younger Dyas, but this implies an unlikely sea level "jump" (rise and fall or just a rapid rise) of about 50 m in less then two thousand years (see Figure 5.3). At this time, this explanation is not supported by any independent evidence from δO^{18} records in the ocean, although a minor sea level fall during the Younger Dryas is now considered plausible in the models put forward by Siddall et al., (2010), and can explain the origin of the deposited formed at ca. -90 meters below sea level (red circle in Figure 5.7).

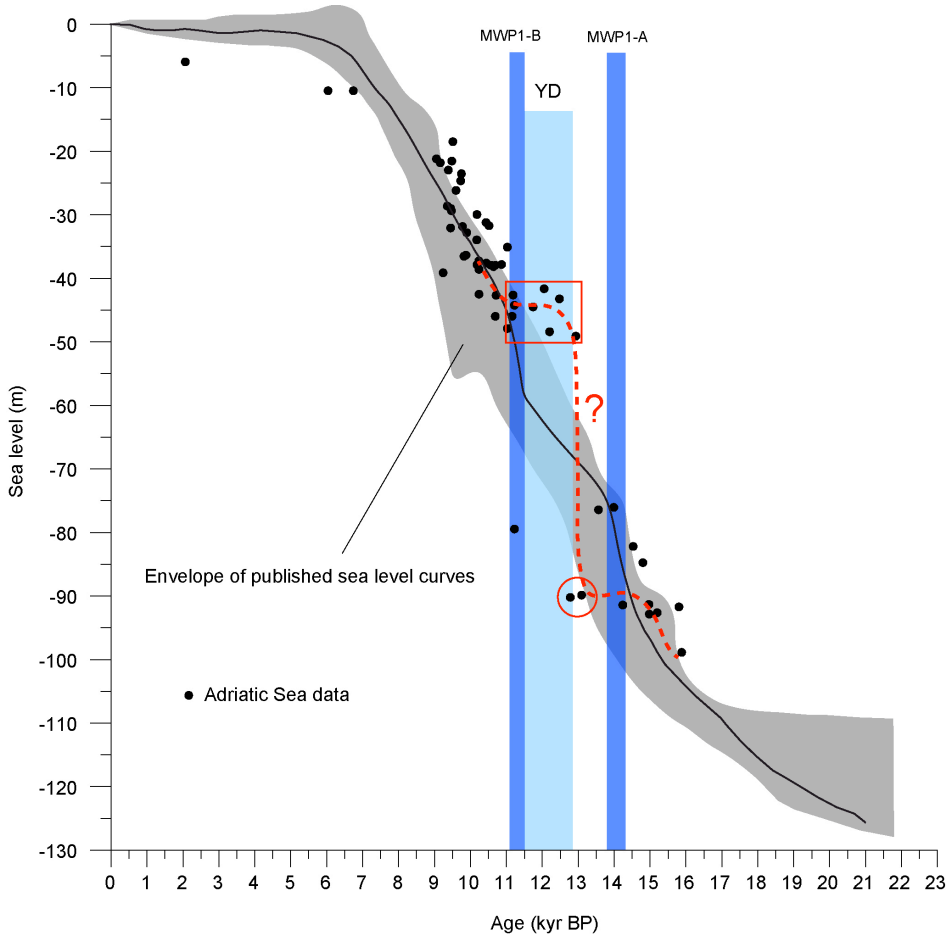

Figure 5.7 - The red dashed line represents one of the possible explanations for the mechanism governing the formation of the barrier-island systems in Site A and B.

2 - The two areas are affected by differential tectonic movements and this implies that the Site A recorded a tectonic uplift of about 20 meters in less then 12 kyr, in a very localized area. At this time, the rates of tectonic uplift or subsidence in this part of the northern Adriatic shelf are not well defined. The only available data can be found in the paper of Amorosi et al. (1999) and Massari et al. (2004), who reported the subsidence rate along the western side of the margin, in the area of Ravenna (subsidence rate 1.0 mm/yr) and Venice (subsidence 0.6 mm/yr) respectively. To explain the huge amount of uplift necessary to justify the elevation of the deposit in Site A (ca. 1.7 mm/yr in the last 12 kyr), only local tectonics movements can be considered, among which salt diapirism, which can explain why this tectonic trend affected only a small area. This hypothesis can be verified by the analysis of deep seismic line, not present at this time in the area.

3 - As highlighted by several Authors, radiocarbon dating techniques are affected by several sources of errors, the most important of which are: 1 - life effects of the dated samples, 2 - reservoir corrections, necessary for marine samples, 3 - calibration methods, 4 - hard-water effect. The most realistic explanation for this dual character of the northern Adriatic Younger Dryas deposits is that the ^{14}C age estimates can be affected by errors, especially referring to the samples of site A

Dating peat layers leaves some of the problems mentioned before, as life effects or reservoir corrections, but are strongly influenced by hard-water effect, a term used to describe the inclusion of old-carbon derived from dissolved carbonate rocks (Grimm et al., 2009). This source of error has long been known (Broecker and Walton, 1959; Andree et al., 1986), but still remain one of the most crucial to remove. Several published papers indicate that the hard-water effect can old the age of a sample up to 2000 yr (Rea and Colman, 1995; Philippsen et al., 2010). If the samples recovered in site A have included older carbon, possibly carried by the Po River, the ^{14}C dating method could reveal an older age: introducing a correction of ca. 1000 yr, all the samples of site A would fit the sea level curve obtained from previous published papers. This hypothesis should be confirmed by independent observations like, for example, those coming from the analysis of pollen spectra: if the age of the samples is correct, the pollen association of the Younger Dryas can be easily recognized for the presence of Artemisia and the scarcity of broad-leave trees.

CONCLUSION

The main results of the three-years PhD thesis work helped to better understand and quantify the tectonics of the central Adriatic region, the mechanisms governing the deposition along the central and northern Adriatic shelves, the timing of the last sea level rise and its impact on the deposition and the preservation of the Adriatic transgressive sedimentary successions.

The main results can be summarized as follows:

1) As subsidence controls the filling pattern of sedimentary basins and is one of the key factors contributing to past sea level changes, the first goal was to quantify its rate along the central Adriatic margin, not yet quantified before. The results, obtained by integrating geohistory analysis of the borehole PRAD1.2, direct investigations of lowstand shoreline deposits, and paleo-environmental reconstructions, indicate that the central Adriatic margin subsides at a rate of ca. 0.3 mm/yr during the last 400 kyr, representing a transfer zone between the northern high subsidence (ca. -1 mm/yr) Adriatic and the uplifting (ca. +0.4 mm/yr) Apulia regions. This subsidence trend, compared with the sedimentation rate obtained through the borehole PRAD1.2, explains also: a) the previously recognized backstepping configuration of the last four depositional sequences of the central Adriatic margin; b) the coarser and shallower nature of the sediment associated with erosional surface ES4, recognized in seismic profiles and in the borehole PRAD1.2; c) the progressive deepening of the margin at the site of the borehole, as illustrated by foraminifera assemblages, which highlights an evolution of the depositional environment from inner-shelf, during MIS 10, to upper-slope conditions during MIS 2.

2) The central Adriatic margin recorded the post LGM sea level rise with the deposition of two correlative sedimentary bodies: in the MAD, where the TST is characterized by a continuous and expanded section of marine mud, and along the central Adriatic shelf, where the TST is composed by a tripartite body more then 30 m thick. In detail, the middle TST unit (mTST), investigated along the central Adriatic shelf, is bounded by two erosional surfaces generated during the two Meltwater Pulses 1A and 1B, and is composed by a prograding wedge, possibly deposited during the Allerød to Younger Dryas transition. Modeling simulations obtained with two coupled models, HydroTrend v.3.0 and 2D-Sedflux 1.0C, integrated with sediment core analyses and with previous studies on pollen spectra and foraminifera associations, indicate that: a) the Younger Dryas cold reversal was characterized by enhanced sediment flux as a consequence of a decline in soil vegetation cover in the catchment area; b) the composite internal geometry of the prograding mTST wedge (and in particular the internal erosional surface) records a still-stand or possibly a fall in sea level close to the end of the Younger Dryas. This conclusion is supported by the evidence of a Younger Dryas paleo-shoreline deposit at ca. -75 m depth in the area between the Tremity High and the Gargano Promontory.

3) The broad and shallow northern Adriatic shelf, recorded the last sea level rise with the deposition of a series of backstepping barrier-island deposits, each associated with the main steps of the last sea level rise. An age-depth plot derived from dating these shoreline indicators (in particular lagoon peat layers or shells of mollusks living close to sea level, such as *Cerastoderma Glaucum*) made it possible to quantify a relative sea level curve for the Adriatic basin. The result obtained is in good agreement with other published sea level curves, although the interval corresponding to the Younger Dryas is more problematic. In particular, at that time, two shoreline indicators appear to characterize the northern Adriatic shelf at very different water depths: one at ca. -90 m offshore of Ancona, and one at ca. -40

m offshore of the modern Po River system. To understand this dual character, several hypotheses have been introduced and confuted, but, at this time, the problem remains unsolved.

REFERENCES

Abdulah, K.C., J.B. Anderson, J.N. Snow and L. Holford-Jack (2004), The Late Quaternary Brazos and Colorado deltas, offshore Texas, USA - their evolution and the factors that controlled their deposition. In: Anderson, J.B., Fillon, R.H. (Eds.), Late Quaternary Stratigraphic Evolution of the Northern Gulf of Mexico Margin, *SEPM Spec. Publ. Soc. Sediment. Geol.*, **79**, 237-269, Tulsa, Oklahoma.

Adhemar, J.A. (1982), Révolutions de la mer, déluges pédiodiques, *Carilian-Goeury et V. Dalmont*, pp.184, Paris, France.

Alley, R.B., D.A. Meese, C.A. Shuman, A.J. Gow, K.C. Taylor, P.M. Grootes, J.W.C. White, M. Ram, E.D. Waddington, P.A. Mayewski and G.A. Zielinski (1993), Abrupt increase in snow accumulation at the end of the Younger Dryas event, *Nature*, **362**, 527-529.

Alley, R.B., and P.U. Clark (1999), The deglaciation of the Northern Hemisphere: A global perspective, *Annual Rev. Earth Planet. Sci*., **27**, 149-182.

Alley, R.B. (2000), The Younger Dryas cold interval as viewed from central Greenland, *Quaternary Science Reviews*, **19**, 213-226.

Amorosi, A., M.L. Colalongo, F. Fusco, G. Pasini and F. Fiorini (1999), Glacio-eustatic control of continental-shallow marine cyclicity from Late Quaternary deposits of the southeastern Po Plain, northern Italy, *Quaternary Research*, **52**, 1-13.

Amorosi, A., M.L. Colalongo, F. Fiorini, F. Fusco, G. Pasini, S. C. Vaiani and G. Sarti (2004), Palaeogeographic and Palaeoclimatic evolution of the Po Plain from 150-ky core records, *Global and Planetary Change*, **40**, 55-78.

Anderson, J.B., A. Rodriguez, K.C. Abdulah, R.H. Fillon, L.A. Banfield, H.A. McKeown and J.S. Wellner (2004), Late Quaternary Stratigraphic evolution of the northern Gulf of Mexico margin: a synthesis. In: Anderson, J.B., and R.H. Fillon (Eds.), Late Quaternary Stratigraphic Evolution of the Northern Gulf of Mexico Margin, *SEPM Spec. Publ. Soc. Sediment. Geol.*, **79**, 1-23, Tulsa, Oklahoma.

Andree, M., H. Oeschger, U. Siegenthaler, T. Riesen, M. Moell, B. Ammann and K. Tobolski (1986), ^{14}C dating of plant macrofossils in lake sediment, *Radiocarbon*, **28**, 411-416.

Antonioli, F., M. Anzidei, K. Lambeck, R. Auriemma, D. Gaddi, S. Furlani, P. Orru, E. Solinas, A. Gaspari, S. Karinja, V. Kovacic and L. Surace (2007), Sea-level change during the Holocene in Sardinia and in the northeastern Adriatic (central Mediterranean Sea) from archaeological and geomorphological data, *Quaternary Science Reviews*, **26**, 2463-2486.

Argnani, A., and F. Frugoni (1997), Foreland deformation in the Central Adriatic and its bearing on the evolution of the Northern Apennines, *Ann. Geof.*, **40**, 771-780.

Argnani, A., and F. Ricci Lucchi (2001), Tertiary Siliciclastic Turbidite Systems. In: Vai, G.B., and I.P. Martini (Eds.), Anatomy of an Orogen: the Apennines and adjacent Mediterranean basins, *Kluwer Academic Pubblication*, 327-350, Dordrecht, Netherlands.

Ariztegui, D., A. Asioli, J.J. Lowe, F. Trincardi, L. Vigliotti, F. Tamburini, C. Chondrogianni, C.A. Accorsi, M. Bandini Mazzanti, A.M. Mercuri, S. Van der Kaars, J.A. McKenzie and F. Oldfield (2000), Palaeoclimate and the formation of sapropel S1: inferences from late Quaternary lacustrine and marine sequences in the central Mediterranean region, *Palaeogeogr. Palaeoclimatol. Palaeoecol*., **158**, 215-240.

Artegiani, A., R. Azzolini and E. Salusti (1989), On dense water in the Adriatic Sea, *Oceanol. Acta*, **12**, 151-160.

Asioli, A., F. Trincardi, J.J. Lowe, D. Ariztegui, L. Langone and F. Oldfield (2001), Sub-millennial scale climatic oscillations in the central Adriatic during the Lateglacial: palaeoceanographic implications, *Quaternary Science Reviews*, **20**, 1201-1221.

Barber, D.C., A. Dyke, C. Hillaire-Marcel, A.E. Jennings, J.T. Andrews, M.W. Kerwin, G. Bilodeau, R. McNeely, J. Southon, M.D. Morehead and J.-M. Gagnon (1999), Forcing of the cold event of 8,200 years ago by catastrophic drainage of Laurentide lakes, *Science*, **400**, 344-348.

Bard, E., B. Hamelin, M. Arnold, L. Montaggioni, G. Cabioch, G. Faure and F. Rougerie (1996), Deglacial sea-level record from Tahiti corals and the timing of global Meltwater discharge, *Nature*, **382**, 241-244.

Bard, E., B. Hamelin and D. Delanghe-Sebatier (2010), Deglacial Meltwater Pulse 1B and Younger Dryas sea levels revisited with boreholes at Tahiti, *Science*, **327**, 1235-1237.

Berger, A. (1984), Accuracy and frequency stability of the Earth's orbital elements during the Quaternary, In: Berger, A., J. Imbrie, H. Hays, G. Kukla and B. Saltzman (Eds.), Milankovitch and Climate – Part 1, *Reidel Publishing*, 3-40, Dordrecht, Netherlands.

Berger, A., and P. Pestiaux (1984), Accuracy and stability of the Quaternary terrestrial insolation, In: Berger, A., J. Imbrie, H. Hays, G. Kukla and B. Saltzman (Eds.), Milankovitch and Climate – Part 1, *Reidel Publishing*, 55-82, Dordrecht, Netherlands.

Berné, S., G. Jouet, M.A. Bassetti, B. Dennielou and M. Taviani (2007), Late Glacial Preboreal sea-level rise recorded by the Rhône deltaic system (NW Mediterranean), *Marine Geology*, **245**, 65-88.

Blanchon, P., and J. Shaw (1995), Reef drowning during the last deglaciation: Evidence for catastrophic sea-level rise and ice-sheet collapse, *Geology*, **23**, 4-8.

Bondesan, M., G.B. Castiglioni, C. Elmi, G. Gabbianelli, R. Marocco, P.A. Pirazzoli and A., Tomasin (1995), Coastal areas at risk from storm surges and sea-level rise in northeastern Italy, *Journal of Coast. Res.*, **11**, 1354-1379.

Broecker, W.S., and A. Walton (1959), The geochemistry of ^{14}C in the freshwater systems, *Geochimica et Cosmochimica Acta*, **16**,15-38.

Broecker, W.S., and J. Van Donk (1970), Insolation changes, ice volume and the O-18 record in deep-sea cores, *Review of Geophysics and Space Physics*, **8**, 169-198.

Broecker, W.S., M. Andree, W. Woli, H. Oeschger, G. Bonani, J. Kennett and D. Peteet (1988), The chronology of the last deglaciation: Implications to the cause of the Younger Dryas event, *Paleoceanography*, **3**, 1-19.

Broecker, W.S. (1998), Paleocean circulation during the last deglaciation: A bipolar seesaw?, *Paleoceanography*, **13**,119-121.

Bryan, K. (1996), The steric component of sea level rise associated with enhanced greenhouse warming; a model study, *Climate Dynamics*, **12**, 545-555.

Cabioch, G., K.A.B. Cutler, W.J. Beck, G.S. Burr, T. Corrège, R.L. Edwards and F.W. Taylor (2003), Continuous reef growth during the last 23 cal kyr BP in a tectonically active zone (Vanuatu, SouthWest Pacific), *Quaternary Science Reviews*, **22**, 1771-1786.

Carminati, E., C. Doglioni and D. Scrocca (2003), Apennines subduction-related subsidence of Venice, *Geophysical Research Letters*, **30 (13)**: 1717, doi: 10.1029/2003GL017001.

Cattaneo, A., and F. Trincardi (1999), The late-Quaternary transgressive record in the Adriatic epicontinental sea: Basin widening and facies partitioning, In: Bergman, K. and J. Snedden (Eds.), Isolated Shallow Marine Sand Bodies: Sequence Stratigraphic Analysis and Sedimentologic Interpretation, *SEPM Spec. Publ. Soc. Sediment. Geol.*, **64**, 127-146, Tulsa, Oklahoma.

Cattaneo, A., A. Correggiari, M. Taviani and F. Trincardi (2001), Sedimentologic expression of the late-Quaternary ravinement surface in the Adriatic Sea, Italy, *International Association of Sedimentology*, 21th Meeting, Davos, Switzerland.

Cattaneo, A., A. Correggiari, L. Langone and F. Trincardi (2003), The late-Holocene Gargano subacqueous delta, Adriatic shelf: Sediment pathways and supply fluctuations, *Marine Geology*, **193**, 61-91.

Cattaneo, A., F. Trincardi, L. Langone, A. Asioli and P. Puig (2004), Clinoformation generation on Mediterranean Margins, *Oceanography*, **17**, 104-117.

Cattaneo, A., F. Trincardi, A. Asioli and A. Correggiari (2007), The Western Adriatic shelf clinoform: energy-limited bottomset, *Continental Shelf Research*, **27**, 506-525.

Channell, J.E.T., B. D'Argenio and F. Horvath (1979), Adria, the African Promontory, in Mesozoic Mediterranean paleo- geography, *Earth Science Rev.*, **15**, 213-292.

Chappell, J., and N.J. Shackleton (1986), Oxygen isotopes and sea level, *Nature*, **324**, 137-140.

Chappellaz, J., T. Blunier, S. Kints, A. Dällenbach, J.-M. Bamola, J. Schwander, D. Raynaud and B. Stauffer (1997), Changes in the atmospheric CH4 gradient between Greenland and Antarctica during the Holocene, *Journal Geophysical Research*, **102**, 15987-l 5999

Church, J.A., J.M. Gregory, P. Huybrechts, M. Kuhn, K. Lambeck, M.T. Nhuan, D. Qin and P.L. Woodworth (2001), Changes in Sea Level, In: Houghton J.T., Y. Ding, D.J. Griggs, M. Noguer, P.J. Van Der Linden, X. Dai, K. Maskell and C.A. Johnson (Eds.), Climate Change 2001, The Scientific basis: Contribution of Working Group 1 to the Third Assessment Report of the Intergovernmental Panel on Climate Change, *Cambridge University Press*, 639-694, Cambridge, New York.

Clark, P.U., R.B. Alley and D. Pollard (1999), Northern Hemisphere Ice-sheet influences on Global Climate Change, *Science*, **286**, 1104-1111.

Clark, P.U., N.G. Pisias, T.F. Stocker and A.J. Weaver (2002a), The role of the thermohaline circulation in abrupt climate change, *Nature*, **415**, 863-869.

Clark, P.U., J.X. Mitrovica, G.A. Milne, J.L. Turon and G. Siani (2002b), Sea level fingerprint as a direct test for the source of global Meltwater Pulse 1A, *Science*, **295**, 2438-2441.

Clark, P.U., A. Marshall McCabe, A.C. Mix and A.J. Weaver (2004), Rapid rise of sea level 19000 years ago and its Global implications, *Science*, **304**, 1141-1144.

Clark, P.U., A.S. Dyke, J.D. Shakun, A.E. Carlson, J. Clark, B. Wohlfarth, J.X. Mitrovica, S.W. Hostetler and A. M. McCabe (2009), The last Glacial Maximum, *Science*, **324**, 720-714.

Cloetingh, S. (1986), Intraplate stresses: A new tectonic mechanism for fluctuations of relative sea level, *Geology*, **14**, 617-620.

Correggiari, A., M. Roveri and F. Trincardi (1996a), Late Pleistocene and Holocene evolution of the North Adriatic Sea, *Il Quaternario*, **9**, 697-704.

Correggiari, A., M. Field and F. Trincardi (1996b), Late Quaternary transgressive large sand dunes on the sediment starved Adriatic shelf, In: De Baptist, M., and P. Jacobs (Eds.), Geology of Siliciclastic Shelf Seas, *Geological Society Special Publications*, **117**, 155-169.

Correggiari, A., A. Asioli, M. Roveri, F. Trincardi, M. Kashgarian, E. Reinhardt and M. Taviani (1997), Rapid sea-level rise during the termination Ia: evidence from low-gradient Adriatic epicontinental shelf, *First IAS/SEPM Meeting on Environmental sedimentology*, 27-29 October, Venice.

Correggiari, A., F. Trincardi, L. Langone and M. Roveri (2001), Styles of failure in heavily-sedimented highstand prodelta wedges on the Adriatic shelf, *Journal of Sedimentary Research*, **71**, 218-236.

Croll, J. (1875), Climate and Time, in their geological relations: A theory of secular changes of the Earth's climate, pp. 577, *D. Appleton & Co.,* New York.

Cushman-Roisin, B., M. Gacic, P.M. Poulain and A. Artegiani (2001), Physical Oceanography of the Adriatic Sea: Past, Present and Future, In: Cushman-Roisin, B., M. Gacic, P.M. Poulain and A. Artegiani (Eds.), *Kluwer Academic Publisher*, pp. 304, Dordrecht, Netherlands.

Cutler, K.B., R.L. Edwards, F.W. Taylor, H. Cheng, J. Adkins, C.D. Gallup, P.M. Cutler, G.S. Burr and A.L. Bloom (2003), Rapid sea-level fall and deep-ocean temperature change since the last interglacial period, *Earth and Planetary Science Letters*, **206**, 253-271.

D'Argenio, B., and F. Horvath (1984), Someremarksonthedefor- mation history of Adria, from the Mesozoic to the Tertiary, *Ann. Geophys.*, **2**, 143-146.

Dällenbach, A., T. Blunier, J. Fluckiger, B. Stauffer, J. Chappellaz and D. Raynaud (1997), Changes in the atmospheric CH4 gradient between Greenland and Antarctica during the Last Glacial and transition to the Holocene, *Geophysical Research Letters*, **27**,1005-1008.

Di Stefano, R., E. Kissling, C. Chiarabba, A. Amato and D. Giardini (2009), Shallow subduction beneath Italy, Three-dimensional images of the Adriatic-European-Tyrrhenian lithosphere system based on high quality P wave arrival times, *Journal Geophysical Research*, **114**, doi: 10.1029/2008JB005641.

Doglioni, C., F. Mongelli and P. Pieri (1994), The Puglia uplift (SE Italy): An anomaly in the foreland of the Apenninic subduction due to buckling of a thick continental lithosphere, *Tectonics*, **13**, 1309-1321.

Doglioni, C., M. Tropeano, F. Mongelli and P. Pieri (1996), Middle–Late Pleistocene uplift of Puglia: an ‘‘anomaly’’ in the Apenninic foreland, *Mem. Soc. Geol. Ital.*, **51**, 101-117.

Doglioni, C., and E. Carminati (2002), The effects of four subductions in NE Italy. Transalp conference, *Mem. Soc. Geol*., **54**, 1-4.

Edwards, R.L., J.W. Beck, G.S. Burr, D.J. Donahue, J.M.A. Chappell, A.L. Bloom, E.R.M. Druffel and F.W. Taylor (1993), A large drop in atmospheric $^{14}C/^{12}C$ and reduced melting in the Younger Dryas, documented with ^{230}Th ages of corals, *Science*, **260**, 962-968.

Fairbanks, R.G. (1989), A 17.000-yr glacio-eustatic sea level record: influence of glacial melting rates on the Younger Dryas event and deep-ocean circulation, *Nature*, **342**, 637-642.

Fairbridge, R.W. (1961), Eustatic changes in sea level, In: Physics and Chemistry of the Earth, **4**, 99-185, *Pergamon Press*, London, United Kingdom.

Fleming, K.P., J. Dan Zwartz, Y. Yokoyama, K. Lambeck and J. Chappell (1998), Refining the eustatic sea-level curve since the Last Glacial Maximum using far- and intermediate-field sites, *Earth and Planetary Science Letters*, **163**, 327-342.

Grimm, E.C., L.J. Maher and D.M. Nelson (2009), The magnitude of error in conventional bulk-sediment radiocarbon dates from central North America, *Quaternary Research*, **72**, 301-308.

Hanebuth, T., K. Stattegger and P.M. Grootes (2000), Rapid flooding of the Sunda shelf: A late-Glacial Sea-level record, *Science*, **288**, 1033-1035.

Haq, B.U., J. Hardenbol and P.R. Vail (1988), Mesozoic and Cenozoic chronostratigraphy and cycles of sea level change, In: Wilgus, C.K., B.S. Hastings, H. Posamentier, J. Van Wagoner, C.A. Ross and C.G.C. Kendall (Eds.), Sea-Level change, *SEPM Spec. Publ. Soc. Sediment. Geol.*, **42**, 71-108, Tulsa, Oklahoma.

Hernández-Molina, F.J., L. Somoza, J. Rey and L. Pomar (1994), Late Pleistocene-Holocene sediments on the Spanish continental shelves: Model for very high resolution sequence stratigraphy, *Marine Geology*, **120**, 129-174.

Imbrie, J., J.D. Hays, D.G. Martinson, A. McIntyre, A.C. Mix, J.J. Morley, N.G. Pisias, W.L. Prell and N.J. Shackleton (1984), The orbital theory of Pleistocene climate: support from a revised chronology of the marine $\delta^{18}O$ record, In: Berger, A., J. Imbrie, H. Hays, G. Kukla and B. Saltzman (Eds.), Milankovitch and Climate – Part 1, *Reidel Publishing*, 269-306, Dordrecht, Holland.

Intergovernmental Panel on Climate Change (IPCC) (1990), Climate Change, The IPCC Scientific Assessment, In: Houghton, J.T., G.J. Jenkins and J.J. Ephraums (Eds.), *Cambridge University Press*.

Isarin, R.F.B., H. Renssen and J. Vandedberghe (1998), The impact of the north Atlantic Ocean on the Younger Dryas climate in northwestern and central Europe, *Journal of Quaternary Science*, **13**, 447-453.

Knorr, G., and G. Lohmann (2003), Southern Ocean origin for the resumption of Atlantic thermohaline circulation during deglaciation, *Nature*, **424**, 532-536.

Labaune, C., G. Jouet, S. Bernè, B. Gensous, M. Tesson and A. Delpeint (2005), Seismic stratigraphy of the Deglacial deposits of the Rhône prodelta and of the adiacent shelf, *Marine Geology*, **222-223**, 299-311.

Lambeck, K., C. Smither and P. Johnston (1998), Sea-level change, glacial rebound and mantle viscosity for northern Europe, *Geophysical Journal International*, **134**, 102-144.

Lambeck, K., and J. Chappell (2001), Sea level change through the Last Glacial cycle, *Science*, **292**, 679-686.

Lambeck, K., Y. Yokoyama and T. Purcell (2002), Into and out of the Last Glacial Maximum: sea level changes during Oxygen Isotope Stage 3 and 2, *Quaternary Science Reviews*, **21**, 343-360.

Lambeck, K., F. Antonioli, A. Purcell and S. Silenzi (2004), Sea-level change along the Italian coast for the past 10,000 yr, *Quaternary Science Reviews*, **23**, 1567-1598.

Lascaratos, A., W. Roether, K. Nittis and B. Klein (1999), Recent changes in deep water formation and spreading in the eastern Mediterranean: an review, *Prog. Oceanogr.*, **44**, 5-36.

Lea, D.W., P.A. Martin, D.K. Pak and H.J. Spero (2002), Reconstructing a 350 kyr history of sea level using planktonic Mg/Ca and oxygen isotopic records from Cocos Ridge core, *Quaternary Science Reviews*, **21**, 283-293.

Lehman, S.J., and L.D. Keigwin (1992), Sudden changes in North Atlantic circulation during the last deglaciation, *Nature*, **356**, 757-762.

Malanotte-Rizzoli, P., and A. Bergamasco (1983), The dynamics of the coastal region of the northern Adriatic Sea, *J. Phys. Oceanogr.*, **13**, 1105-1130.

Malinverno, A., and W.B.F. Ryan (1986), Extension in the Tyrrhenian Sea and the shortening in the Apennines as a result of arc migration driven by sinking of lithosphere, *Tectonics*, **5**, 227-245.

Manca, B.B., V. Kovacevic, M. Gacic and D. Viezzoli (2002), Dense water formation in the Southern Adriatic Sea and interaction with the Ionian Sea in the period 1997–1999, *Journal of Mar. Syst.*, **33-34**, 133-154.

Martinson, D.G., N.G. Pisias, J.D. Hays, J. Imbrie, T.C. Moore and N.J. Shackleton (1987), Age dating and the Orbital theory of Ice Ages: Development of a high-resolution 0 to 300,000 year chronostratigraphy, *Quaternary Research*, **27**, 1-29.

Massari, F., D. Rio, R. Serandrei Barbero, A. Asioli, L. Capraro, E. Fornaciari and P.P. Vergerio (2004), The environment of Venice area in the past two million years, *Palaeogeogr. Palaeoclimatol. Palaeoecol.*, **202**, 273-308.

Maslin, M.A., and A.J. Ridgwell (2005), Mid-Pleistocene revolution and the 'eccentricity myth', *Geological Society Special Publications*, **247**, 19-34, London, United Kingdom.

Milankovitch, M. (1941), Kanon der Erdbestrahlung und seine Andwendung auf das Eiszeitenproblem, *Spec. Pub*., **133**, pp. 633, Royal Serbian Academy.

Mix, A.C., and W.F. Ruddiman (1985), Structure and timing of the last deglaciation: Oxygen-isotope evidence, *Quaternary Science Reviews*, **4**, 59-108.

Mörner, N.-A. (1996), Rapid changes in coastal se level, *Journal of Coast. Res.*, **12**, 797-800.

Myers, P.G., K. Haines and E.J. Rohling (1998), Modeling the paleocirculation of the Mediterranean: the last glacial maximum and the Holocene with emphasis on the formation of Sapropel S1, *Paleoceanography*, **6**, 586-606.

Ori, G.G., and P.F. Friend (1984), Sedimentary basins formed and carried piggyback on active thrust sheets, *Geology*, **12**, 475-478.

Ori, G.G., M. Roveri and F. Vannoni (1986), Plio-Pleistocene sedimentation in the Apenninic-Adriatic foredeep (central Adriatic Sea, Italy), In: Allen, P., and P. Homewood (Eds.), Foreland Basins, *Int. Ass. Sediment., Spec. Pub*., **8**, 183-198, *Blackwell Sci.*, Oxford, United Kingdom.

Paillar, D. (2001), Glacial cycles: Toward a new paradigm, *Review of Geophysics*, **39**, 325-346.

Paschini, E., A. Artegiani and N. Pinardi (1993), The mesoscale eddy field of the middle Adriatic during fall 1988, *Deep-Sea Res.*, *40*, 1365-1377.

Paul, F., (2011), Sea-level rise: Melting glaciers and ice caps, *Nature Geoscience*, **4**, 71-72.

Peltier, W.R. (1994), Ice Age Paleotopography, *Science*, **265**, 195-201.

Peltier, W.R. (2004), Global Glacial Isostasy and the Surface of the Ice-Age Earth: the ICE-5G (VM2) Model and GRACE, *Annu. Rev. Earth Planet. Science*, **32**, 111-159.

Peltier, W.R., and R.G. Fairbanks (2006), Global glacial ice volume and Last Glacial Maximum duration from an extended Barbados sea level record, *Quaternary Science Reviews*, **25**, 3322-3337.

Philippsen, B., H. Kjeldsen, S. Hartz, H. Paulsen, I. Clausen and J. Heinemeier (2010), The hardwater effect in AMS 14C dating of food crusts on pottery, *Nuclear Inst. And Met. In Phys. Res. B.*, **268**, 995-998.

Piva, A., A. Asioli, R. R. Schneider, F. Trincardi, N. Andersen, E. Colmenero-Hidalgo, B. Dennielou, J.-A. Flores and L. Vigliotti (2008a), Climatic cycles as expressed in sediments of the PROMESS1 borehole PRAD1.2, central Adriatic, for the last 370 ka: 1. Integrated stratigraphy, *Geochem. Geophys. Geosyst.*, **9**, Q01R01, doi:10.1029/2007GC001713.

Piva, A., A. Asioli, N. Andersen, J. O. Grimalt, R. R Schneider and F. Trincardi (2008b), Climatic cycles as expressed in sediments of the PROMESS1 borehole PRAD1.2, central Adriatic, for the last 370 ka: 2. Paleoenvironmental evolution, *Geochem. Geophys. Geosyst*., **9**, Q03R02, doi:10.1029/2007GC001785.

Patacca, E., R. Sartori and P. Scandone (1990), Tyrrhenian Basin and Apenninic arcs: Kinematic relations since Late Toronian times, *Mem. Soc. Geol. It*., **45**, 425-451.

Pieri, M., and G. Groppi (1981), Subsurface geological structure of the Po Plain, Italy, Progetto Finalizzato Geodinamica, CNR Publ., **414**, pp. 23, Roma, Italy.

Poulain, P.M. (2001), Adriatic Sea surface circulation as derived from drifter data between 1990 and 1999, *Journal Marine Systems*, **29**, 3-32.

Rea, D.K., and S.M. Colman (1995), Radiocarbon ages of pre-bomb clams and the hard-water effect in Lakes Michigan and Huron, *Journal of Paleolimnology*, **14**, 89-91.

Reynolds, D.J., M.S. Steckler and B.J. Coakley (1991), The role of the sediment load in Sequence Stratigraphy: The influence of flexural isostasy and compaction, *Journal of Geophysical research*, **96**, 6931-6949.

Ricci Lucchi, F. (1986), The Oligocene to recent foreland basins of the Northern Apennines, In: Allen, P.A., and P. Homewood (Eds.), Foreland Basins, *Int. Ass. Sediment., Spec. Pub*., **8**, 105-139, *Blackwell Sci.*, Oxford, United Kingdom.

Ridente, D., and F. Trincardi (2002), Eustatic and tectonic control on deposition and lateral variability of Quaternary regressive sequences in the Adriatic basin (Italy), *Marine Geology*, **184**, 273-293.

Ridente, D., and F. Trincardi (2005), Pleistocene "muddy" forced-regression deposits on the Adriatic shelf: A comparison with prodelta deposits of the late Holocene highstand mud wedge, *Marine Geology*, **222-223**, 213-233.

Ridente, D., and F. Trincardi (2006), Active foreland deformation evidenced by shallow folds and faults affecting Late Quaternary shelf-slope deposits (Adriatic Sea, Italy), *Basin Research*, **18**, 171-188.

Ridente, D., F. Foglini, D. Minisini, F. Trincardi and G. Verdicchio (2007), Shelf-edge erosion, sediment failure and inception of Bari Canyon on the South-Western Adriatic Margin (Central Mediterranean), *Marine Geology*, **246**, 193-207.

Ridente, D., F. Trincardi, A. Piva, A. Asioli and A. Cattaneo (2008), Sedimentary response to climate and sea level changes during the past 400 ka from borehole PRAD1.2 (Adriatic margin), *Geochem. Geophys. Geosyst.*, **9**, 1-20.

Ridente, D., F. Trincardi, A. Piva and A. Asioli (2009), The combined effect of sea level and supply during Milankovitch cyclicity: Evidence from shallow-marine $\delta^{18}O$ records and sequence architecture (Adriatic margin), *Geology*, **32**, 1003-1006.

Rohling, E.J., M. Fenton, F.J. Jorissen, P. Bertrand, G. Ganssen and J.P. Caulets (1998), Magnitudes of sea level lowstands of the past 500.000 years, *Nature*, **394**, 162-165.

Rohling, E.J., R. Marsh, N.C. Wells, M. Siddall and N.R. Edwards (2004), Similar Meltwater contributions to glacial sea level changes from Antarctic and northern ice sheets, *Nature*, **430**, 1016-1021.

Royden, L.E., E. Patacca and P. Scandone (1987), Segmentation and configuration of subducted lithosfere in Italy: an important control on thrust-belt and foredeep-basin evolution, *Geology*, **15**, 714-717.

Ruddiman, W.F. (2006), Orbital changes and climate, *Quaternary Science Reviews*, **25**, 3092-3112.

Scrocca, D. (2006), Thrust front segmentation induced by differential slab retreat in the Apennines (Italy), *Terra Nova*, **18**, 154-161.

Scrocca, D., E. Carminati, C. Doglioni and D. Marcantoni (2007), Slab retreat and active shortening along the Central-Northern Apennines, In: Lacombe, O., J. Lavu, F. Roure and J. Verges (Eds.), Thrust belts and Foreland Basins: from fold kinematics to hydrocarbon systems. Frontier in Earth Science, 471-487, *Springer*.

Severinghaus, J.P., T. Sowers, E.J. Brook, R.B. Alley and M.L. Bender (1998), Timing of abrupt climate change at the end of the Younger Dryas interval from thermally fractionated gases in polar ice, *Nature*, **391**, 141-146.

Severinghaus, J.P. (2009), Southern see-saw seen, *Nature*, **457**, 1093-1094.

Shackleton, N.J., and N.D. Opdyke (1973), Oxygen isotope and paleomagnetic stratigraphy of equatorial Pacific core V28-238: oxygen isotope temperatures and ice volume on a 10^5 and 10^6 year scale, *Quaternary Research*, **3**, 39-55.

Shackleton, N.J. (1987), Oxygen isotopes, ice volume and sea level, *Quaternary Science Reviews*, **6**, 183-190.

Siddall., M., E.J. Rohling, A. Almogi-Labin, C. Hemleben, D. Melschber, I. Schmelzer and D.A. Smeed (2003), Sea level fluctuations during the last glacial cycle, *Nature*, **523**, 853-858.

Siddall, M., M.R. Kaplan, J.M. Schaefer, A. Putnam, M.A. Kelly and B. Goehring (2010), Changing influence of Antarctic and Greenlandic temperature records on sea-level over the last glacial cycle, *Quaternary Science Reviews*, **29**, 410-423.

Stanley, D.J., and A.G. Warne (1994), Worldwide initiation of Holocene marine deltas by deceleration of sea-level rise, *Science*, **265**, 228-231.

Stephens, B.B., and R. Keeling (2000), The influence of Antarctic sea ice on glacial-interglacial CO_2 variations, *Nature*, **404**, 171-174.

Stocker, T.F., D.G. Wright and W.S. Broecker (1992), The influence of high-latitude surface forcing on the global thermohaline circulation, *Paleoceanography*, **7**, 529-541.

Storms, J.E.A., G.J. Weltje, G.J. Tierra, A. Cattaneo and F. Trincardi (2008), Coastal dynamics under conditions of rapid sea-level rise: Late Pleistocene to Early Holocene evolution of barrier-lagoon systems on the northern Adriatic shelf (Italy), *Quaternary Science Reviews*, **27**, 1107-1123.

Taylor, K.C., P.A. Mayewski, R.B. Alley, E.J. Brook, A.J. Gow, P.M. Grootes, D.A. Meese, E.S. Saltzman, J.P. Severinghaus, M.S. Twickler, J.W.C. White, S. Whitlow and G.A. Zielinski (1997), The Holocene/Younger Dryas transition recorded at Summit, Greenland, *Science*, **278**, 825-827.

Törnqvist, T.E., J.L. Gonzalez, L.A. Newsom, K. Van der Borg, A.F.M. De Jong and C.W. Kurnik (2004), Deciphering Holocene sea-level history on the U.S. Gulf Coast: A high-resolution record from the Mississippi Delta, *Geological Society of America Bulletin*, **116**, 1026-1039.

Trincardi, F., A. Correggiari and M. Roveri (1994), Late Quaternary transgressive erosion and deposition in a modern epicontinental shelf: the Adriatic Semi-enclosed Basin, *Geo-Marine Letters*, **14**, 41-51.

Trincardi, F., and A. Correggiari (2000), Quaternary forced regression deposits in the Adriatic basin and the record of composite sea-level cycles. In: Hunt, D., Gawthorpe, R. (Eds.), Depositional Response to Forced Regression, *Geological Society Special Publication*, **172**, 245-269.

Trincardi, F., and A. Argnani (2001), Note illustrative della Carta Geologica d'Italia alla scala 1:250000 – Foglio NL33-10 "Ravenna", ISPRA – Servizio Geologico d'Italia.

Trincardi, F., F. Foglini, G. Verdicchio, A. Asioli, A. Correggiari, D, Minisini, A. Piva, A. Remia, D. Ridente and M. Taviani (2007), The impact of cascading currents on the Bari Canyion System SW-Adriatic Margin (Central Mediterranean), *Marine Geology*, **246**, 208-230.

Trincardi, F., A. Argnani and A. Correggiari (in press, a), Note illustrative della Carta Geologica d'Italia alla scala 1:250000 – Foglio NL33-7 "Venezia", ISPRA – Servizio Geologico d'Italia.

Trincardi, F., A. Argnani and A. Correggiari (in press, b), Note illustrative della Carta Geologica d'Italia alla scala 1:250000 – Foglio NK33-12 "Ancona", ISPRA – Servizio Geologico d'Italia.

Vilibic, I., and M. Orlic (2002), Adriatic water masses, their rates of formation and transport through the Otranto Strait, *Deep-Sea Res*., Part 1, *Oceanogr. Res. Pap*., **49**, 1321-1340.

Waelbroek, C., L. Labeyrie, E. Michel, J.C. Duplessy, J.F. McManus, K. Lambeck, E. Balbon and M. Labracherie (2002), Sea level and deep water temperature changes derived from benthic foraminifera isotopic records, *Quaternary Science Reviews*, **21**, 295-305.